LIQUEFACTION PROBABILITY MAPPING IN GREATER BOSTON

by

Youssef M.A. Hashash

B.S. Civil Engineering, MIT 1987

SUBMITTED TO THE DEPARTMENT OF CIVIL ENGINEERING IN PARTIAL FULFILLMENT OF THE REQUIREMENTS FOR THE DEGREE OF

MASTER OF SCIENCE IN CIVIL ENGINEERING

at the

MASSACHUSETTS INSTITUTE OF TECHNOLOGY

April 1988

Signature of Author _____
Department of Civil Engineering
April 28, 1988

Certified by _____
Prof. Daniele Veneziano
Thesis Co-Supervisor

Certified by _____
Prof. Herbert H. Einstein
Thesis Co-Supervisor

Accepted by _____
Prof. Ole S. Madsen
Chairman, Departmental Graduate Committee

LIQUEFACTION PROBABILITY MAPPING IN GREATER BOSTON

by

Youssef M.A. Hashash

Submitted to the Department of Civil Engineering on April 28, 1988 in partial fulfillment of the requirements for the degree of Master of Science in Civil Engineering

Abstract

Three different methods to produce liquefaction maps are presented. In the first method standard penetration test data from the area to be mapped is used to characterize the local soil liquefaction resistance. This data, combined with local seismicity information, is the input to a probabilistic liquefaction model which produces liquefaction recurrence rates. This methodology is applied at two sites, BackBay in Boston and Lowell in northern Massachusetts, liquefation hazard maps are produced. In the second method, historic records of liquefaction at a site are used as additional information to estimate the liquefaction hazard. An application of this method to glaciomarine deposits in Newburyport which partially liquefied during the 1727 earthquake is presented. In the last method, geological and some geotechnical data are used to construct liquefaction danger maps in areas north of Boston.

Thesis Co-Supervisor: Prof. Daniele Veneziano
Title: Professor of Civil Engineering

Thesis Co-Supervisor: Prof. Herbert H. Einstein
Title: Professor of Civil Engineering

Acknowledgments

The author would like to acknowledge the help and support he received from his thesis supervisors Prof. Daniele Veneziano and Prof. Herbert Einstein. The author thanks Prof. Herbert Einstein for his guidance throughout the course of this work and for being a superb academic advisor. Also, many thanks to Prof. Veneziano for his patience, comments and encouragement during our many long meetings and discussions. It has been a pleasure working under both supervisors.

The author would also like to acknowledge the help of the following individuals:

Mr. Don Degroot for several of the computer program used.

Mr. Luc Chouinard for the data on local seismicity and the contouring program.

Mr. Raymond Ty for some of the BSCE Borehole data and many of the computer programs.

My parents and my sister Mariam for their love and support and their help in compiling the BackBay data during their visit last Summer. My sister Naila for her comments on some of the chapters.

Mr. Matt Grebner for his help in some of the figures and for putting up with the fluctuating moods of his office-mate.

The author would like to express his deep gratitude to the above individuals. This work would have been impossible to accomplish without their help.

Table of Contents

List of Figures

List of Tables

Chapter 1

INTRODUCTION

Mapping of natural hazards is an important part of hazard prevention programs in many countries. Hazard maps are becoming increasingly important. In many parts of the world, and due to the pressure of increasing population, areas which are prone to natural disasters are being inhabited. Hazard maps are necessary components is the decision making process on land use and management.

This thesis is part of the research project "Liquefaction Risk Map of the Boston Area", sponsored by the United States Geological Survey. The thesis is one of a series of reports produced for this project (see Hawkes, 1987, Ty, 1987). In the two earlier reports extensive information was collected on natural and artificial soil deposits in Boston. In this thesis liquefaction maps[1] are produced for selected areas within greater Boston.

1.1 Objective

The objective of this work is two fold:

(a) Develop procedures to produce liquefaction maps;

(b) Apply such procedures to specific sites within the Boston area.

---

[1]Liquefaction maps are maps which show the liquefaction potential or risk of soil deposits within a selected area.

1.2 Contents

The following two chapters give some background on the phenomenon of liquefaction and on liquefaction mapping. Specifically, Chapter 2 describes the main mechanisms of liquefaction and the parameters that affect the liquefaction behavior of soils. Several methods have been developed to produce liquefaction hazard maps, in the U.S. and abroad. Chapter 3 describes the different types of such maps and reviews the methods currently in use to produce them.

The mapping procedures employed in this thesis build up on some of the methods introduced in chapters 4 and 5. Three techniques of liquefaction mapping are developed and exemplified:

(1) A technique, described in Chapter 4, combines blow count records and seismicity information at the site with a probability of liquefaction model. The technique is used to produce liquefaction hazard maps for the artificial fills in BackBay (Chapter 4) and for fluvial and fluvioglacial deposits in Lowell (Chapter 5).

(2) A method that, in addition to the geologic and blow count records, uses information about the occurrence or non-occurrence of liquefaction at the site during strong historical earthquakes. The method is described in Chapter 6 where it is applied to glaciomarine deposits in Newburyport which experienced partial liquefaction during the 1727 earthquake.

(3) In areas where borehole data is insufficient, liquefaction danger maps based on surficial geology information can be produced. Chapter 7 describes this mapping technique and applies it to two areas north of Boston.

Chapter 8 presents a brief summary of methods and results and makes suggestions for future work.

Chapter 2

LIQUEFACTION POTENTIAL EVALUATION

2.1 Introduction

This chapter presents a brief review of the liquefaction phenomenon. It discusses some of the basic mechanisms of liquefaction and different methods developed to evaluate liquefaction potential. It is not intended to be comprehensive. Its main objective is to present aspects of liquefaction that are relevant to later chapters. A more detailed review of the literature on liquefaction can be found in a recent report by the National Research Council, on "Liquefaction of Soils During Earthquakes", NRC(1985).

2.2 Liquefaction

Liquefaction is the phenomenon by which soil deposits suffer a substantial loss of strength due to the increase in pore pressure and the consequent decrease in effective stress. Liquefaction of a soil deposit can result from static or dynamic (cyclic) loading. This review deals mainly with earthquake induced liquefaction, which is most frequently observed in saturated cohesionless soils. There is doubt as to whether cohesive soil can liquefy, see El Hosri et al. (1984).

Liquefaction manifests itself through different types of ground failure. It can cause landslides in embankments and slopes, and boils, and lateral spreading, and loss of bearing capacity in level deposits. The result may be extensive damage to structures, power supplies, pipelines and other utility services. As an example, during the 1906 San Francisco Earthquake, firefighting efforts were hampered by the damage to water pipes resulting from liquefaction.

The deposits which liquefy most frequently are geologically young fine-to-medium sands which are medium dense to loose. Liquefaction can occur at the same site more than once (Youd, 1984).

It is important to distinguish between initial liquefaction and ground failure. Initial liquefaction is the state in which the vertical effective stress in the deposit decreases and approaches zero, whereas ground failure is the surface damage caused by this decrease in effective stress. It is, therefore, possible for a soil to experience initial liquefaction without producing ground failure. This distinction is important to correctly interpret the results of different methods used to evaluate liquefaction.

In earlier liquefaction work, it was assumed that water had no time to drain during rapid earthquake loading and, therefore, that liquefaction would occur under fully undrained conditions. This is indeed one possible mechanism of liquefaction, but not the only one. Whitman, (1985), for example, describes three failure mechanisms due to cyclic straining of the soil: (1) loss of static shearing resistance during truly undrained shear, (2) loss of static shearing resistance within parts of the cohesionless soil owing to redistribution of water within the soil, and (3) loss of static shearing resistance in the material surrounding cohesionless soils, due to high pore pressure buildup.

2.3 Soil Parameters

The effect of some soil parameters, such as density, uniformity, grain size,... on the behavior of a deposit during an earthquake is critical. Liquefaction occurs mainly in cohesionless granular soils. Particularly prone to liquefaction are uniform soils with D_{50} = 0.01-0.25mm and with uniformity coefficient C_u=2-10 (DM7, 1982). Soil resistance to liquefaction is affected by the percentage of fines (silt and clay size particles) in the soil. Tokimatsu and Yoshimi (1984) observe that sands containing fines are more resistant to liquefaction than clean sands.

Liquefaction resistance increases with the increase in relative density and seems to be influenced by the grain shape: at low confining stresses, Vaid et al (1984) find that angular sand is more resistant than round sand; however, the two types of sand are found to exhibit similar behavior at higher stresses, probably due to crushing of the angular grains.

2.4 Liquefaction Evaluation Methods

Over the years, several methods have been developed to evaluate the liquefiability of a soil deposit. Some of the methods are based on laboratory testing, while others use insitu test data. Still other methods are based on theoretical modeling of the liquefaction phenomenon or on the probabilistic evaluation of liquefaction potential using historical liquefaction data. These four types of liquefaction analyses are briefly reviewed next.

2.4.1 Evaluation Based on Lab Testing

The critical void ratio concept has been used to evaluate the liquefaction resistance of soils. This is based on the assumption that soils undergo full undrained cyclic shearing during earthquake loading and that there is no change in the insitu void ratio during that loading. According to this hypothesis, the soil strength against liquefaction equals the residual strength at the insitu void ratio; see fig 2-1. However, several authors have observed a behavior different from what this method predicts. Casagrande (1975), and Seed (1987) attribute these observations to the redistribution of the pore pressure and the changes in the insitu void ratio during ground shaking. Seed (1987) suggests that the void ratio might even reach infinity, with water layers forming within the soil during liquefaction. Poulos (1985) proposes a correction of laboratory measurements to account for changes in void ratio due to sampling disturbance but does not consider other possible changes in insitu void ratio during liquefaction.

Another method to estimate soil resistance to liquefaction is by measuring the soil

strength after a specified number of cyclic loads. Conventionally, undrained cyclic shear tests have been used to measure this strength, but some researchers suspect that, in the field, partial drainage may occur during cyclic loading. Zen et al (1985) report some results on the increase of cyclic shear strength when partial drainage is allowed, fig. 2-2.

During ground shaking, soil deposits experience a rotation in the direction of the principal stresses and changes in the relative magnitude of the intermediate principal stress. Symes et al (1984) observe that the cyclic rotation of the principal stresses and the initial anisotropy of the soil are important factors in determining the likelihood of liquefaction.

Evaluating liquefaction on the basis of lab tests has its limitations. Disturbance of the sand during sampling or the use of reconstituted samples of sand can lead to erroneous results. Undisturbed samples obtained by freezing techniques (Yoshimi et al, 1985) have been found to have higher undrained cyclic strength than reconstituted samples of the same material, at the same relative density.

2.4.2 Evaluation Based on Insitu Testing

Analysis of liquefaction potential based on insitu testing complements lab evaluation techniques and improves the accuracy of the evaluation process. Seed et al (1983) propose to evaluate liquefaction resistance of soils based on blow counts obtained from Standard Penetration Tests (SPT). They base their correlation on case histories of liquefaction and non liquefaction. They also propose two different limiting curves based on the D_{50} of the deposit, as shown in fig. 2-3. Their analysis was made possible by the availability of an extensive data base of SPT records.

One of the shortcomings of the SPT records is that they are only taken at discrete intervals in the soil. Therefore, it is possible to miss a loose layer of sand in an otherwise dense deposit. Typically, SPT values have a maximum resolution of one foot, and cannot adequately reflect weak layers less than one foot in thickness.

The Cone Penetration Test (CPT) is becoming increasingly popular for evaluating liquefaction potential. The advantage of using CPT is that one can obtain a continuous profile of the soil. Robertson and Campanella (1985) correlate CPT to the cyclic stress ratio that produces failure and obtain liquefaction curves similar to those based on SPT data, see fig. 2-4. The main problem with using CPT correlations is the lack of an extensive data base. Some researchers, Kasim et al (1986) and Jamiolkwoski et al (1985), have established relationships between CPT and SPT, which enable one to use the liquefaction results in terms of SPT.

2.4.3 Evaluation Based on Numerical Models

The main idea of liquefaction models is to incorporate parameters that affect the liquefaction potential in a deposit in a mathematical representation of the phenomena. Liquefaction models can be of two types:

- Models for small scale liquefaction analysis such as for foundation or dam design where soil parameters are well defined. For example, Yegian (1984) and Pires et al (1984) model the pore pressure buildup in the soil during cyclic loading and assume liquefaction to occur when the vertical effective stress is zero.

- Models for large scale liquefaction evaluation (such as for liquefaction mapping) where spatial variability of soil properties is significant. Liao(1986) presents a method to evaluate the probability of liquefaction based on case histories of liquefaction and non liquefaction. Kavazanjian, (1984) estimates the probability of liquefaction based on the number of load cycles needed to liquefy the soil. In chapters 4 and 5 we will describe and use Liao's probabilistic liquefaction model. In Chapter 6 we will present a method of evaluating liquefaction potential using historical liquefaction data in the area of interest.

2.5 Conclusion

Several approaches to evaluate liquefaction potential in a soil deposit have been summarized. The choice of a liquefaction evaluation method depends on the type of information available. Lab evaluation methods can be inaccurate because of sample disturbance and incorrect modeling of the liquefaction phenomenon. A good practice would be to use more than one method, whenever possible. In chapters 4, 5 and 6 liquefaction evaluation is based on a probabilistic model which uses insitu SPT data. In Chapter 7 liquefaction evaluation is based on geologic characterization of soil deposits combined with some geotechnical information.

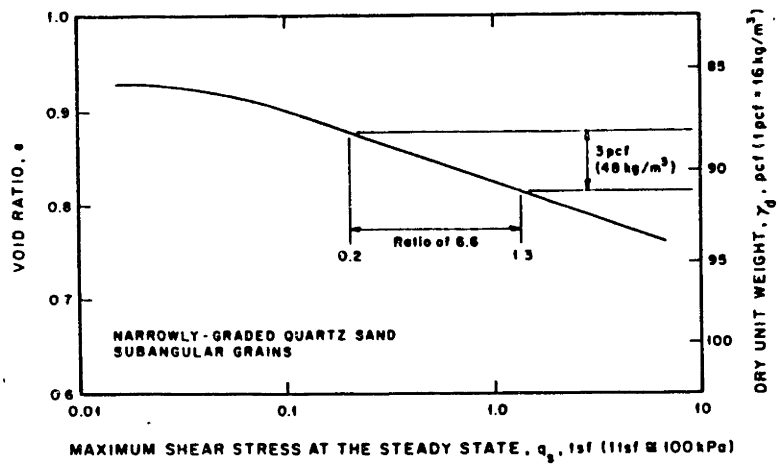

Figure 2-1: Steady-State Line for Clean Sand (Poulos, 1985)

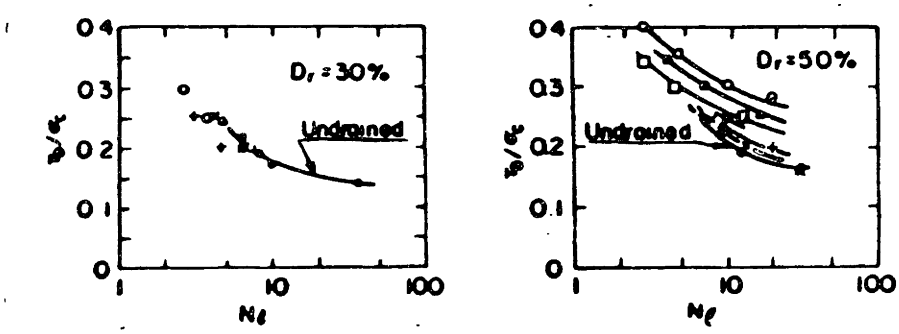

Figure 2-2: Effect of Partial Drainage on Cyclic Strength (Zen, 1985)
N_l= number of load cycles

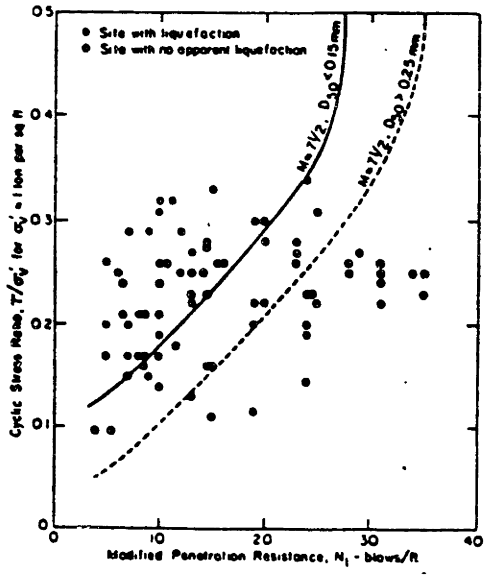

Figure 2-3: Liquefaction Evaluation Using SPT (Seed et al, 1983)

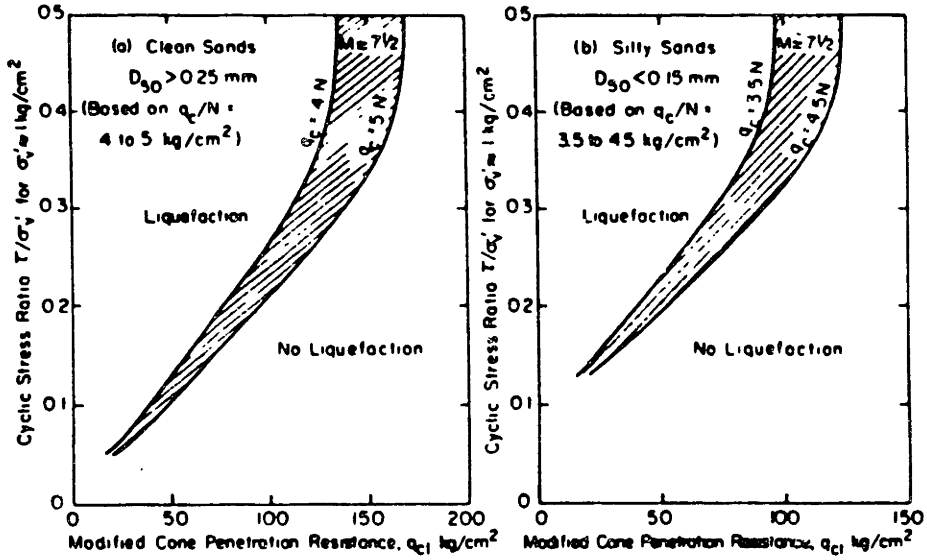

Figure 2-4: Liquefaction Evaluation Using CPT (Robertson and Campanella, 1985)

Chapter 3

LIQUEFACTION POTENTIAL MAPPING

3.1 Introduction

In this chapter we are interested in the procedures of mapping the risk of liquefaction induced by earthquakes. The chapter is divided into two parts. In the first part a liquefaction mapping framework, which describes the steps involved in producing different liquefaction maps, is presented. The second part is a review of some of the liquefaction mapping methods published in the literature.

3.2 Liquefaction Mapping

For the purpose of liquefaction mapping, one needs information in two areas. The first area is seismicity and attenuation which, when combined, characterize the frequency at which ground motions of different intensities occur at the site. The second area is that of soil susceptibility to liquefaction and includes geologic and geotechnical information about the soil as well as information on ground water. Liquefaction maps are then obtained in various ways by combining information on seismicity and soil deposit characteristics.

The main difficulty in liquefaction mapping is in the acquisition of data on soil characteristics. In many cases, the availability of these data determines the level of complexity and the detail of a liquefaction study.

3.3 Classes of Liquefaction Maps

Liquefaction maps can be of different types depending on the purpose of their use and the level of information they contain. A liquefaction mapping framework categorizing the different types of liquefaction maps is suggested in this section. The mapping framework, to be described later, is adopted from the landslide mapping framework described by Einstein (1988) with some modifications. This framework represent a coherent approach to the liquefaction mapping procedure, however, not the only one It is in the opinion of the author of this thesis that the framework by Einstein (1988) is wider in scope than the terminology and the descriptions used in the literature dealing with liquefaction mapping. The following is a detailed description of the proposed liquefaction mapping sequence.

3.3.1 Class A; State of Nature Maps

This includes all information available about the area to be mapped; such as geological and geotechnical characteristics, seismicity, topography, etc...

3.3.2 Class B; Danger Maps

In these maps, areas which might be subject to liquefaction are identified. Preliminary geologic and geotechnical information from class A maps usually constitute the basis for the identification procedure. These maps could either be "black & white" and classify the deposits as being liquefiable or not, or they could be "color" maps where different colors represent different degrees of susceptibility to liquefaction. This class of maps can have two levels of detail:

Level 1 (Class B1): These maps are based mainly on geologic descriptions of the deposits in a certain area and on some past cases of liquefaction in similar deposits.

Level 2 (Class B2): With the aid of B1 maps, one performs laboratory and insitu tests

to determine whether the deposits are liquefiable. Also, one would include information about the water table (including seasonal variations) to determine whether the identified deposits are below or above the water table.

3.3.3 Class C; Hazard Maps

One can combine danger maps with seismicity information to obtain an estimate of the return periods of liquefaction events in different subregions within the mapped area. Mapping may again be at two levels:

Level 1 (Class C1): Evaluation of the return period is qualitative, and for example obtained by dividing the deposits into regions of low, moderate, and high liquefaction rate. One basis for the classification might be an estimate of the critical acceleration at which local deposits liquefy; then the return period of these or larger accelerations can be used to estimate the return period of liquefaction events.

Level 2 (Class C2): The return period of liquefaction events is formally computed using liquefaction models. For example, the liquefaction rate[2] can be calculated in the following manner:

$$\lambda_L(\underline{x})=\sum_a P_L(SoilResistance,a)\lambda_a(\underline{x}) \tag{3.1}$$

where

$\underline{x}$= coordinates of the site

a= peak ground acceleration

$\lambda_L(\underline{x})$= rate of liquefaction events at location $\underline{x}$

P_L= probability of liquefaction as a function of soil liquefaction resistance and peak ground acceleration a

---

[2]The rate is the reciprocal of the return period.

$\lambda_a(\underline{x})$= rate at which events with peak ground acceleration a occur at location $\underline{x}$

3.3.4 Class D; Risk Maps

At this level, one estimates the potential consequences of liquefaction on the population as well as on properties and infrastructure and on the natural environment. The resulting maps consider these potential consequences in combination with the frequency of liquefaction events. Lew (1984) identifies as main components of liquefaction risk (Risk= hazard.vulnerability.value):

-The earthquake hazard in terms of liquefaction probability.

-The liquefaction vulnerability of the facility under consideration.

-The value of the facility.

3.3.5 Class E; Land Management and Land Use Maps

These maps are used by regulatory agencies to determine which area may or may not be inhabited, to specify design requirements for structures, or simply to improve emergency response measures in liquefaction prone areas. Depending on their use, class E maps can be based on class B, class C, or class D maps.

3.4 Development of Liquefaction Maps

Over the past two decades many maps have been developed to represent the spatial variation of liquefaction potential. Most of the work has been done in the United States, Japan and Italy. The main difficulty encountered in producing these maps lies in establishing the spatial variability of soil liquefaction resistance parameters.

The following is a brief description of the different methods used to develop liquefaction maps.

As discussed earlier, two components, seismicity and soil resistance, are needed to produce liquefaction maps. Ziony (1976) evaluates seismicity from regional faulting, and estimates potential local wave amplification based on the SPT values. The two components are qualitatively combined with information on water table to produce a B2 class map for the San Francisco Bay region, (fig. 3-1).

Several of the liquefaction maps developed in the U.S.A. are based on a method developed by Youd and Perkins (1978). In that method, one arrives at a ground failure potential map by combining a ground failure opportunity map and a ground failure susceptibility map. The ground failure opportunity map, fig. 3-2, estimates the return periods of potential ground failure events based on the seismicity of the area and on local attenuation. The ground failure susceptibility map (class B2) is based on geologic descriptions, grain size distribution curves, and water table information and describes the relative resistance of the soil deposit to liquefaction; see fig 3-3. The combined C-class map, fig. 3-4, shows the potential of a liquefaction induced ground failure. The basis of the map is that liquefaction potential increases with seismic activity and is greater for younger soils and for ground water closer to the surface. An application of this procedure can be found in Youd et al (1978).

Several modifications have been introduced to the previously described method For example, Kavazanjian et al (1985) use a probabilistic approach to determine the liquefaction potential of a soil deposit, rather than rely on qualitative evaluation. Initial liquefaction is assumed to occur when a zero vertical effective stress occurs. Then, using a pore pressure model, the conditional probability of liquefaction for each given ground acceleration "a" can be calculated. The return period of liquefaction events , therefore, correspond to the return period of the the different accelerations "a", see Table 3-I.

Youd and Perkins (1987) present a liquefaction susceptibility map of San Mateo County in California using the technique they developed in 1978, except that they treat

parameters as uncertain quantities, of which they estimate the probability distribution. Liquefaction potential is then quantified in terms of the relative susceptibility (RS) of sand and silt to liquefaction, where:

RS=P(Layer in ground) x P(layer liquefiable) x P(layer saturated) (3.2)

The values of RS are divided into intervals of high, moderate (0.1%<RS<1.%), low (0.01%<RS<0.1%) and very low (RS<0.01%) susceptibility to liquefaction.

The marginal probabilities are estimated based on geologic and hydrogeologic information from the area, as shown in Table 3-II. Specifically, the probability that the layer exists is estimated from geologic profiles. The probability that the soil is liquefiable is estimated from standard penetration tests. The probability that the layer is saturated is estimated using a ground water map. Youd and Perkins (1987) do not describe the numerical formulations used in the above estimations.

A different method of evaluating the liquefaction potential is presented by Anderson and Keaton (1982). In this method, the cyclic stress ratio at which liquefaction occurs is found from laboratory tests. Then using for the cyclic stress ratio τ/σ_{ave} the equation:

$$\frac{\tau}{\sigma_{ave}} = 0.65 \frac{a_{max}}{g} \frac{\sigma_{tot}}{\sigma_{eff}} r_d \quad (3.3)$$

where

a_{max}= peak ground acceleration

g= acceleration due to gravity, 9.81m/sec^2

σ_{tot}= total overburden stress

σ_{eff}= vertical effective stress

r_d= depth correction factor (see eq. (4.17))

Anderson and Keaton backcalculate the critical acceleration a_{cr} at which liquefaction

occurs. Then they use the the probability of exceedence of a_{cr} in 100 years as the probability of liquefaction in the same time period.

One can go a step further and attempt to quantify the expected damage that might result from a liquefaction event (Class D mapping). Youd and Perkins (1987) introduce the concept of liquefaction severity index (LSI). LSI has a range of 1-100, where 1 indicates very little damage and 100 indicates extensive destruction. They give the following expression for LSI as a function of earthquake magnitude M and distance from the source R:

$$\text{Log(LSI)} = -3.39 - 1.86\log(R) + 0.98M \qquad (3.4)$$

LSI represents the maximum observed or expected severity of ground failure. It is an empirical variable that is derived from ground failure data during past earthquakes. Contour Maps of LSI can be constructed for earthquake events of different return periods, see fig. 3-5.

Budhu et al (1987) use a different method to map liquefaction hazard based on the liquefaction model of Liao (1986) (see Chapter 4). The method assumes the peak ground acceleration at the site to be 0.15g (g=9.81 m/sec^2). SPT values are obtained from borehole data. A class C1 map, fig. 3-6, is produced where liquefaction is :

H if $P_L > 50\%$ (High)

M if $P_L = 10\%$-50% (Moderate)

L if $P_L < 10\%$ (Low)

where P_L is calculated using equation (4.15).

3.5 Conclusion

A liquefaction mapping framework is proposed in this chapter. The different components of the framework are described in detail. Some of the different methods published in the literature and used to produce liquefaction maps are reviewed briefly.

The type of liquefaction maps that one can produce depend very much on the geologic and geotechnical information available. In Chapter 4 we build up on the method presented by Budhu (1987) to produce liquefaction hazard maps. In Chapter 7 we use a method similar to the one presented by Ziony (1976) to produce liquefaction danger maps for areas north of Boston.

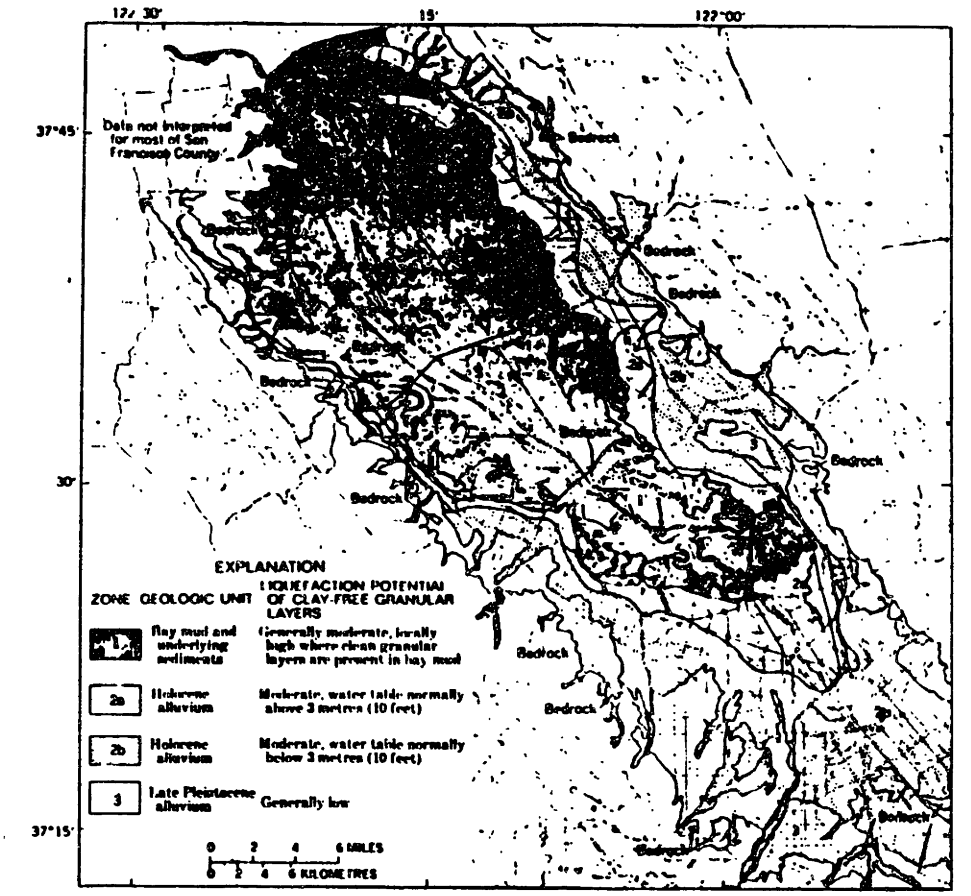

Figure 3-1: Liquefaction Potential from Geologic Conditions (Ziony, 1976)

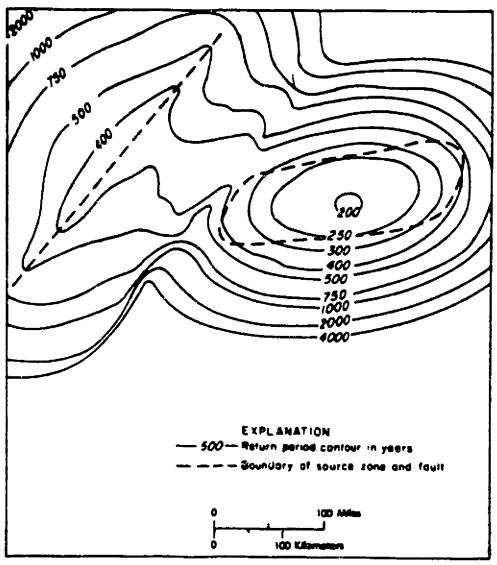

Figure 3-2: Ground Failure Opportunity Map, Youd and Perkins (1978)

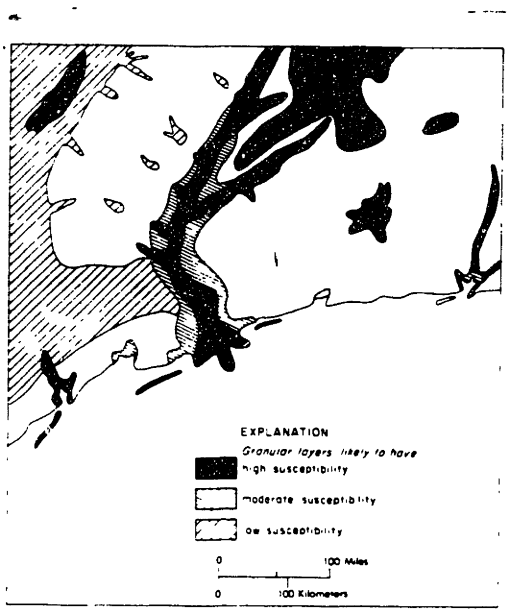

Figure 3-3: Ground Failure Susceptibility Map, Youd and Perkins (1978)

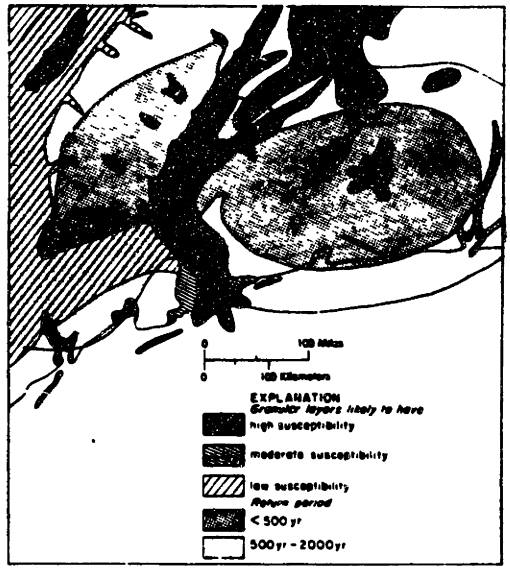

Figure 3-4: Ground Failure Potential Map, Youd and Perkins (1978)

Location (1)	Soil type (2)	Relative density, as a percentage (3)	Effective vertical stress (PSI) (4)	Total vertical stress (PSI) (5)	PROBABILITY OF LIQUEFACTION Return Period, in Years		
					20 (6)	50 (7)	100 (8)
Yerba Buena Cove	SP	81	1.9	4.1	0.01	0.98	1.0
Yerba Buena Cove	SM	60	3.8	8.1	0.01	0.99	1.0
Telegraph Hill	GW	93	3.8	8.1	—	0.14	0.98
North Beach	GW	60	1.9	4.1	—	0.97	1.0
North Beach	SM	70	3.8	8.1	—	1.0	1.0
Mission Bay	SP	81	1.9	4.1	0.01	0.98	1.0
Mission Bay	SM	85	1.9	4.1	—	0.67	1.0
South Beach	GW	64	3.8	8.1	—	0.93	1.0
Dune Sand*	SP	90	13.98	17.5	—	—	0.84

*Water table depth equal to 12 ft. Water table at ground surface for other locations.

Table 3-I: Probability of Initial Liquefaction, Kavazanjian et al (1985)

Geologic unit	Geologic age	Description	Ground-water depth (meters)	Sand or silt layers estimated probability			Relative susceptibility	
				lie below surface (percent)	are liquefiable[2] (percent)	are saturated (percent)	percent[1]	probability
(1)	(2)	(3)	(4)	(5)	(6)	(7)	(8)	(9)
Qm	Holocene	Bay mud	<3	9	73	100	1.8	High[3]
		Below mud	<3	35	33	100		
Qal	Holocene	Stream alluvium	<3	50	42	100	2.1	High
			3-6	50	42	20	0.42	Moderate
			>6	50	42	10	0.21	Moderate
Qs	Holocene	Beach and dune sand	Unmapped	100	42	50	2.1	High
Qyf	Holocene	Alluvial fan (inner)	<3	50	22	100	1.1	High
			3-6	50	22	20	0.22	Moderate
			>6	50	22	10	0.11	Moderate
Qyfo	Holocene	Alluvial fan (outer)	<3	20	22	100	0.44	Moderate
			3-6	20	22	20	0.088	Low
			>6	20	22	10	0.044	Low
Qb	Holocene	Basin deposits	>3	5	22	100	0.1	Moderate
			3-6	5	22	20	0.02	Low
			<6	5	22	10	0.01	Low
Qcl	Holocene	Colluvium	Unmapped	4	10	5	0.008	Very low
Qof	Pleisto-cene	Alluvial fan	<3	25	11	100	0.28	Moderate
			3-6	25	11	20	0.055	Low
			>6	25	5	5	0.006	Very low
Qob	Pleisto-cene	Basin deposit	<3	5	11	100	0.06	Low
			3-6	5	11	20	0.01	Low
			>6	5	5	10	0.003	Very low
Qc	Pleisto-cene	Colma Formation	<3	75	11	100	0.83	Moderate
			3-6	75	11	20	0.17	Moderate
			>6	75	5	10	0.04	Low
Qmt	Pleisto-cene	Marine terrace	Unmapped	25	5	5	0.006	Very low

Table 3-II: Liquefaction Susceptibillity Ratings, Youd and Perkins (1987)

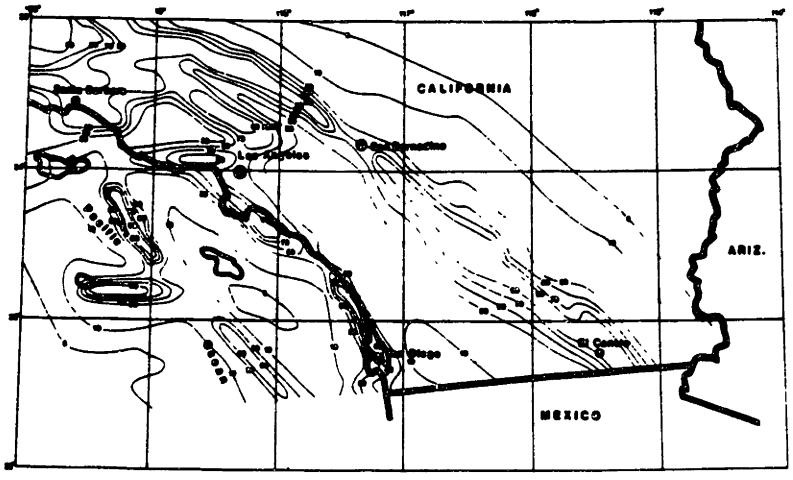

LSI Contours for Southern California with 90% Probability of Nonexceedance in 50 Years or Average Return Period of 500 Years

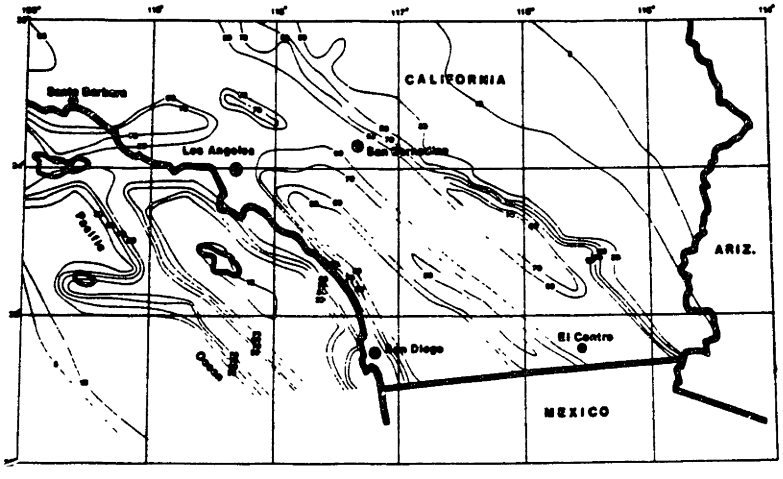

LSI Contours for Southern California with 90% Probability of Nonexceedance in 250 Years or an Average Return Period of 2,500 Years

Figure 3-5: LSI Maps, Youd(1987)

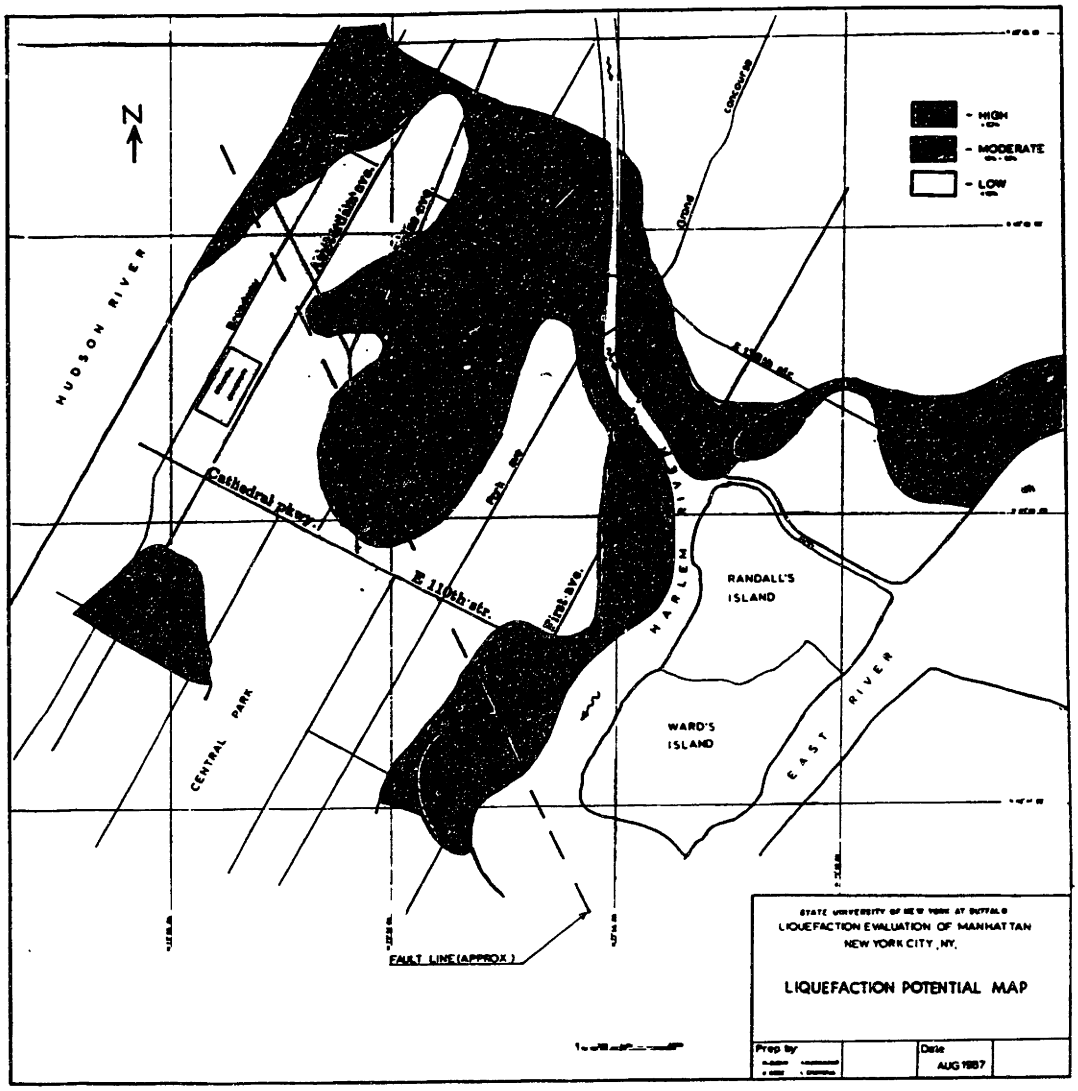

Figure 3-6: Liquefaction Hazard Map, Budha et al (1987)

Chapter 4

LIQUEFACTION HAZARD MAP OF BACKBAY BOSTON, MASSACHUSETTS

4.1 Introduction

The objective of this chapter is to evaluate the liquefaction hazard in the BackBay area of Boston, shown in fig. 4-1.

This area has been chosen mainly because of the availability of extensive standard penetration test (SPT) data. A typical soil profile, fig. 4-2, consists of fill, mostly sand and some gravel, followed by organic silts and clays and then by Boston Blue Clay. While none of the natural deposits is expected to liquefy, it is suspected that the sandy fill is liquefiable. Some portions of the fill have very low blow count numbers.

The SPT values have been analyzed statistically and a procedure has been developed to quantify uncertainty on the SPT number at locations where no SPT data is available. Over a grid of locations in the BackBay area, we have combined the uncertainty on the SPT value N, the recurrence of various peak ground accelerations a, and the conditional probability of liquefaction given N and a to obtain the liquefaction rate, λ_L. The final product of the study is a map of λ_L.

The value of λ_L averaged over the area is $\lambda_L=5\text{x}10^{-4}$ liquefaction events/year. As the SPT data is poorly correlated in space, λ_L converges quickly to the average value as soon as one moves away from the geographical points of the SPT data base.

4.2 BackBay Fill

BackBay was filled over a period of about 100 years, from the early nineteenth century to the late 1920's. A thorough description of the filling process is available in Ty (1987). The depth of the fill layer is between 5ft and 30ft. The fill material consists mainly of sand and gravel transported from Needham and form the Boston Peninsula, but includes also city ashes and refuse and dredged material from the Charles river. Whether this artificial deposit is liquefiable or not is a question that cannot be answered fully. Although the SPT counts are sometimes very low, the presence of gravel, refuse, and ash in the sand might provide drainage paths, and prevent significant pore pressure buildup in the event of an earthquake. Also, the influence of building foundations and other structures on the water table (the presence of water is obviously necessary for liquefaction) is hard to quantify. The depressed Turnpike, the subway tunnels, the sewer mains, the underground basements, ... etc tend to lower the water level. At the same time, water mains and flooded sewers tend to raise the water level. A description of the water level in BackBay can be found in Aldrich (1970,1986).

For the purpose of this study, we assume that the SPT values are the sole indicators of the liquefiability of the fill. Local variations in the water table are largely unknown and ignored.

4.3 Blow Count Records

SPT data are obtained from boreholes drilled for a variety of exploration projects and over a span of several decades. These boreholes can be placed in two major categories: these listed in the BSCE (1969-1970), and these drilled for several construction projects (CP) during the last thirty years.

The BSCE logs include the profile of the soil and the average SPT value for each

layer, but do not report the elevations that correspond to the SPT measurements. The geographical location of the boreholes can be determined with an accuracy of 50-100ft.

The CP data include the soil profile and a detailed record of the SPT tests performed within each layer. Elevations are available for most of the logs, but location accuracy is of the same order as that of the BSCE data.

The accuracy of the SPT values is different in the two data sets. Hence, we did not combine them. Rather, we have used each set for a specific phase of the analysis: the BSCE data has been used to determine general trends and establish preliminary properties of the SPT values in the fill, whereas the CP data has been used to quantify the variability of the SPT values and to calculate the liquefaction recurrence rates.

4.4 Preliminary Analysis of SPT Data

The fill in BackBay consists of four distinct materials (Ty, 1987); city ashes and refuse, gravel from one of the hills of the Boston Peninsula, sand and gravel from Needham, and material from the Charles River (mud). The major part of the fill is sand and gravel, as evidenced by the BSCE borehole logs. The fill material has been transported and dumped by various means: carts, shovels/railway, hydraulic dredging,... over the period from 1814 to 1931. Analysis[3] of the effect of these factors on the BSCE SPT data does not reveal any major influence or trend. For example, we have not been able to relate the lower SPT values to a specific transportation/dumping mechanism or to a particular historical period. However, we have found that city refuse and ash have a relatively high mean blow count number , 13.30 blows/ft, as this material behaves as if it were cemented. Gravel from the Boston Peninsula and sand and gravel from Needham have a mean blow count number of about 10-11 blows/ft. The dredged material from the Charles river has a lower mean blow count number, of about 5.5 blows/ft.

---

[3]Part of this analysis was performed by Raymond Ty.

The city ashes and refuse (mostly cemented) and the dredged silt and clay are not liquefiable materials. On the other hand, the sand is potentially liquefiable.

Based on the above analysis we conclude that the sand and gravel components of the fill are rather "homogeneous" with regard to SPT data. The term "homogeneous" means here that the probability distribution of the SPT value does not depend on geographical location or depth. (This conclusion will be supported later by analysis.) We also conclude that any liquefaction analysis should include only the sand-and-gravel components of the fill, as identified in borehole logs. Therefore, in what follows, we shall use the term "fill" to denote sand-and-gravel material in the fill.

The fill material in many of the CP boreholes is described as "fine sand with some silt and gravel". However, no grain size distribution curve was available at the time of the study to establish the gradation of the material. The analysis that follows is based on the assumption that the fill material is liquefiable. The SPT blow count number is used as the indicator of liquefiability.

4.5 The Data Set

The data base consists of one SPT value for each borehole (CP category), chosen to correspond to the layer with minimum corrected SPT value (The correction procedure will be explained later). The layer should have the description " sand and gravel &... (fill)". This choice is based on the reasoning that, should liquefaction occur, this phenomena would occur first in the layer with minimum corrected SPT.

For many of the boreholes, the SPT values are expressed in blows/6 inches, but for others, the SPT values are given in blows/1 ft; we have multiplied the former by 2 to get comparable data. For each data point we have recorded the borehole location, the depth of the layer at which the minimum corrected SPT was found and the ground surface elevation

at that location. The SPT values are comparable, because they were all obtained using a two-inch split sampler driven by a 140 lb hammer falling 30 inches. Hence, no energy correction for the SPT values was needed. No correction of the SPT values for the weight of rod (WOR) was applied, because the WOR is not typically available.

The data base consists of 280 points (Table 4-I). Figs 4-3 and 4-4 show a map of SPT locations and values. It can be seen that the data is concentrated within certain subareas of BackBay. This condition unfortunately limits our ability to extrapolate the SPT data to distant locations.

For the purpose of analysis we have referenced all elevations to Boston City Base (BCB), which is at about -5.65ft below USC&GS Mean Sea Level of 1929. The locations (X&Y) are based on the coordinate system shown in fig. 4-1.

To obtain a corrected value of the blow count number, to be used in the expression of the liquefaction probability, we have used the formula developed by Liao & Whitman (1985),

$$N_1 = N \sqrt{1/\sigma_{v_{eff}}} \qquad (4.1)$$

where

N = Field Blow Count Number

N_1= Corrected Blow Count Number

$\sigma_{v_{eff}}$ = Vertical Effective Stress in tons/square ft

To calculate the effective vertical (and later total vertical) stress, we have assumed the following unit weights:

Unit weight of dry fill, $\gamma_{fd} = 95$ lb/ft^3

Unit weight of wet fill, $\gamma_{fw} = 110$ lb/ft^3

Hence:

$$\sigma_{v_{tot}} = (Z_s - Z_w)\gamma_{fd} + (Z_w - Z_l)\gamma_{fw} \quad (4.2)$$

$$\sigma_{v_{eff}} = (Z_s - Z_w)\gamma_{fd} + (Z_w - Z_l)(\gamma_{fw} - \gamma_w) \quad (4.3)$$

where

Z_s= ground surface elevation

Z_w= water table elevation

Z_l= layer elevation

For a layer to be liquefiable, it must lie below the water table; hence Z_w cannot be less than Z_l.

Since many borehole logs do not include a record of the water table, we have assumed that the water table is at elevation 7.5 ft (BCB), or at ground level if the ground surface elevation is below 7.5 ft (BCB).

In what follows the minimum corrected SPT value will be referred to as N_1, the associated uncorrected value as N, and the depth to the critical layer (depth to minimum corrected SPT) as D.

4.6 Data Trends

As a first step of the analysis, we have looked for any trend that N or N_1 might have with depth. One might for example expect to see N increase with depth. It is also possible that the fill contains a "weak" layer.

Figure 4-5 shows a plot of the critical depth on the BackBay map. The minimum corrected blow count N_1 occurs at a wide range of depths. Specific regions exhibit some regularity in D, but in the region where the bulk of the data exists, N_1 occurs at a variety of depths. Because of the erraticity of D in figure 4-5, we can make the simplifying assumption that at all locations where the N values are not reported, D has the (marginal)

probability distribution estimated from the entire data set. Figure 4-6 shows a histogram of the critical depth D.

Figure 4-8 shows a plot of the natural logarithm of N_1 versus D. One can see that the points follow a distinct trend (notice the upward curvature). However, a similar plot of N vs. D, fig 4-9, does not show such a trend. This means that N_1 values vary with depth according to the correction factor $\sqrt{1/\sigma_{eff}}$. Fig 4-10 shows a plot of the correction factor versus depth assuming a water table at ground surface and at 7.5 ft below surface. Notice that the correction factors for the various data points do not fit any of the two curves exactly, due to variations in the depth of the water table (see fig. 4-11).

The distribution of N_1 does not show significant regional dependence (i.e. no patches of low or high N_1). This conclusion has been reached by analyzing the data in different subregions.

The logarithms of the N values are fitted well by a normal distribution, with mean m=1.88 and variance σ^2=0.9425; see Figure 4-7. The associated lognormal density of N is:

$$f(N)= \frac{1}{N} \frac{1}{\sqrt{2\pi}0.971} e^{-.5[\frac{\ln(N)-1.88}{0.971}]^2} \qquad (4.4)$$

4.7 Spatial Dependence and Interpolation Procedure

4.7.1 Spatial Correlation

As a second step, we have analyzed the SPT data for spatial dependence (3-Dimensional Analysis). The purpose of this analysis is to derive a correlation function that allows one to estimate N or N_1 at locations away from available boring logs. For the logarithm of N at locations (X1,Y1,Z1) and (X2,Y2,Z2) we have assumed a covariance of the exponential type:

$$cov(1,2)=\sigma^2 e^{-d_{12}/d_o} \tag{4.5}$$

where

$$d_{12}=[(X1-X2)^2+(Y1-Y2)^2+c^2(Z1-Z2)^2] \tag{4.6}$$

is a generalized distance between the two points 1 and 2, σ^2 is the variance of ln(N) and d_0 is the so-called correlation distance. The parameter c in the definition of d is a constant such that in the space of $(X,Y,Z^*=cZ)$, the random field $\ln[N(X,Y,Z^*)]$ is isotropic. It has been often found that, for natural deposits, c has values around 10-30. Lower values may be expected for soil deposits that have been disturbed, as for land fills where the soil has not been deposited in successive layers. Let d_{ij} be the "distance" between the location of the i^{th} and j^{th} measurement of N and denote by $\underline{\underline{\sum}}$ the covariance matrix of the values of ln(N) at the measured points. Therefore, $\underline{\underline{\sum}}$ has $(i,j)^{th}$ coefficient equal to $\sigma^2 \exp\{-d_{ij}/d_0\}$ and the likelihood of c and d_0 given the observations is:

$$l(c,d_0|\ln(\underline{N})) \quad \alpha \quad \frac{1}{det\underline{\underline{\sum}}^{0.5}} \; e^{-0.5[ln(\underline{N})-\underline{m}]^T \underline{\underline{\sum}}^{-1}[ln(\underline{N})-\underline{m}]} \tag{4.7}$$

Where $\ln(\underline{N})$ is the vector of the logarithms of the observed uncorrected SPT values and $\underline{m}$ is a vector with all components equal to the mean value of ln(N). The right hand side of eq. (4.7) depends on c and d_0 through the matrix $\underline{\underline{\sum}}$. In order to estimate c and d_0, we have evaluated the likelihood function in eq. (4.7) for several combinations of these parameters. The results, which are shown in Table 4-II, indicate that the maximum likelihood value of the correlation distance d_0 is about 50 ft and that a reasonable estimate of the depth extension factor c is 10. Although this is not exactly the maximum likelihood value of c, it appears from fig. 4-12 that the likelihood is quite flat for c>10.

Unfortunately, having a correlation distance of 50 ft is an indication that the SPT

values are poorly correlated in space and therefore that estimation of N away from the boring locations is not very accurate.

4.7.2 The Updating Model

Based on the above analysis, one can develop a method to update the distribution of N at any location in BackBay. At points that are far away (more than 100 ft) from the points of the data set, the distribution of N is very close to the marginal distribution and no updating is necessary. At locations that are closer than 100 ft from the points of the data set, the distribution of N is different from the marginal distribution. Updating has been done on a grid of points with 100 ft spacing in both the X and Y directions and at various elevations/depths. Figure 4-13 shows the points where the distribution of N is updated. At each such point where updating is performed, we use as relevant information the values of N for borings within a distance of 100 ft.

4.7.3 Updating Technique

From the likelihood analysis, the covariance between ln(N) at two points A and *i* is:

$$covar(A,i)=\sigma^2\times e^{-d/d_o} \tag{4.8}$$

where

d= generalized distance between A and *i*

d_0= correlation distance (= 50 ft)

σ^2= variance of ln(N) (= 0.94)

Consider the problem of updating the distribution of ln(N) at a point A and suppose that there are r points in the data set within a distance of 100 ft from A. In this case, ln(N) at A has normal distribution, with mean value m_A and variance σ_A given by:

$$m_A = m + \sum_{Ar} \times \sum_{rr}^{-1} \times (\underline{ln(N)} - \underline{m}) \quad (4.9)$$

$$\sigma_A^2 = \sigma^2 - \sum_{Ar} \times \sum_{rr}^{-1} \times \sum_{Ar}^{T} \quad (4.10)$$

where

m = marginal mean of ln(N) (1.88)

σ^2 = marginal variance of ln(N) (0.94)

$\underline{ln(N)}$= column vector whose elements are the natural logarithms of N at the r nearest neighbors of A,

$\underline{m}$= column vector whose elements are all equal to m.

$\sum_{Ar}$= row vector whose elements are covar(A,1), covar(A,2), ...,covar(A,r).

$\sum_{Ar}^{T}$= transpose of the above vector.

$\sum_{rr}^{-1}$= inverse of the covariance matrix of ln(N) at the r nearest neighbor points.

4.7.4 Ground Shaking Recurrence Rate

The recurrence rates of the various peak ground accelerations at the site were obtained through a standard seismic hazard procedure, by combining a seismicity model with an attenuation function. The seismicity model is that estimated by Veneziano and Chouinard (1987) using an earthquake catalogue of the Northeastern U.S. (fig 4-14). According to the model, the frequency of events of epicentral MM intensity I inside a unit area around location $\underline{x}$ is given by:

$$\lambda(\underline{x},I) = \exp(a(\underline{x}) - b(\underline{x})(I - I^*)), \; I < I_1(\underline{x}) \quad (4.11)$$

where I^* is a given intensity, $I_1(\underline{x})$ is the maximum possible MM intensity at location $\underline{x}$, and $a(\underline{x})$ and $b(\underline{x})$ are parameters to be estimated from historical data. Contour plots of $a(\underline{x})$ and $b(\underline{x})$ are shown in fig 4-15.

In order to calculate the hazard function at the site, one needs also an attenuation relationship which estimates peak ground acceleration (PGA) as a function of MM epicentral intensity I and epicentral distance r. For this purpose, we have used a model developed by Heidari(1987), which is:

$$PGA = \exp\{2.00 - 1.14 m_{lg} - 1.03 \ln(R) + \varepsilon\} \quad (4.12)$$

$$m_{lg} = 1 + 0.6 I_o \quad (4.13)$$

R= Hypocentral distance in kilometers for a focal depth of 10 km.

ε= normal random variable with zero mean and standard deviation 0.6

Using these seismicity and attenuation models, the rate at which a given peak ground acceleration PGA is exceeded at the site is calculated through the following integral:

$$\Lambda(PGA) = \int_x \int_I \Lambda(I,\underline{x}) P[>PGA|I,\underline{x}] dx dI \quad (4.14)$$

Figure 4-16 shows a plot of the exceedence rate vs. PGA. For the Boston area it is found that the main contribution to these rates is from sources within 50 km. Earthquake sources farther than 100 km from the site give very low contributions (fig 4-17).

4.7.5 Liquefaction Probability

In order to quantify the probability of liquefaction P_L given the magnitude of the earthquake, the maximum ground acceleration and the normalized corrected SPT value, we use the model developed by Liao(1986) for silty or clean sand (combined model):

$$P_L(a,N_1) = \frac{1}{1+e^{-Q_L}} \quad (4.15)$$

$$Q_L = 10.2 + 4.19 \ln(CSRN) - 0.24 (N_1)_{60} \quad (4.16)$$

$(N_1)_{60}$ = modified corrected SPT value for 60% energy

$= C_N . C_E . N$

C_N= SPT correction factor

C_E= Normalized energy correction
= ER/60.C_{ROD}.C_{LIN}

ER= % of theoretical energy transmitted

C_{ROD}= WOR correction for shallow depths
= 0.75 if d < 10ft

= 1.00 if d >= 10ft

C_{LIN}= 1.0 (Assumed)

C_{LIN} is a function of the inside diameter of SPT (Liner). Since we do not have information about the liners we assume it to be 1.0 (see Liao,1986).

$$CSRN=0.65 \frac{a}{g} \frac{\sigma_{v_{so}}}{\sigma_{v_{eff}}} \frac{r_d}{r_m} \tag{4.17}$$

g = acceleration of gravity, 9.81m/sec^2

r_d=1.0-0.00765d if d<9.15m (30 ft)
=1.174-0.0276d if d>9.15m (30 ft)

d=depth from ground surface in meters

r_m=0.032×M^2–0.631×M+3.934

M=magnitude of earthquake (here set to 6.5)

The magnitude of the earthquake is chosen to be 6.5 because Boston is located relatively far away from earthquake sources in the region. Hence, we need a large enough earthquake to cause liquefaction. Ideally, one should in the analysis integrate over all possible earthquake magnitudes and use their corresponding recurrence rates and PGA values. This would make calculations more complex. We believe that the results are not much affected by setting M=6.5.

One should understand the P_L model is based on actual liquefaction/nonliquefaction

case histories, where liquefaction is manifested in the form of ground failure. Therefore, the present analysis estimates the rate of ground failure not of initial (local) liquefaction.

4.8 Liquefaction Hazard Maps

4.8.1 Liquefaction Rate at the Points of the Data Set

At the points where N_1 is known, the liquefaction rate is calculated as:

$$\lambda_l=\sum_a \lambda(a)P_L(a,N_1) \tag{4.18}$$

Results are shown in figures 4-18 and 4-19(a,b). Note that some of the rates are very small ,less than $1x10^{-4}$/year, whereas others are as high as $3x10^{-3}$/year. The average rate is $5.4x10^{-4}$/year. Figure 4-20 shows the cumulative distribution of the liquefaction rate. For example, 80% of the sites have a liquefaction rate less than 10^{-3}/year.

4.8.2 Updated Liquefaction Rates

At a site (X,Y) where SPT data are not directly available, the liquefaction rate has been found as follows. Suppose first that the critical depth D is known. Then the liquefaction rate $\lambda_L(X,Y,D)$ can be found from:

$$\lambda_L(X,Y,D)=\sum_a \sum_N \lambda(a)\times P_L(a,N_1)\times P(N|D,X,Y) \tag{4.19}$$

where P(N|D,X,Y) is the probability of N derived from the SPT count updating procedure described earlier and N_1 is the corrected SPT value that corresponds to N. For calculation of the liquefaction rate $\lambda_L(X,Y)$ with D not specified, one must take expectation with respect to D,

$$\lambda_L(X,Y)=\sum_D\sum_a\sum_N \lambda(a)\times P_L(a,N_1)\times P(D)\times P(N|D,X,Y) \tag{4.20}$$

where P(D) is the probability that D the critical depth.

Two estimates of $\lambda_L(X,Y)$ have been made using eq. (4.20), by making different assumptions on the surface elevation and on water depth. In both cases we have limited the summation over depth to Z=-5 ft(B.C.B.) because on the average the fill in BackBay does not extend below that elevation. The ground surface elevation at the updated sites is assumed to be the average ground surface elevation of the nearby points. Also, in both cases, a 'generic site' is assumed to represent the sites at which updating of the distribution of N is not made.

The main difference between the two estimates is the elevation of the water table. In the first analysis we assume that the water table has a fixed elevation. In the second analysis, we assume that the water table is at a fixed depth below ground surface. We believe that these assumptions about the water table position represent extreme opposite cases with respect to the water table elevation.

First Analysis

In this case the water table is assumed to be at elevation Z=+7.5 ft (BCB) and the surface elevation for the generic site is fixed at +15 ft (BCB). Figure 4-21 shows the associated map of the liquefaction rate. All points in the white area have a liquefaction rate of $\lambda_L=5.3\text{x}10^{-4}$/year, which is the rate calculated for the generic site. Figure 4-22 shows a contour plot of the liquefaction rates, at $1\text{x}10^{-4}$/year intervals. The actual value of λ_L on the contours can be determined through comparison with fig. 4-21. Notice that there are sites which have rather high rates. These rates correspond to locations where the ground surface

elevation is lower than 7.5 ft (BCB); at such sites, the present analysis assumes that the water table is at the ground surface.

Figure 4-23 shows the probability of having λ_L below a certain value at the generic site. The curve is similar to the one obtained from the sites where SPT values are available. However, the curve in fig. 4-23 has a slightly different interpretation: for example, fig. 4-23 indicates that there is 80% probability that the generic site will liquefy about once every 1000 years.

Second Analysis

In this analysis, the water table is assumed to be at a depth of 7.5 ft. below ground surface, on condition that water level cannot be below Z=0.0 ft BCB for locations where the ground surface is below 7.5ft BCB. The depth range over which the rates are integrated is from 7.5 ft. to 31 ft. below ground surface. The results are shown in fig. 4-24 in the from of a liquefaction rate map. The white area has a liquefaction rate of $\lambda_L=6.2\text{x}10^{-4}$/year, which is the value calculated for the generic site. Figure 4-25 shows a contour plot of the liquefaction rates, at $1\text{x}10^{-4}$/year intervals. The rates in fig. 4-24 are rather uniform and do not show the extreme values of solution 1. This is because, in the present analysis, the ground water level is several feet below ground surface at all locations.

Figure 4-26 is analogous to fig. 4-23 and for example indicates that there is 75% probability that the generic site liquefies once every 1000 years.

4.9 Discussion

The results form the two analysis are quite similar. In both cases the model looses "information" quickly as one moves away from points of the data set. This is due to weak spatial correlation of the data. The assumption about the marginal probability distribution of the critical depth D is not entirely correct. Problems that might be encountered using this assumption are described in Chapter 5.

4.10 Conclusions

The above analysis of the liquefaction recurrence rates in the BackBay area of Boston leads us to the following conclusions:

1- On average, the area has a liquefaction recurrence rate of $5\text{-}6 \times 10^{-4}$ liquefaction events /year. (This is the rate of liquefaction at a generic point in the area, not the rate of liquefaction events anywhere in BackBay.)

2- The SPT data has low spatial correlation. In particular, it is difficult to predict N_1 using standard penetration test data at a distance greater than about 50 ft.

For this reason, in order to accurately evaluate the liquefaction rate at a specific site in BackBay, it is recommended that local site investigations be performed. Studies at nearby sites should be used only as an index guide, not a basis for decision making.

NUMBER OF DATA POINTS: 280				BLOWS/FT	
X (FT)	Y (FT)	Z (FT) (BCB)	DEPTH (FT)	LB(SPT) UNCORRECTED	LB(SPT) CORRECTED
6476.10	5989.00	-5.9	20.3	1.386	1.649
6295.10	5674.50	6.3	10.3	2.079	2.518
4347.00	5764.00	-2.1	18.3	2.773	3.045
4453.00	5649.00	-1.9	17.8	0.693	0.993
4425.00	5600.00	1.0	16.8	2.890	3.161
4409.40	5728.00	0.1	15.3	3.091	3.437
4323.50	5724.00	-0.1	16.8	3.466	3.759
5300.00	1300.00	6.5	5.5	2.708	3.475
5300.00	1200.00	-0.4	12.4	2.197	2.701
5300.00	1500.00	1.0	11.0	1.386	1.932
5208.00	1400.00	6.5	5.5	2.197	2.965
5408.00	1400.00	5.0	7.0	3.045	3.742
5500.00	1400.00	4.0	8.0	2.565	3.219
5750.00	2287.00	5.0	15.8	0.693	0.916
5650.00	2300.00	6.8	14.8	1.792	2.028
5933.30	4933.30	6.8	11.3	1.386	1.758
6076.00	4867.00	-3.3	21.3	2.639	2.827
6133.00	4733.00	-0.8	18.8	1.386	1.609
6267.00	4667.00	-6.3	24.3	3.258	3.401
6333.00	4533.00	2.3	15.8	3.332	3.616
6467.00	4467.00	-3.5	21.5	3.401	3.566
5867.00	4867.00	-7.8	25.8	3.332	3.456
5933.00	4733.00	1.8	16.3	0.693	0.956
6067.00	4667.00	2.3	15.8	2.639	2.923
6133.00	4533.00	6.8	11.3	1.386	1.758
6267.00	4467.00	2.8	15.3	2.303	2.595
6333.00	4333.00	1.8	16.3	0.693	0.956
5833.30	4667.00	5.8	9.3	1.386	1.902
5078.00	5326.00	4.8	11.8	0.693	1.099
5072.30	5273.60	1.3	17.3	0.693	0.956
5100.00	5256.00	-3.3	21.8	2.079	2.251
4852.00	2789.00	1.9	15.3	1.792	2.104
4828.00	2848.00	5.1	5.3	1.792	2.660
4862.00	2783.00	3.6	5.1	2.639	3.614
4953.00	2861.00	-0.4	11.3	1.792	2.370
2299.00	6272.00	2.0	13.0	2.079	2.485
2298.00	6274.00	2.5	12.5	1.945	2.370
2118.00	6660.00	4.0	11.0	2.079	2.542
2046.00	6584.00	3.5	11.5	2.639	3.086
2108.00	6312.00	5.5	9.5	2.303	2.803
2142.00	6124.00	4.0	11.0	2.079	2.542
2631.00	6497.00	-1.1	30.3	2.485	2.425
2345.00	6763.00	-0.1	4.3	3.912	4.605
2442.00	6655.00	-1.7	6.3	2.639	3.332
2539.00	6564.00	-0.3	4.3	1.386	2.079
2162.00	6825.00	-0.6	4.8	0.693	1.386
2250.00	6887.00	-3.4	7.8	0.693	1.856
2020.00	6990.00	2.8	13.8	0.693	1.030
2383.00	6807.00	2.3	7.3	1.386	2.186
2010.00	7000.00	4.2	11.0	2.079	2.534
2033.00	6995.00	2.9	21.3	1.792	1.887
2086.00	6964.00	4.0	20.3	2.303	2.416
2030.00	7000.00	-0.8	5.8	2.303	3.645
2161.00	7019.00	-0.9	5.8	2.079	3.437
2040.00	7000.00	0.7	7.3	0.693	1.589
2050.00	7000.00	-3.3	10.3	3.689	4.473
2050.00	6990.00	2.1	10.3	1.386	1.946
2050.00	6992.00	0.1	14.5	1.792	2.175
2360.00	6169.00	-0.2	21.3	2.079	2.219
2242.00	6165.00	4.6	9.3	3.178	3.723
2151.00	6143.00	7.5	10.5	4.220	4.617
2341.00	5953.00	7.4	10.3	0.693	1.099
2191.00	6046.00	3.3	15.3	3.332	3.616
8300.00	6600.00	4.3	5.8	2.639	3.503
8300.00	6525.00	-0.8	10.8	2.890	3.517
6193.00	5664.00	3.3	16.3	0.693	0.956
6024.00	5675.00	0.1	12.8	0.693	1.194
6147.00	5646.00	4.5	16.5	0.000	0.182
6213.00	5607.00	-3.3	24.3	0.693	0.788
6103.00	5746.00	-1.3	20.8	0.693	0.875
6000.00	3400.00	0.8	15.3	2.079	2.416
5667.00	5267.00	-1.8	20.8	2.079	2.262
3067.00	4800.00	6.1	11.8	2.079	2.451
5056.00	4727.00	1.1	15.3	1.792	2.116
4986.00	4771.00	0.6	16.7	4.078	4.357
4927.00	4676.00	1.8	15.7	0.693	0.993
4897.00	4629.00	1.8	15.5	2.996	3.300
4882.00	4773.00	0.9	15.8	3.178	3.487
4891.00	4724.00	7.3	9.9	3.219	3.645
4822.00	4677.00	1.8	15.4	2.773	3.077
4756.00	4718.00	1.2	16.0	2.398	2.695
4986.00	4846.00	1.1	15.3	1.792	2.116
4960.00	4813.00	-5.7	22.7	2.485	2.667
4958.00	4726.00	2.1	15.1	3.714	4.027
3317.00	5577.00	5.8	4.6	3.526	4.220
3372.00	5531.00	0.9	9.5	2.485	3.144
3371.00	5503.00	2.1	9.3	2.639	3.270
3169.00	5469.00	-1.0	12.8	2.303	2.803
3230.00	5430.00	3.3	9.5	3.178	3.752
3292.00	5402.00	5.2	7.0	3.638	4.325
3303.00	5368.00	5.0	10.4	2.773	3.239
3265.00	5335.00	-1.3	16.8	2.485	2.797
3364.00	5312.00	2.5	16.0	1.792	2.067
3164.00	5319.00	2.0	16.4	1.792	2.054
6847.00	5964.00	3.3	13.3	0.693	1.065
6922.00	3939.00	3.0	13.8	0.693	1.030
6943.00	3926.00	3.9	13.0	0.000	0.336
6767.00	3959.00	4.8	11.3	0.693	1.131
6884.00	3911.00	6.0	10.8	1.386	1.808
6856.00	3942.00	5.1	11.8	1.386	1.775
6767.00	3960.00	2.6	13.8	2.639	2.996
6818.00	3964.00	6.4	10.3	0.693	1.131
6806.00	4024.00	4.9	10.3	2.639	3.114
6970.00	3941.00	5.5	11.3	0.693	1.099
6797.00	3929.00	5.5	10.8	3.332	3.766
5400.00	4670.00	6.8	13.3	0.693	0.993
5410.00	4670.00	0.5	19.5	0.000	0.182
5420.00	4670.00	6.3	13.8	0.693	0.993
5440.00	4670.00	7.8	12.3	0.693	1.030
5450.00	4670.00	4.8	15.3	1.792	2.054
5460.00	4670.00	1.0	19.0	0.000	0.182
5470.00	4670.00	7.3	12.8	0.693	0.993
5500.00	4670.00	5.3	14.8	0.693	0.956
5400.00	4680.00	5.8	14.3	0.693	0.956
4700.00	4700.00	4.8	15.3	1.386	1.649
5400.00	4720.00	3.3	16.8	0.693	0.916
5200.00	4500.00	5.8	14.3	0.693	0.956

Table 4-Ia: BackBay Data Base

5210.00	4510.00	4.8	15.3	1.386	1.649
5240.00	4540.00	3.8	16.3	1.386	1.629
5270.00	4570.00	6.1	13.8	1.792	2.079
5280.00	4580.00	4.8	15.3	0.693	1.548
3773.00	4102.00	7.4	10.3	2.303	2.715
3985.00	4113.00	3.1	15.3	3.091	3.378
3875.00	4192.50	1.9	10.8	1.792	2.322
4057.00	4020.00	2.4	16.3	1.792	2.054
3775.00	4270.00	3.1	15.3	1.792	2.079
3810.00	4097.00	-0.1	13.8	0.693	1.099
3766.00	4018.00	-6.8	23.3	0.693	0.875
3944.00	4021.00	6.2	11.8	2.485	2.851
3915.00	4247.00	7.0	10.3	2.079	2.501
4043.00	4168.00	2.0	16.3	2.303	2.573
5264.00	4976.00	-9.3	26.8	1.386	1.504
5729.50	4707.00	-3.6	21.8	0.693	0.875
5443.00	4725.00	7.4	6.8	2.303	2.923
5134.50	4770.00	0.5	16.8	1.386	1.668
5614.00	4476.00	0.9	17.8	0.000	0.262
5700.00	4500.00	5.9	11.8	1.386	1.758
5500.00	4400.00	-9.1	26.3	0.000	0.095
5302.00	5040.00	-10.8	28.3	0.000	0.095
5760.00	4773.00	1.3	16.8	1.386	1.649
5800.00	4700.00	-9.3	27.3	0.693	0.788
5600.00	4650.00	6.1	11.3	2.890	3.285
5700.00	4750.00	-1.6	18.8	0.693	0.956
5061.00	4735.50	-4.1	21.3	2.079	2.282
5587.00	4437.00	1.1	17.8	1.386	1.609
5500.00	4500.00	-11.0	30.8	1.386	1.411
5361.00	4920.00	0.5	17.3	0.693	0.956
5459.00	4869.00	-4.0	21.8	2.079	2.262
5558.00	4819.00	-4.1	21.8	1.792	1.974
5650.00	4755.00	1.1	16.8	2.079	2.351
5195.00	4868.00	-6.3	23.3	0.693	0.875
5224.00	4794.00	1.4	13.0	0.000	0.405
5564.00	4649.00	4.3	11.3	1.386	1.825
5675.00	4583.00	6.5	11.3	1.386	1.775
5228.00	4702.50	1.1	16.3	0.693	0.993
5331.00	4641.00	0.3	17.5	0.000	0.262
5416.50	4589.00	-3.8	21.8	0.693	0.875
5915.00	4530.00	7.0	11.3	1.792	2.163
3338.00	6344.00	4.6	10.3	0.693	1.163
3445.50	6281.00	4.1	10.3	2.303	2.803
3277.50	6242.00	6.5	14.8	1.792	2.028
3385.00	6178.50	5.0	14.8	0.693	0.956
3306.30	6414.00	4.3	4.3	2.773	3.466
2765.00	6312.00	-1.1	30.3	2.485	2.425
2835.00	6190.50	6.5	24.3	4.060	4.048
2847.00	6070.00	1.6	24.3	4.500	4.542
2513.00	5889.00	3.3	10.8	3.091	3.586
2405.00	6075.00	5.9	6.3	2.079	2.803
4699.00	4148.00	6.6	1.8	1.386	2.079
4640.00	4228.00	3.8	5.3	1.792	2.754
4584.00	4318.00	7.4	1.8	1.792	2.485
4512.00	4479.00	7.4	1.3	2.773	3.466
4697.50	4307.00	3.5	15.3	2.485	2.766
4610.50	4661.00	-10.*	25.3	2.485	2.588
4597.00	4629.00	1.0	16.3	2.890	3.182
4530.00	4639.00	-0.9	15.3	2.890	3.258
4573.00	4605.00	7.1	5.3	2.485	3.250
4586.00	4657.00	5.0	11.3	1.792	2.208
4643.00	4616.00	-4.9	20.8	1.792	2.028
4623.00	4534.00	5.6	10.3	2.996	3.453
4670.00	4438.00	-2.3	20.3	2.079	2.303
4730.00	4352.00	-4.3	20.3	2.639	2.827
4801.00	4248.00	-0.3	16.3	1.792	2.015
4844.00	4340.00	-3.4	20.8	2.079	2.282
5205.00	3361.00	-0.1	5.8	2.485	3.721
4792.00	3801.00	2.0	20.8	1.386	1.504
1957.00	4529.00	4.7	4.3	2.485	3.178
5095.00	3457.00	-1.8	25.8	2.079	2.128
5075.00	3500.00	-5.4	30.5	1.386	1.361
4688.50	3872.00	-2.4	26.3	0.693	0.742
4680.00	3957.00	4.9	20.3	2.485	2.588
4562.00	4077.00	5.0	20.8	2.303	2.389
4439.00	4178.00	5.5	21.3	2.773	2.681
4321.50	4269.00	6.3	20.3	1.792	1.872
4202.00	4326.00	0.6	25.8	2.303	2.322
4205.00	4541.00	2.4	10.3	2.303	2.056
4045.00	4541.00	7.3	5.3	4.431	5.183
3731.50	4454.00	1.4	16.3	2.079	2.361
4051.00	4546.00	7.2	5.3	0.693	1.065
3589.00	4471.00	2.0	11.3	2.079	2.580
3342.00	4563.00	5.0	6.3	0.693	1.253
3045.00	4584.00	5.4	6.3	0.693	1.459
2665.00	4485.00	6.1	21.8	2.303	2.370
2627.50	4614.00	-9.0	36.3	2.485	2.389
2385.00	4588.00	7.3	10.3	2.079	2.361
2137.00	4592.00	-5.3	22.3	0.693	0.875
1878.00	4598.00	4.9	11.3	1.792	2.104
1611.00	4612.00	0.6	15.8	1.792	2.104
1325.00	4528.00	6.1	25.3	2.890	2.815
1326.00	4674.00	-1.1	30.3	2.079	2.028
1168.00	4527.00	-0.1	14.8	2.079	2.451
1169.00	4625.00	0.4	11.8	2.996	3.515
4971.00	3590.00	0.5	11.3	1.386	1.932
4602.00	3948.00	1.6	21.3	1.386	1.504
4603.00	3995.00	-0.2	25.3	1.792	1.825
4579.00	4157.00	3.2	5.3	2.773	3.777
4497.00	4242.00	2.8	6.3	1.386	2.272
4426.00	4306.00	2.4	6.8	0.693	1.548
4337.00	4377.00	-2.6	11.8	2.639	3.258
4248.50	4432.00	3.2	6.3	1.386	2.251
4176.00	4460.00	3.1	6.3	0.693	1.569
4123.00	4369.00	-1.5	21.8	3.258	3.411
3923.00	4513.00	7.2	2.3	4.094	4.787
3788.00	4486.00	2.7	6.8	2.303	3.135
3356.00	4460.50	1.4	11.3	1.792	2.313
3171.00	4566.00	4.8	6.3	1.386	2.163
3090.00	4468.00	1.6	11.3	1.386	1.982
2905.00	4584.00	0.7	16.8	0.693	0.956
2780.00	4576.00	-1.8	12.8	1.386	1.917
2707.00	4472.00	2.3	16.8	1.792	2.041
2654.00	4577.00	2.5	26.3	1.792	1.775
2592.00	4401.00	-1.3	26.3	2.303	2.332
2516.00	4588.00	1.8	11.3	0.693	1.194
2392.00	4498.00	4.1	13.3	0.693	1.030
2248.00	4604.50	5.5	[illegible]0	1.386	2.175
2174.50	4499.00	3.6	10.8	0.693	1.163
1986.70	4599.60	-4.4	16.0	0.000	0.405
1776.00	4527.00	5.3	9.3	1.386	1.902
1747.00	4627.00	3.1	11.3	0.693	1.163
1531.00	4514.00	2.7	11.3	2.303	2.785
1407.00	4625.00	5.3	25.8	3.466	3.391
1392.00	4654.00	-0.9	30.3	2.639	2.580
1388.00	4511.00	5.2	25.3	2.079	2.054
1267.00	4619.00	2.5	10.3	1.792	2.342
1057.00	4644.00	-16.4	29.3	1.386	1.526
5285.00	3265.50	2.0	4.3	2.996	3.761
5145.00	3487.00	3.1	2.3	1.792	3.144
5081.50	3569.00	-0.3	5.3	2.773	3.466
4940.00	3761.00	-0.3	6.3	1.386	2.526
4863.00	3850.00	1.0	5.8	1.386	2.501
4628.00	4044.00	0.4	6.3	3.401	4.475
3908.00	4463.00	2.2	5.8	4.025	5.031
3439.00	4502.00	6.5	1.8	3.258	4.168
3273.00	4508.00	6.1	2.3	2.079	3.016
3059.00	4514.00	2.5	6.3	2.773	3.684
2723.00	4524.00	2.6	6.3	0.693	1.589
2463.00	4532.00	-1.9	11.3	2.079	2.708
2267.00	4537.00	3.1	6.8	1.792	2.603
2107.00	4542.00	3.4	6.8	3.178	3.976
1851.00	4550.00	5.6	5.3	2.890	3.733
1666.00	4555.00	4.4	6.8	1.792	2.542
1478.00	4562.00	5.9	5.8	3.951	4.724
1315.00	4566.00	1.1	11.3	2.079	2.612
1062.00	4573.00	2.8	11.0	2.773	3.246
1297.00	4278.00	2.9	20.8	0.693	0.788
1849.00	4857.00	2.3	14.8	0.693	1.030
1825.00	4250.00	2.9	15.3	2.079	2.370
2370.00	4846.00	5.5	11.3	2.303	2.708
2345.00	4262.00	-3.0	20.8	1.386	1.589
2894.40	4833.00	0.9	16.3	2.079	2.370
2666.00	4233.00	6.5	11.3	2.079	2.468
3427.00	4819.00	0.6	16.3	0.693	0.993
3642.00	4442.00	-4.9	19.3	2.639	2.929
3298.50	4413.00	6.0	5.3	2.303	2.701
3190.00	4433.00	-4.4	21.3	2.303	2.510
1320.00	4877.00	2.9	21.3	2.485	2.588
3053.00	4573.00	1.1	10.8	0.693	1.253
3731.00	4465.00	7.3	10.3	2.079	2.493
3728.00	4437.00	1.7	15.8	1.386	1.686
4557.00	3952.30	-4.1	26.3	1.386	1.459
0000.00	0000.00	0.0	00.00	0.000	0.000

Table 4-Ib: BackBay Data Base

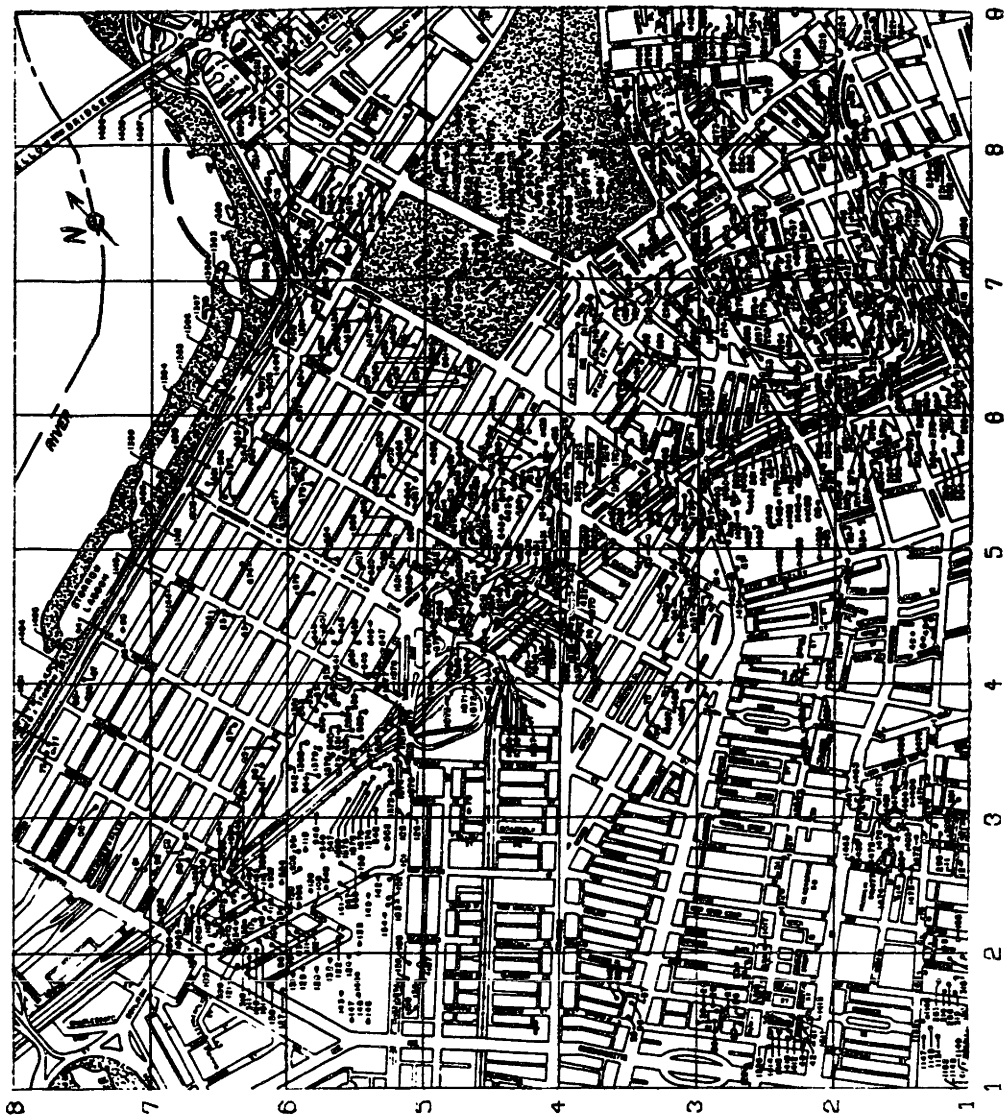

Figure 4-1: Geographical Setting of BackBay

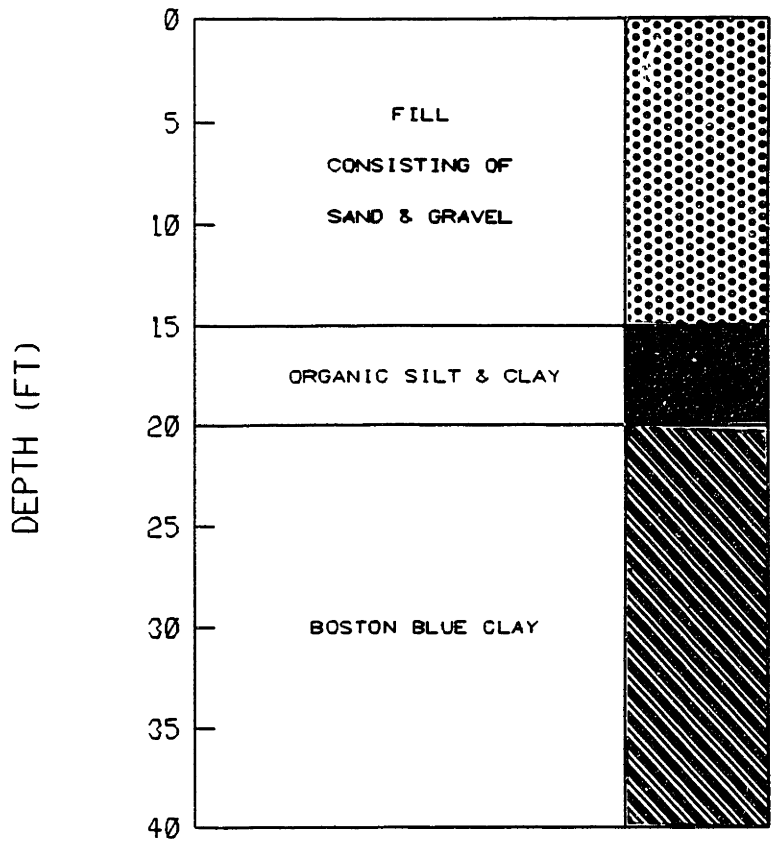

Figure 4-2: Geologic Profile, BackBay

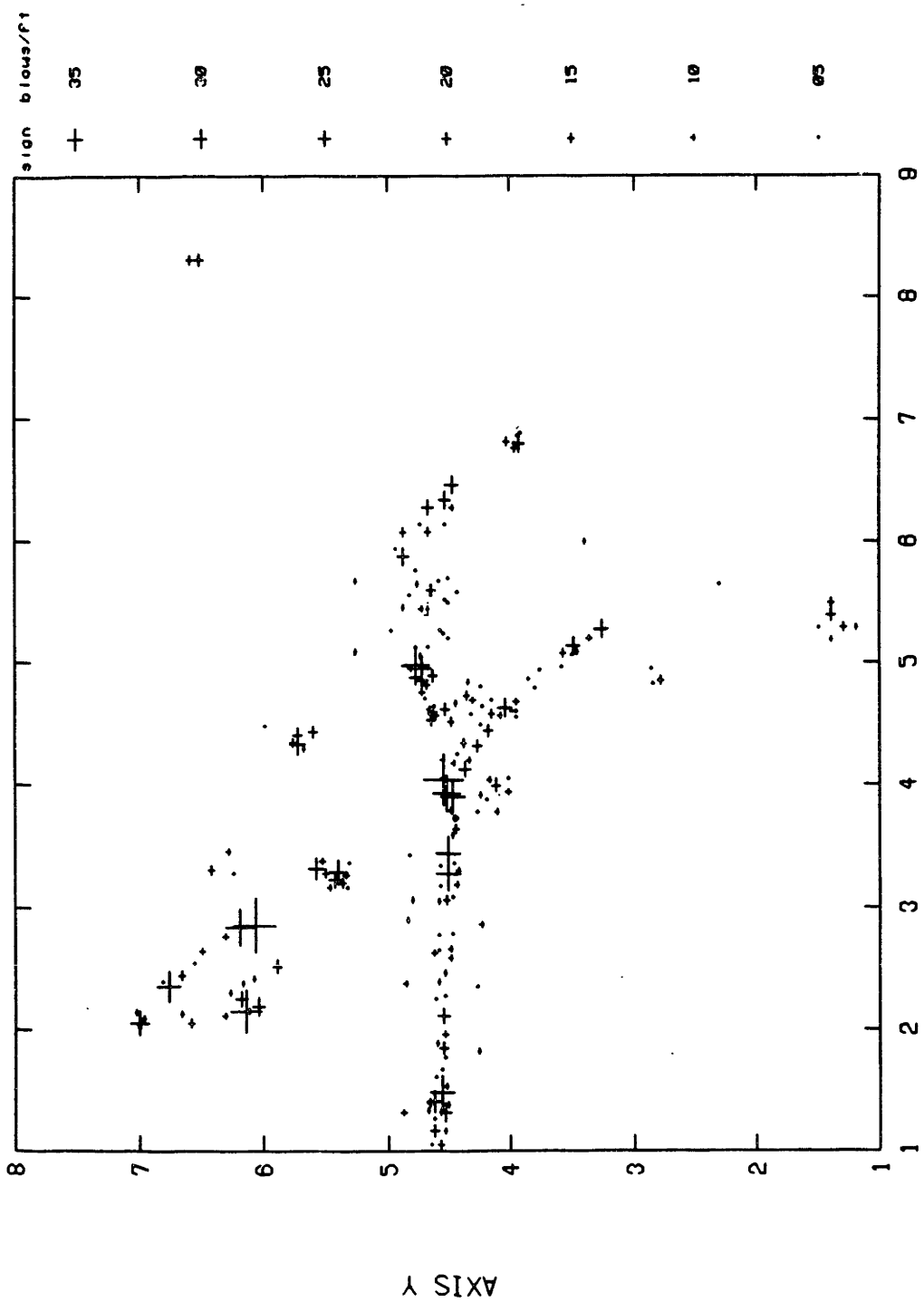

Figure 4-3: Map of Uncorrected Blow Count Data

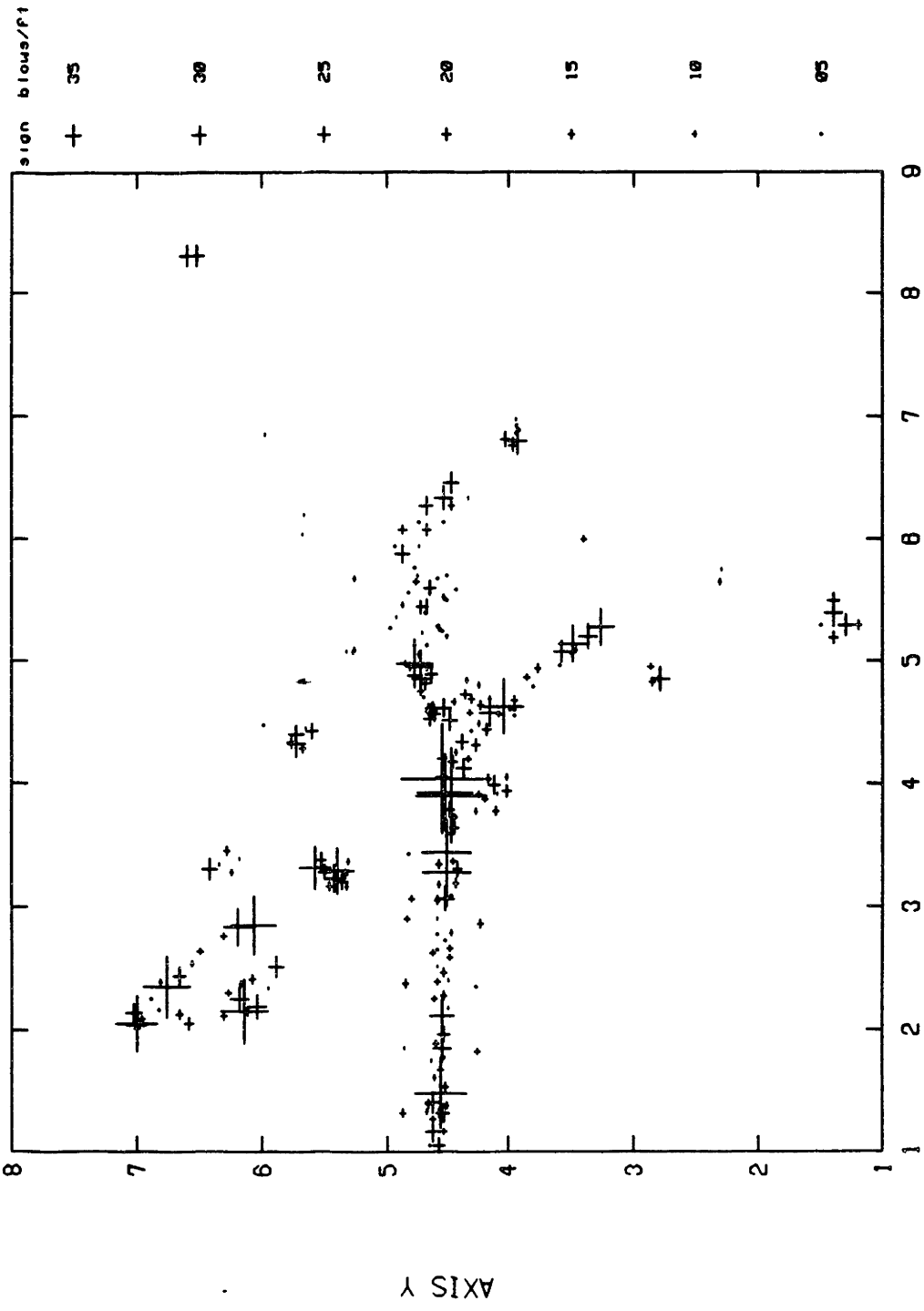

Figure 4-4: Map of Corrected Blow Count Data

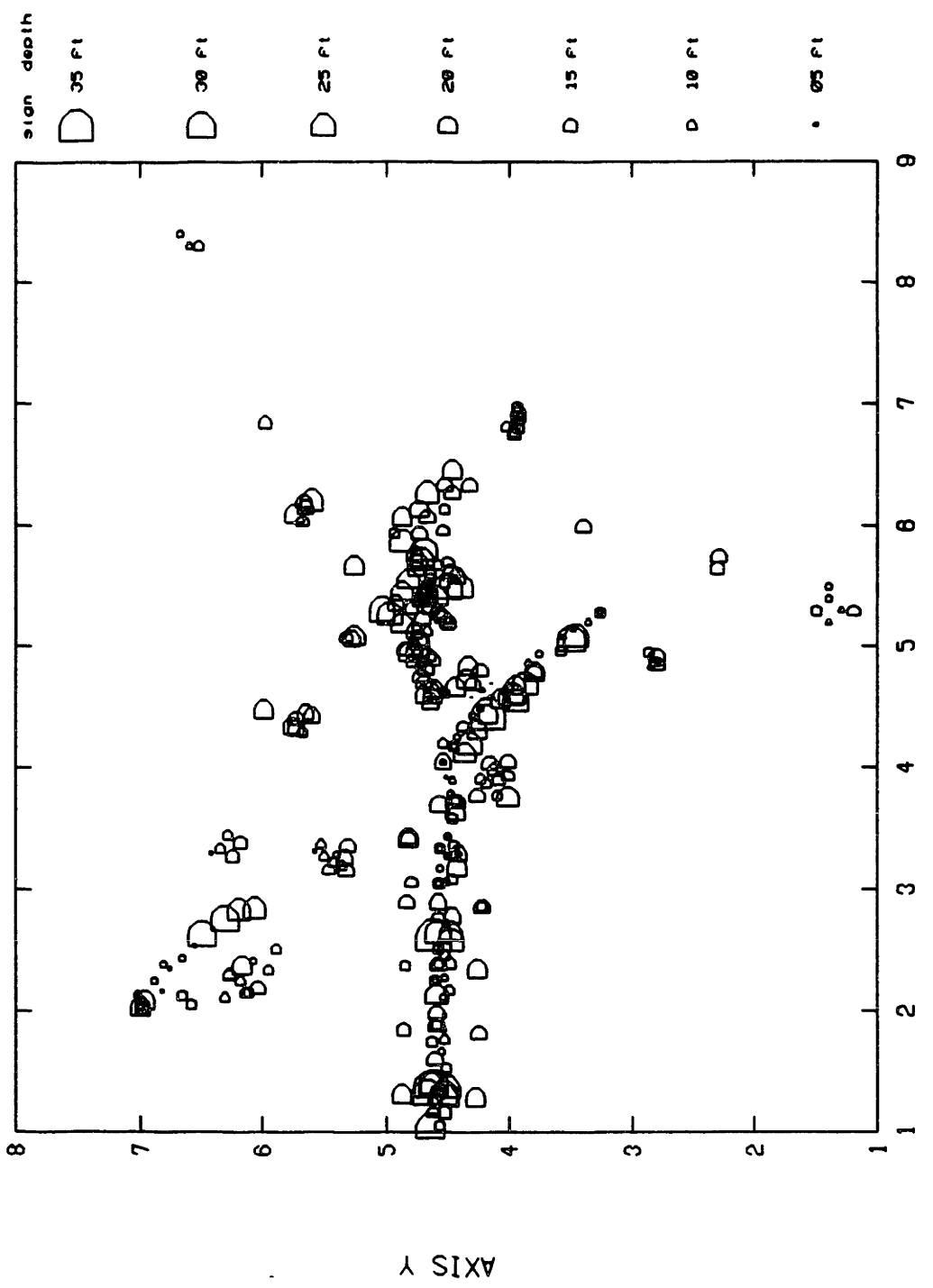

Figure 4-5: Map of Critical Depth

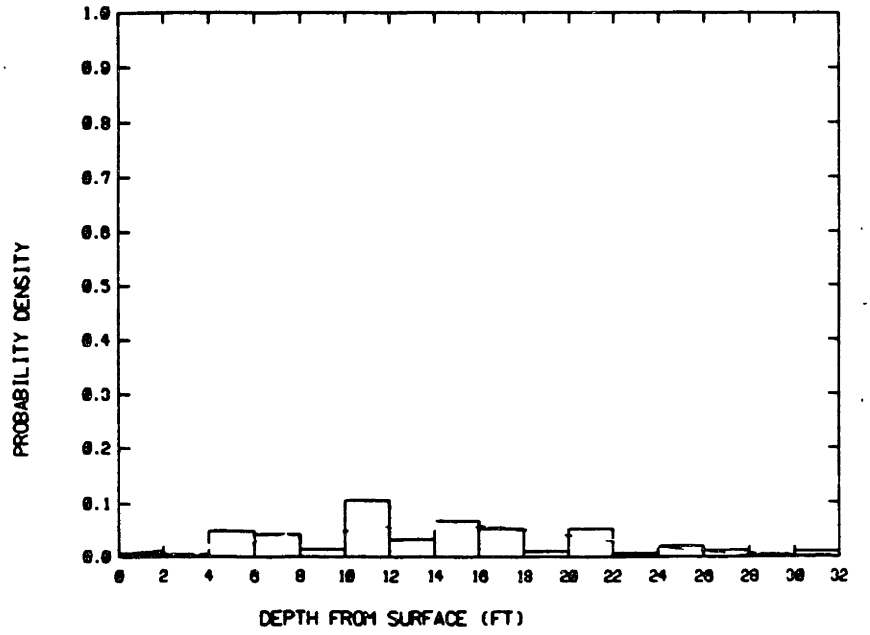

Figure 4-6: Histogram of Critical Depth

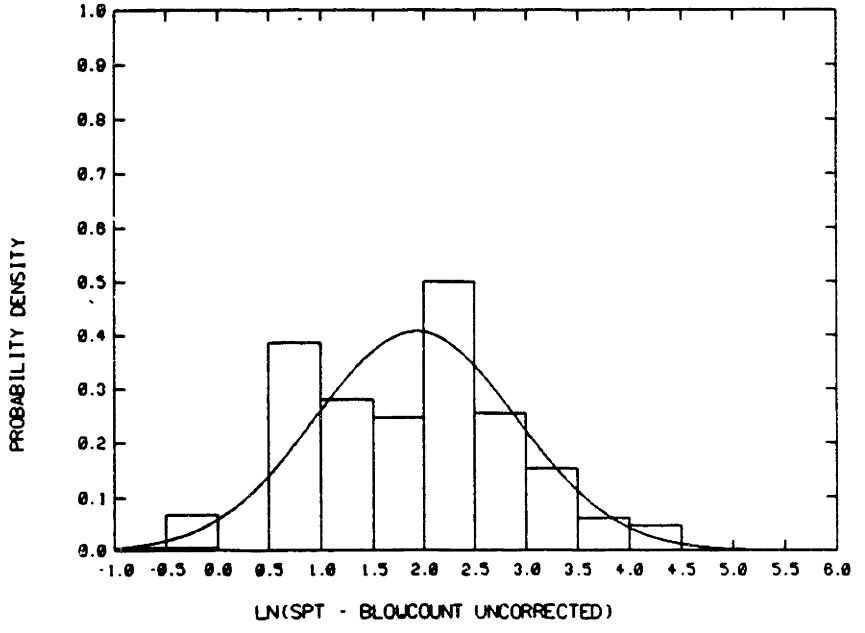

Figure 4-7: Distribution of ln(N)

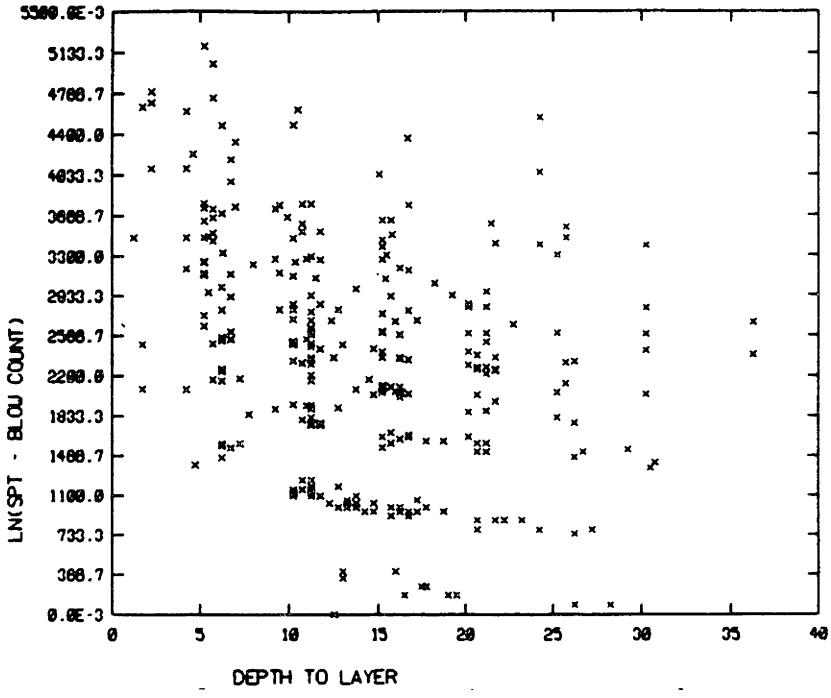

Figure 4-8: $\ln(N_1)$ vs. Critical Depth

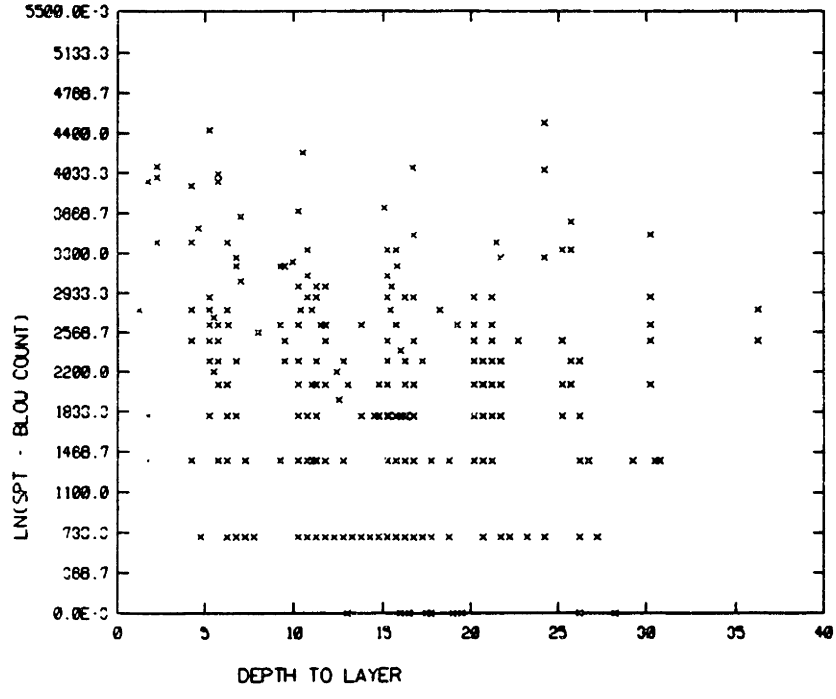

Figure 4-9: ln(N) vs. Critical Depth

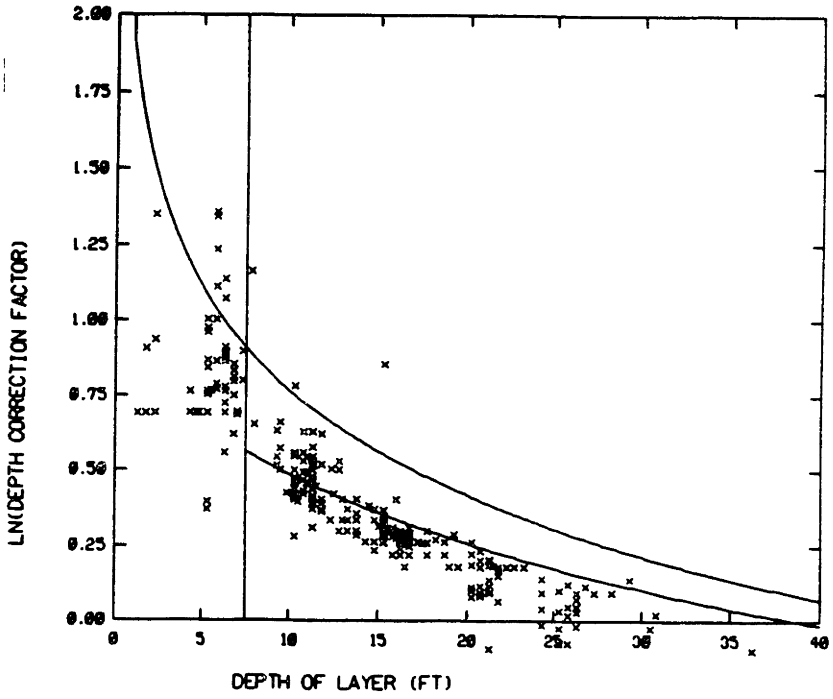

Figure 4-10: ln(Depth correction Factor) vs. Critical Depth

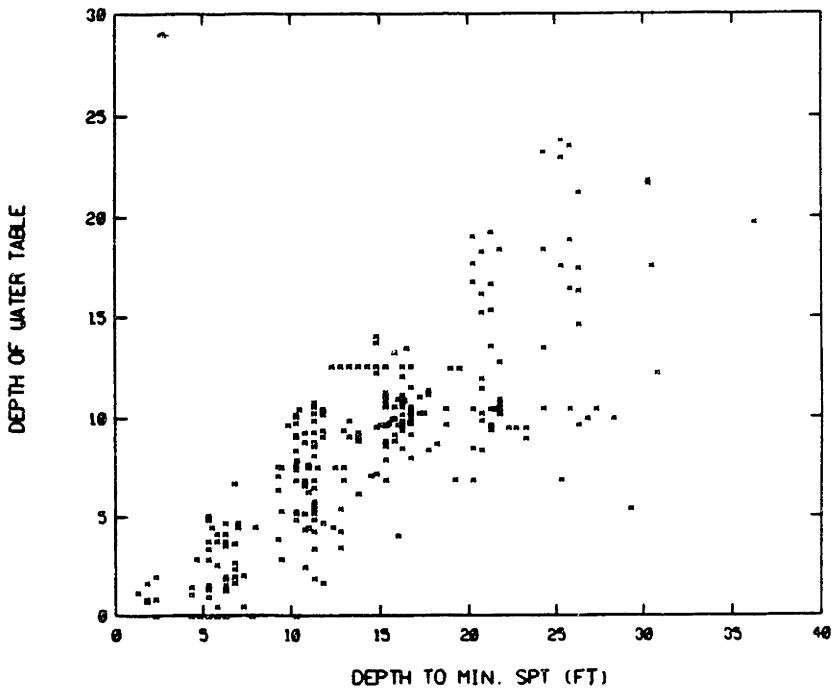

Figure 4-11: Depth of Water Table vs. Critical Depth

DEPTH EXTENSION FACTOR	CORRELATION DISTANCE (FT) 10	30	50	70	90
0	-138.093	-157.690	-184.129	-216.654	-253.436
2	-131.288	-132.407	-139.613	-152.757	-170.123
4	-130.288	-127.907	-130.167	-138.201	-150.332
6	-130.884	-126.509	-126.332	-131.728	-141.141
8	-130.976	-126.124	-124.476	-128.149	-135.764
10	-131.082	-126.190	-123.626	-126.084	-132.406

Table 4-II: Values of the Likelihood Function

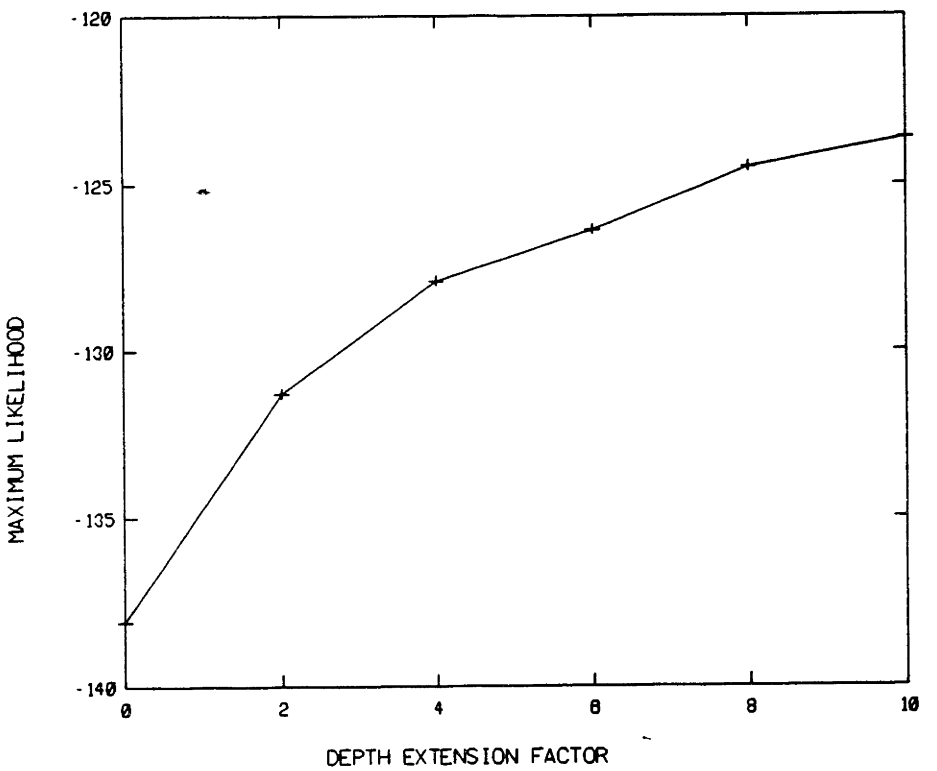

Figure 4-12: Maximum Likelihood vs. Vertical Extension Factor

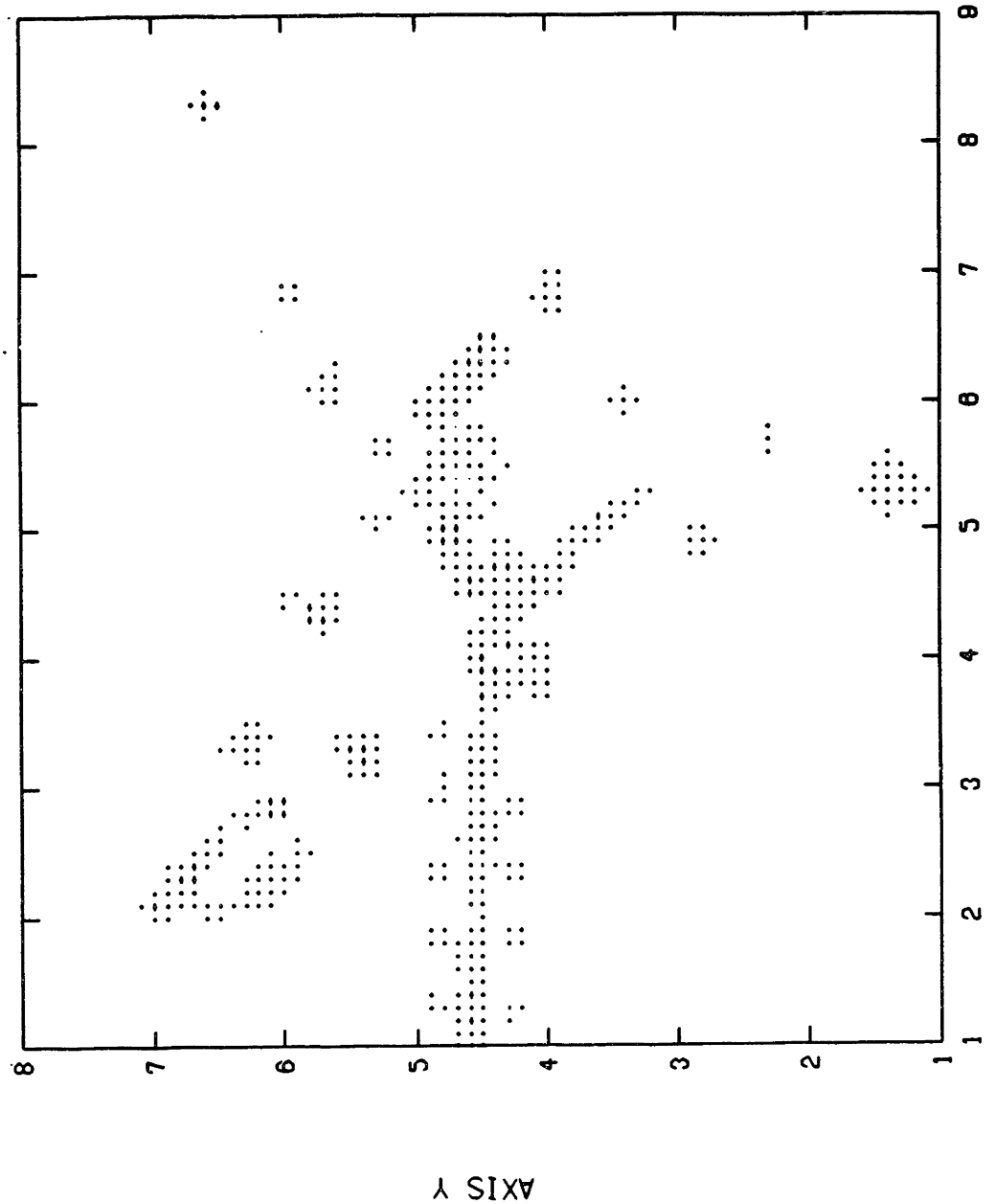

Figure 4-13: Region of N Distribution Updating

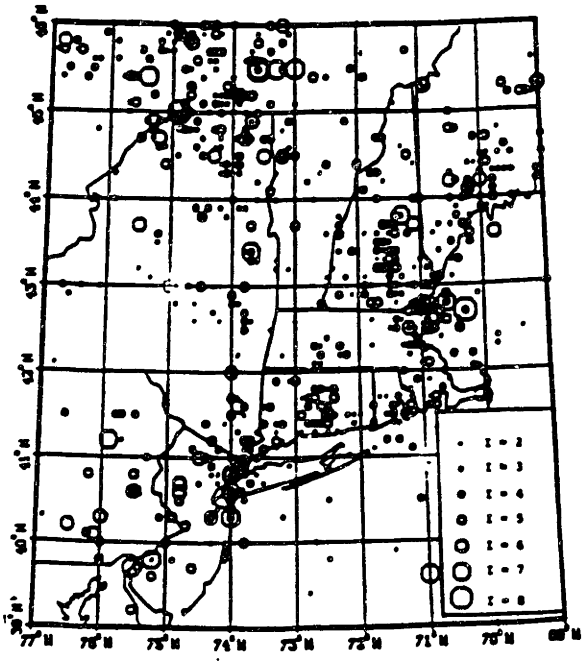

Figure 4-14: Earthquake Catalogue 1627-1981 (Veneziano and Chouinard, 1987a)

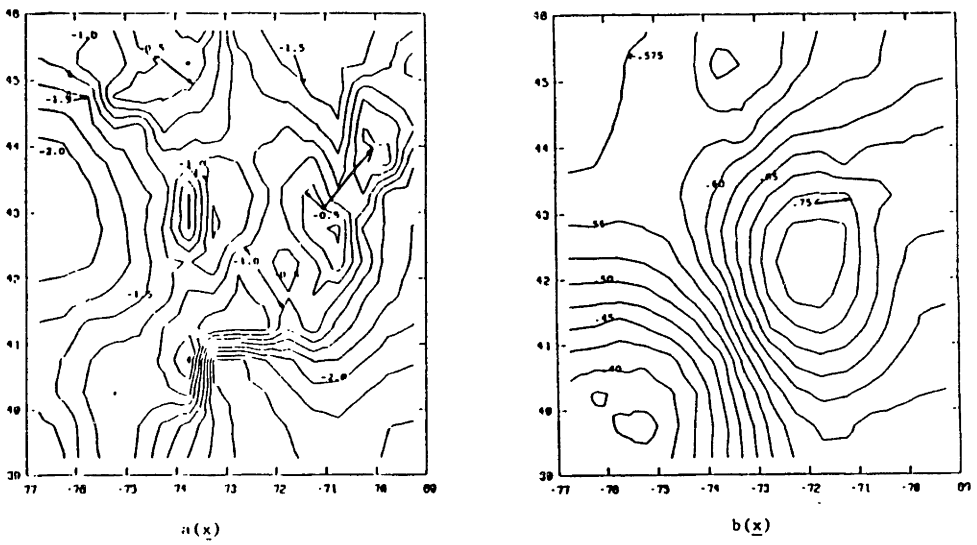

Figure 4-15: Contours of a(x) and b(x) (Veneziano and Chouinard, 1987b)

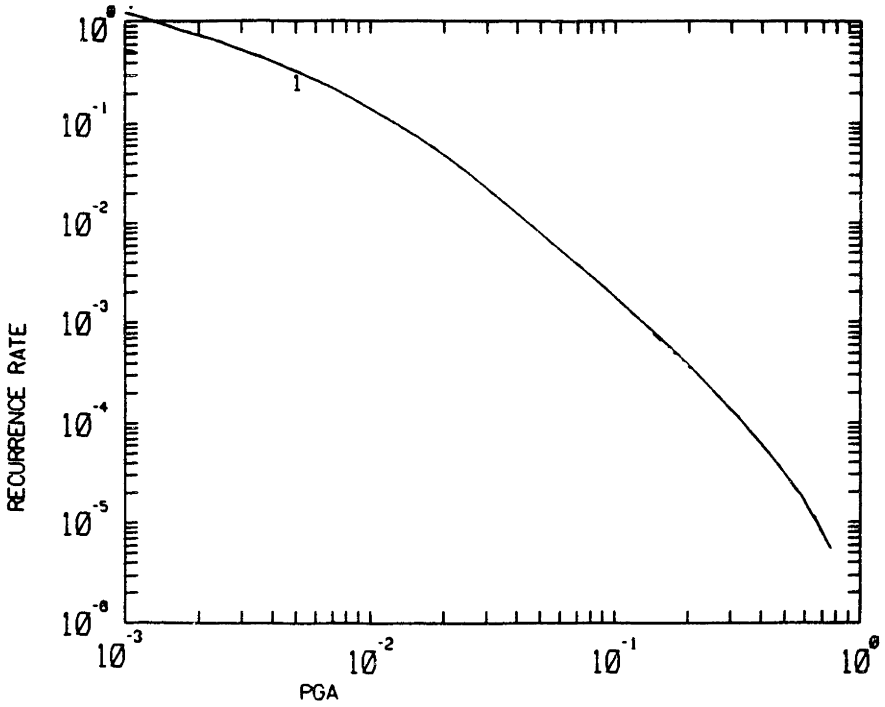

Figure 4-16: Exceedence Rate vs. PGA

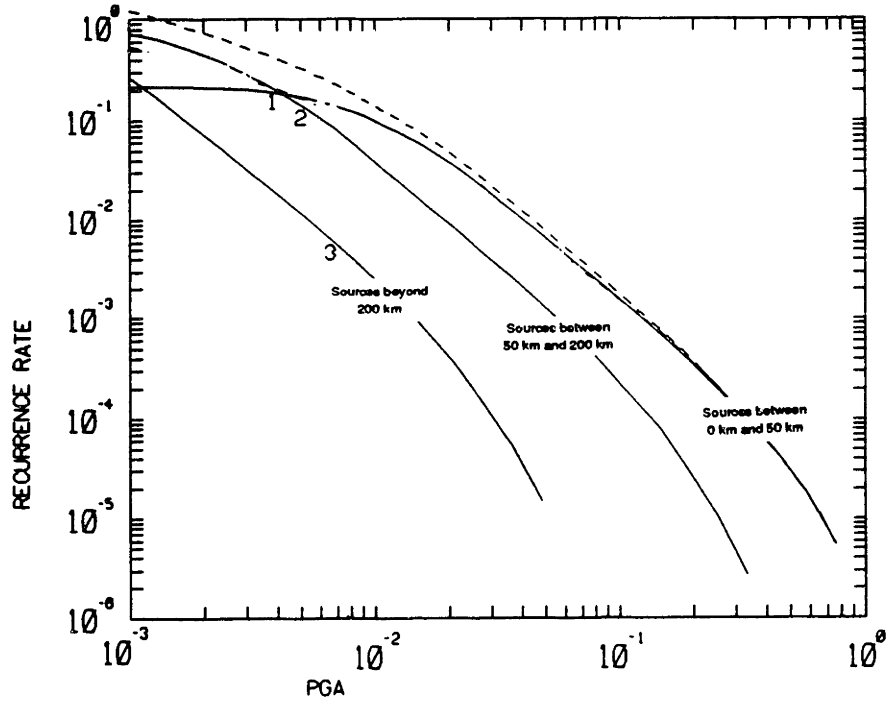

Figure 4-17: Contribution to Exceedence Rate

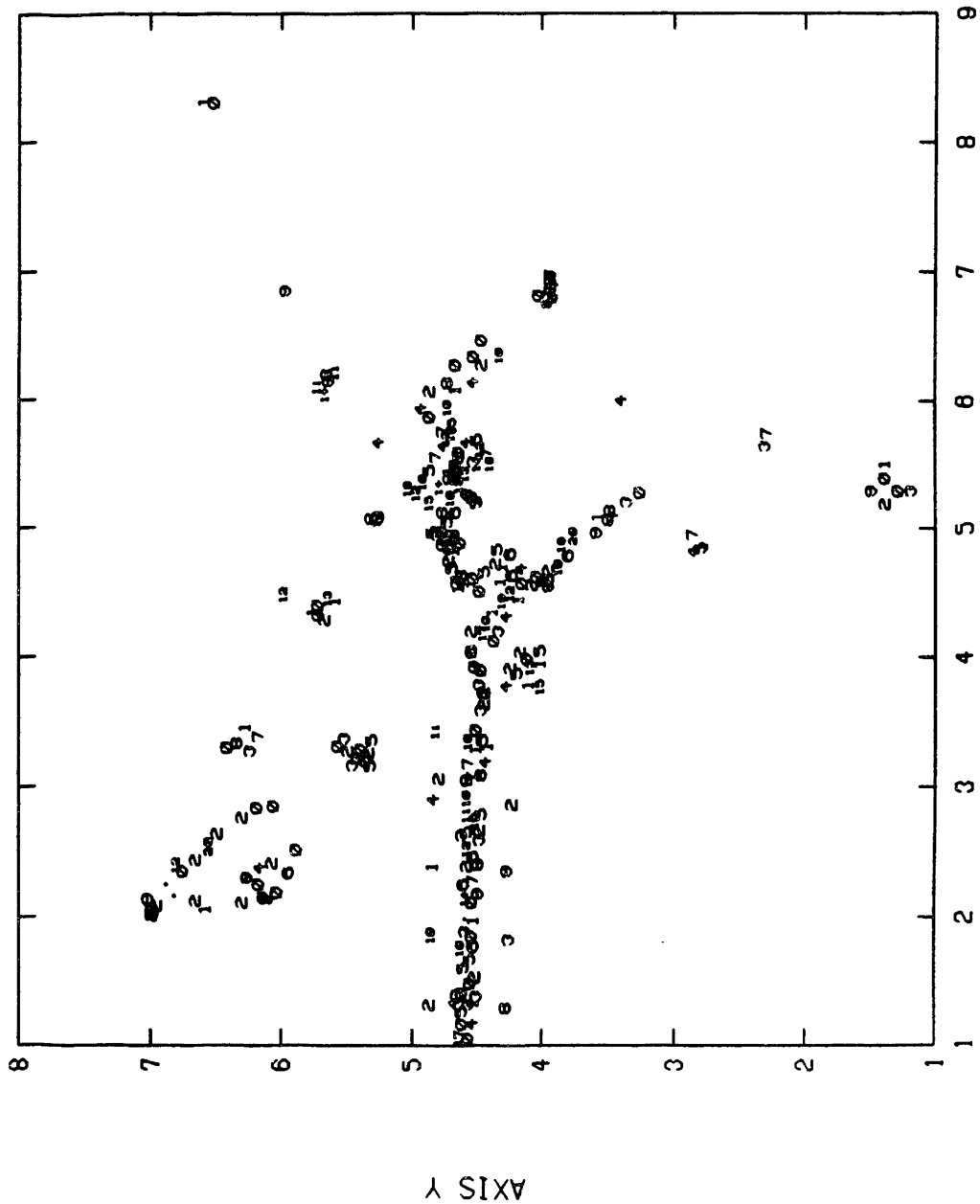

Figure 4-18: Liquefaction Rates x10^4 at the Data Points

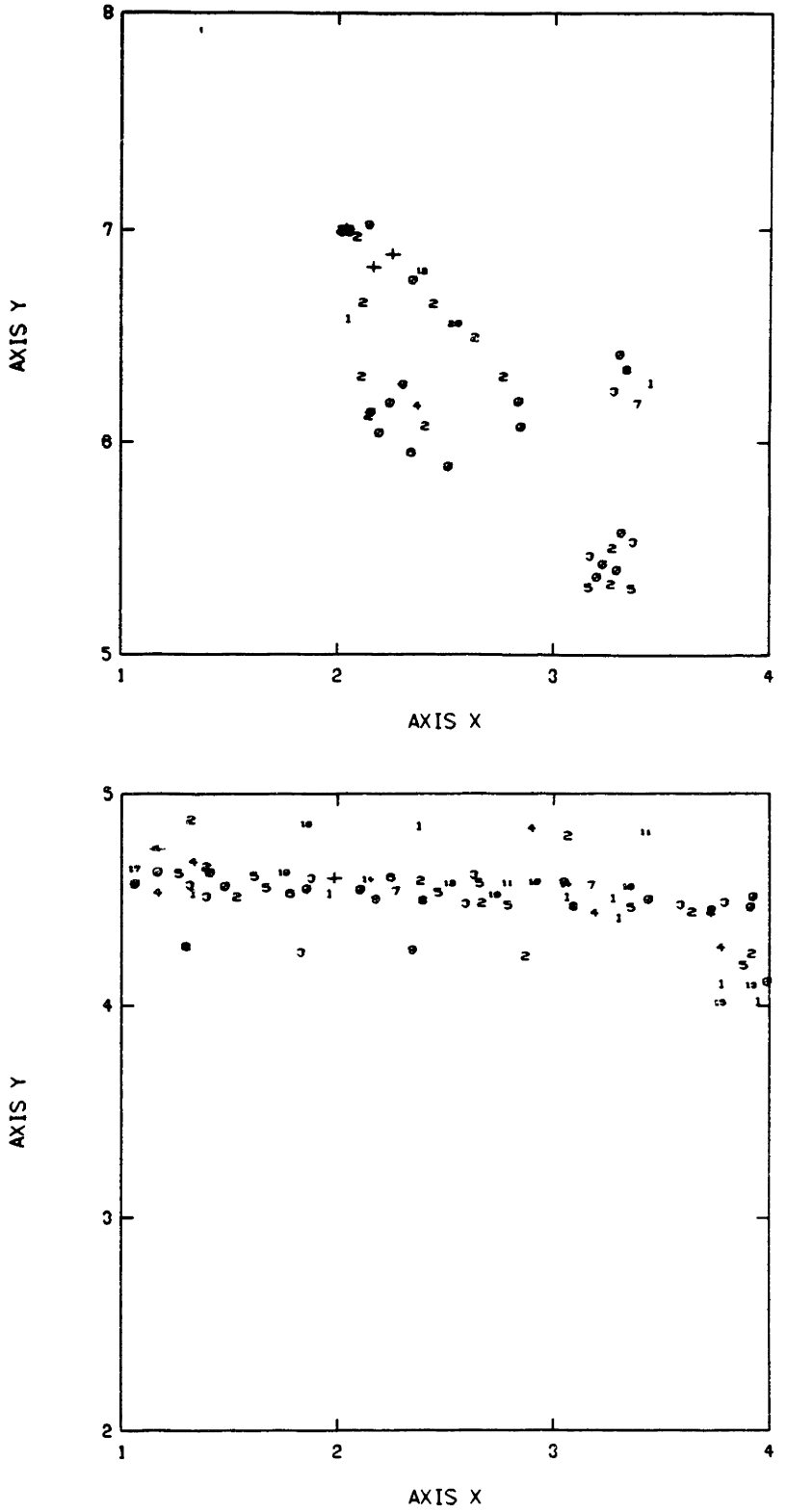

Figure 4-19a: Liquefaction Rates x10^4 in Subregions

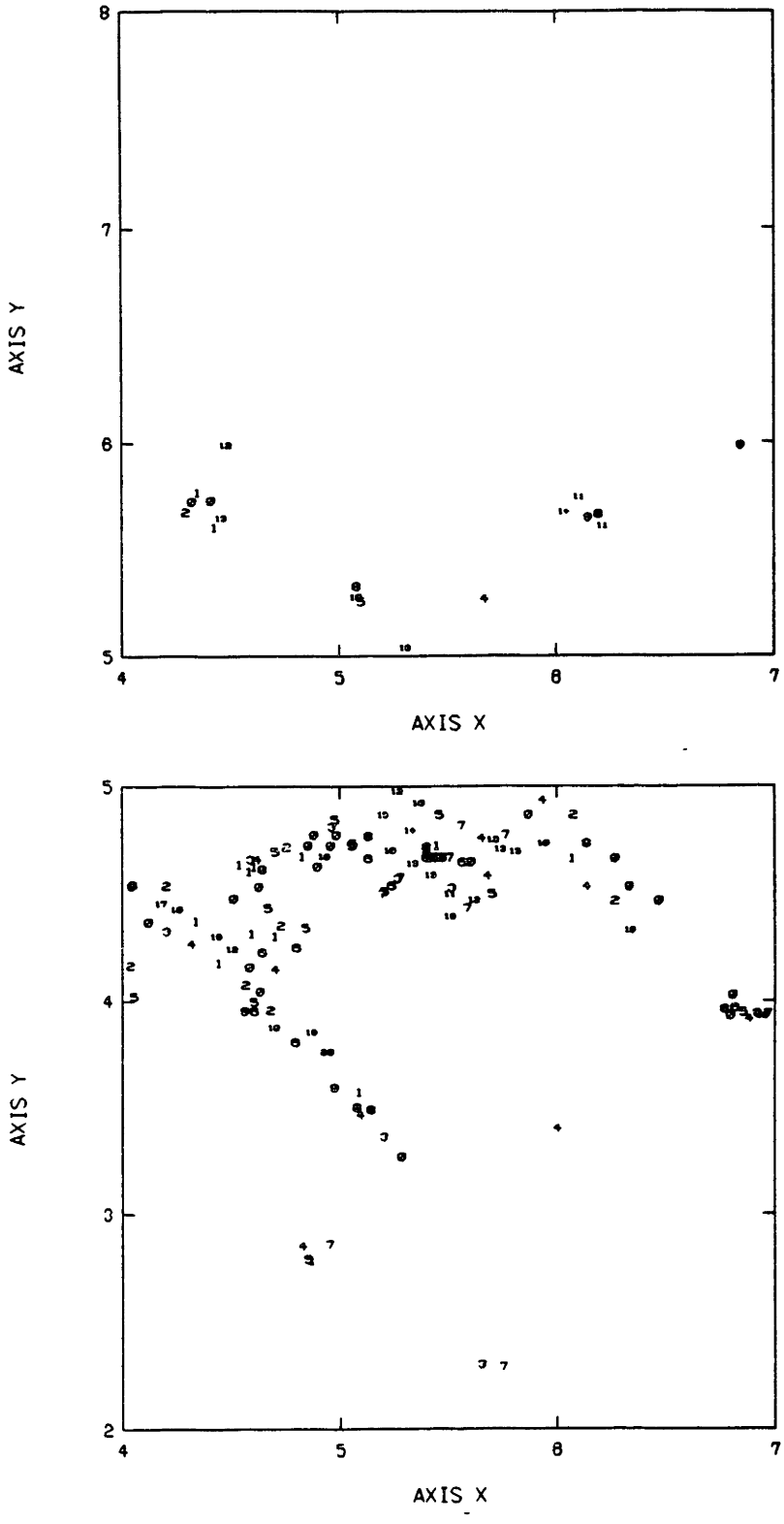

Figure 4-19b: Liquefaction Rates x10^4 in Subregions

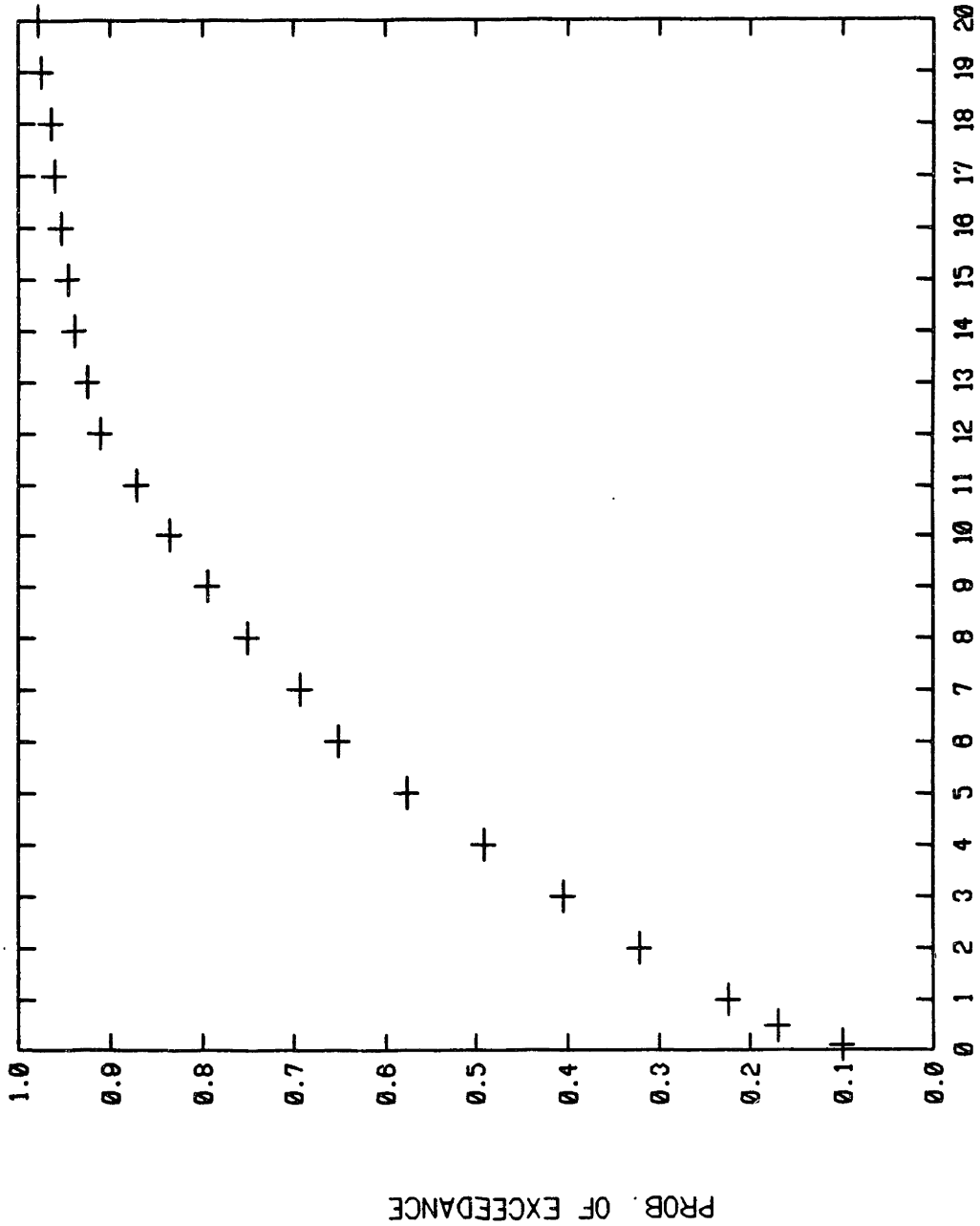

Figure 4-20: Prob. of Exceedence of Liquefaction Rate at the Data Points

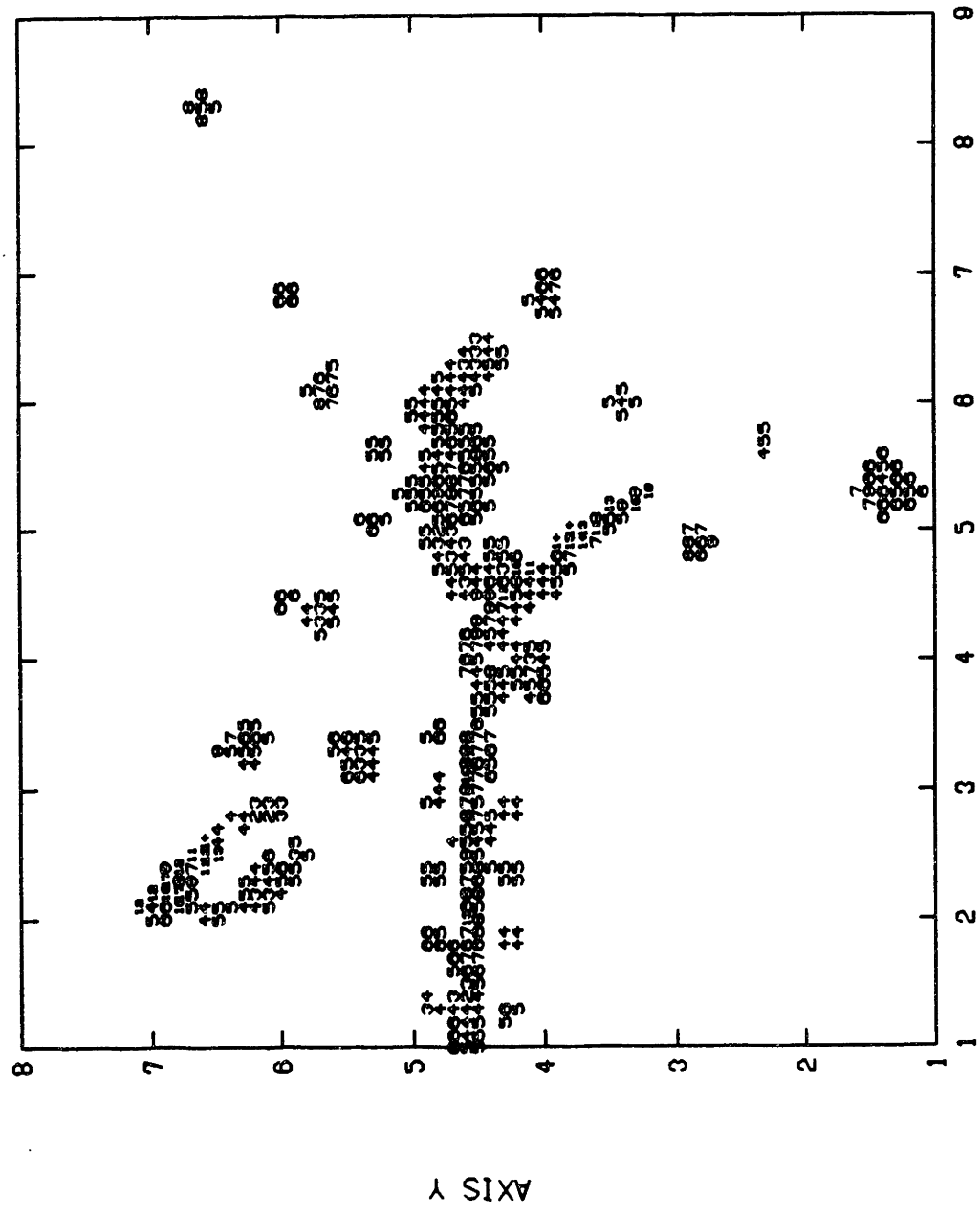

Figure 4-21: Liquefaction Hazard Map (1) (Rate x10^4/year)

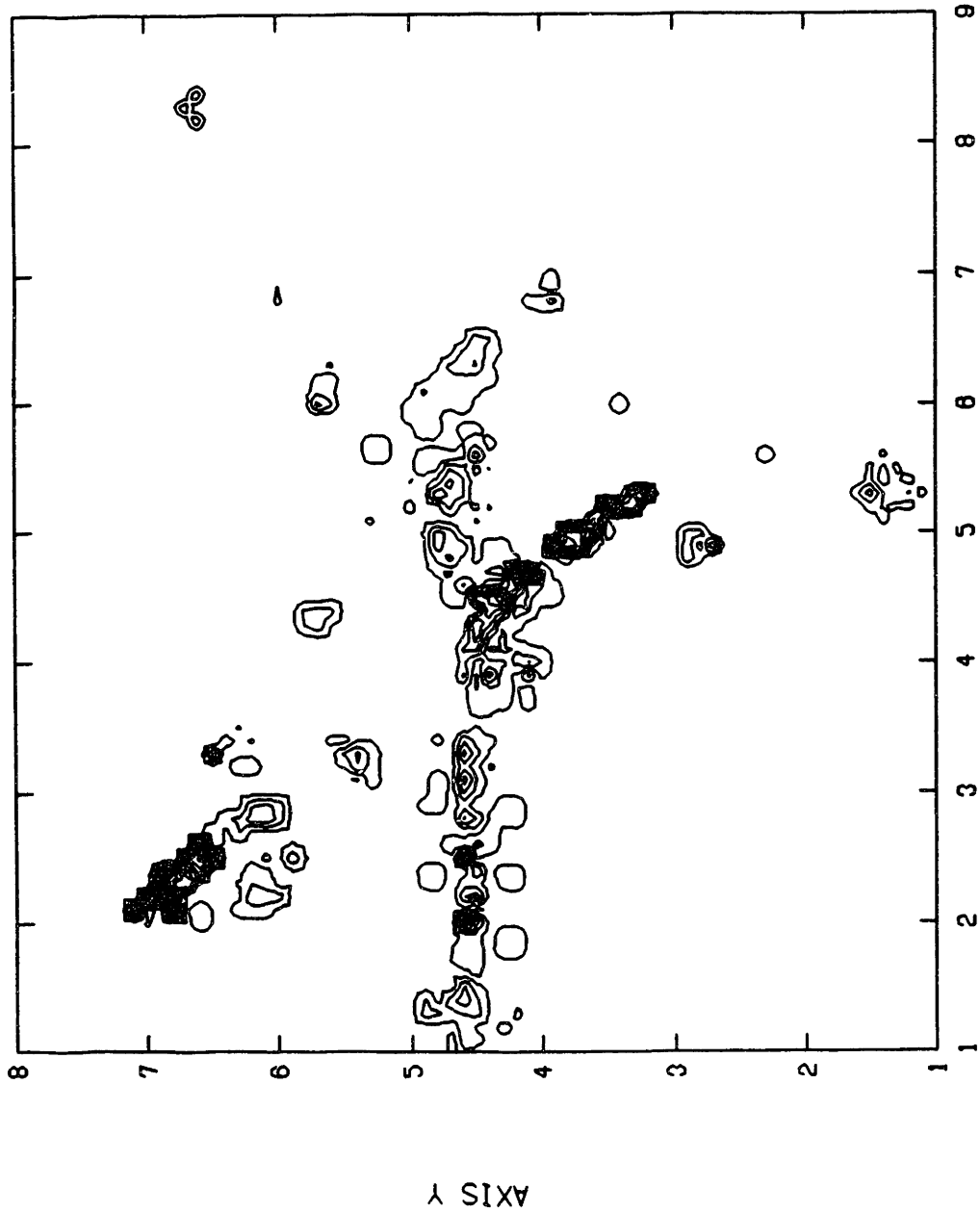

Figure 4-22: Liquefaction Hazard Map (1) (Contours of Rates)

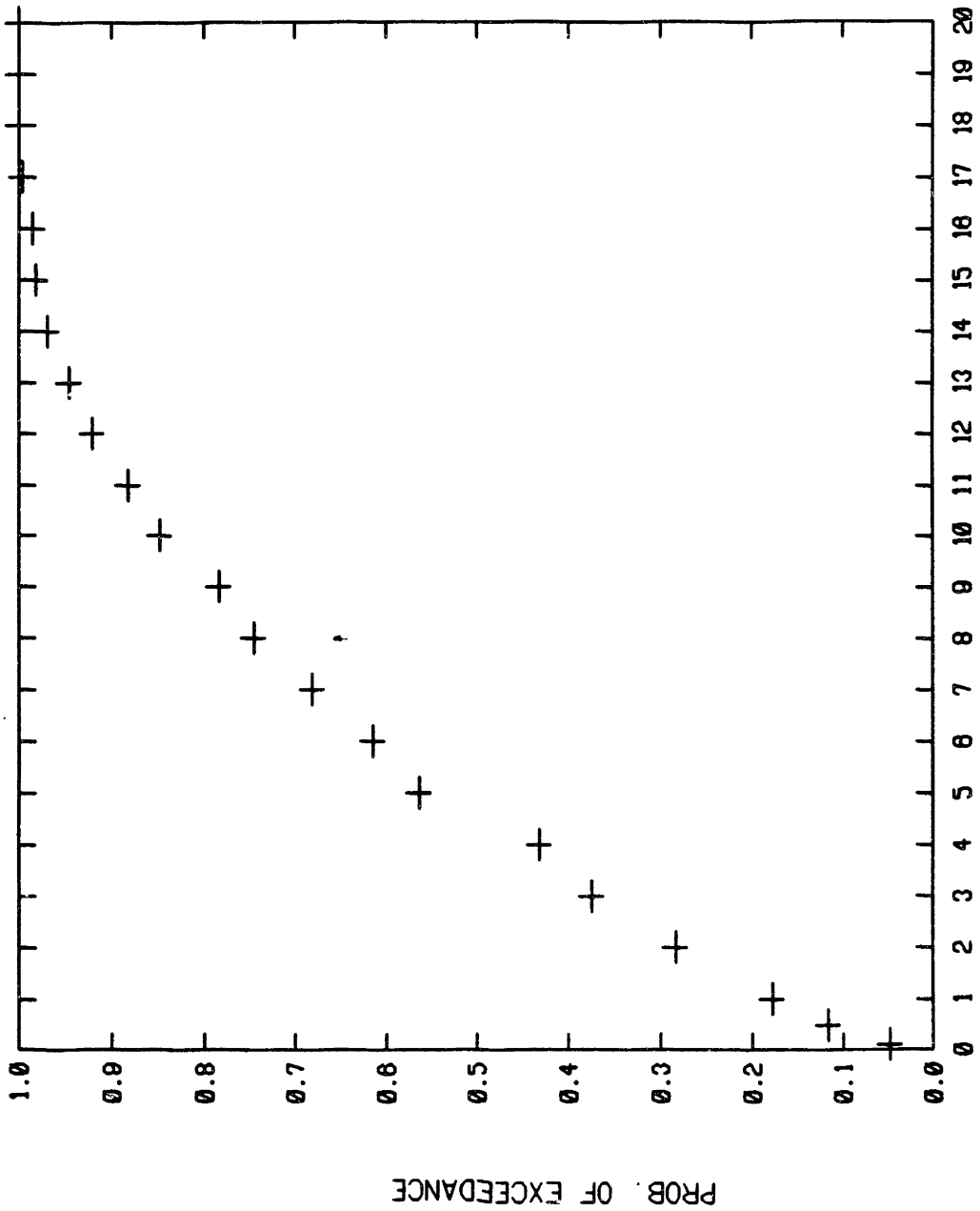

Figure 4-23: Prob. of Exceedence of Liquefaction Rate (1)

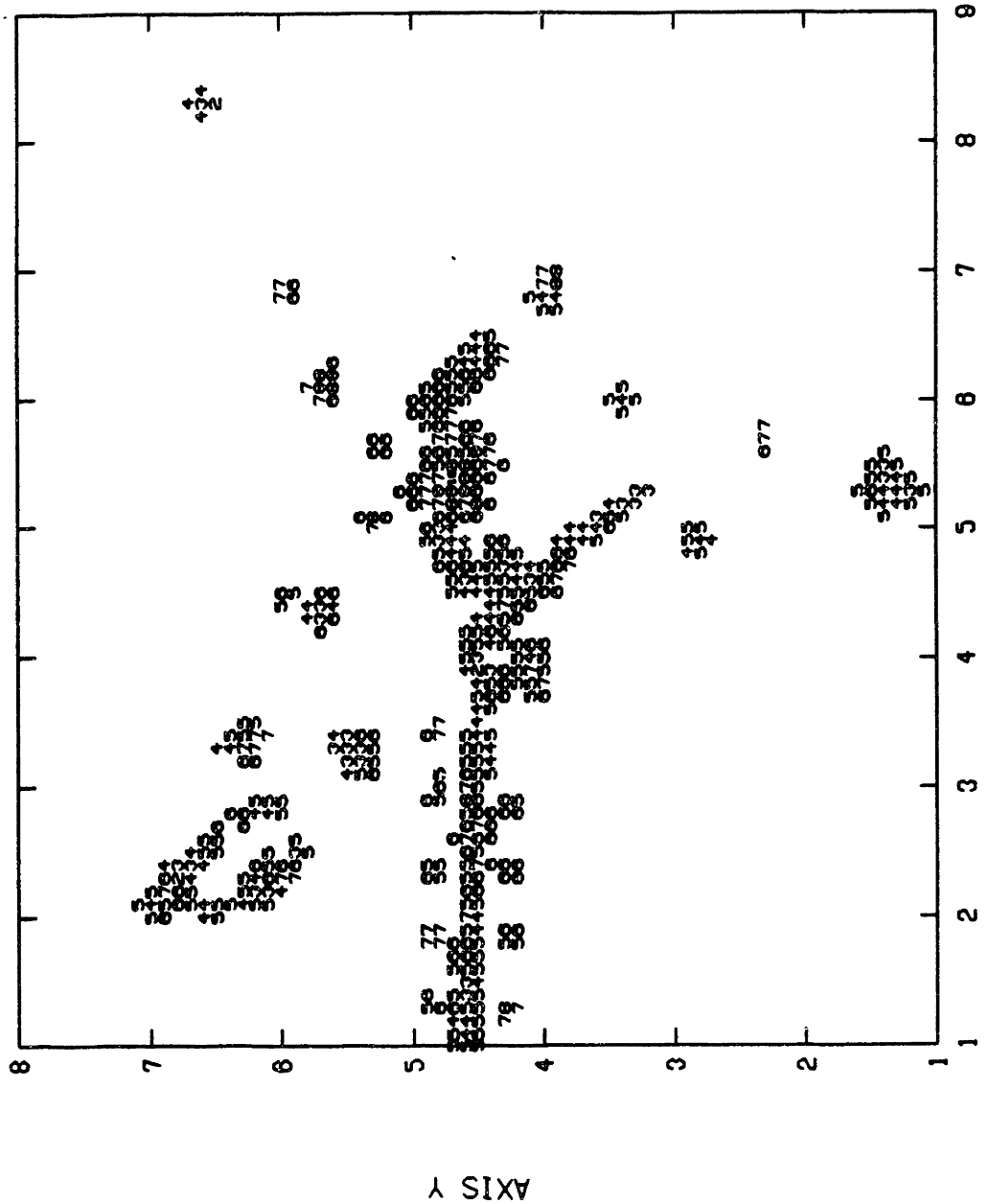

Figure 4-24: Liquefaction Hazard Map (2) (Rate x10^4/year)

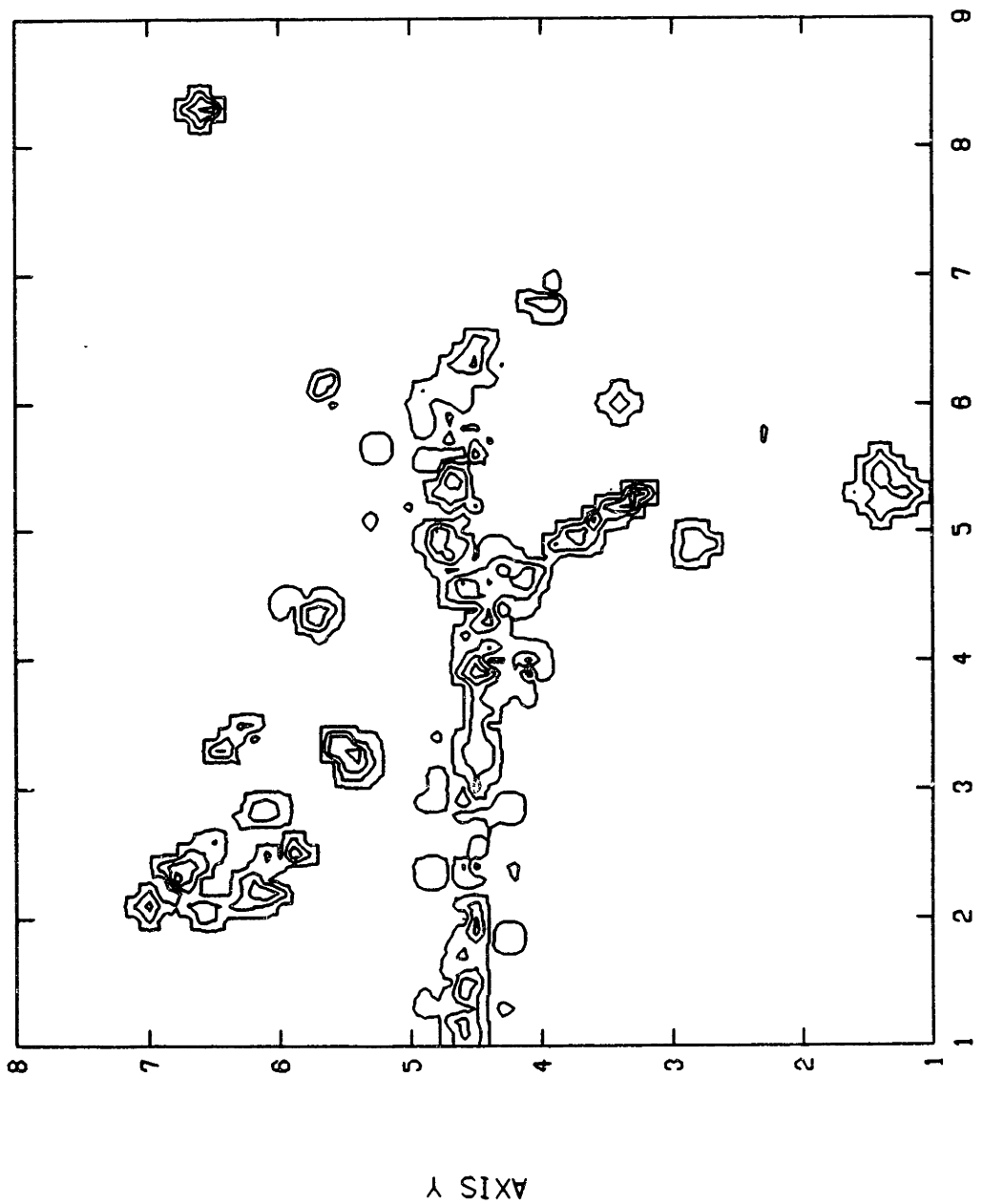

Figure 4-25: Liquefaction Hazard Map (2) (Contours of Rates)

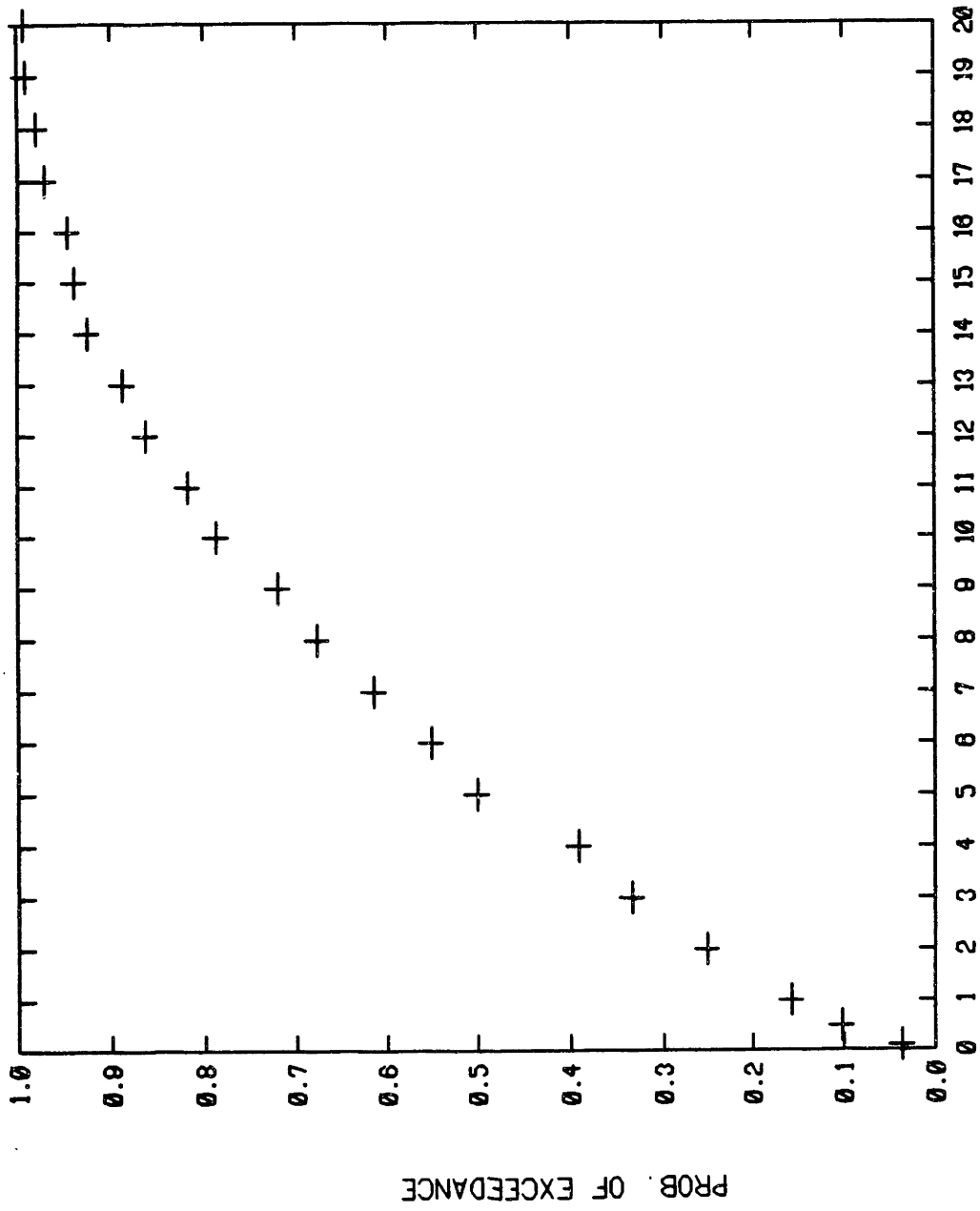

Figure 4-26: Prob. of Exceedence of Liquefaction Rate (2)

Chapter 5

LIQUEFACTION HAZARD MAP OF NATURAL DEPOSITS IN THE LOWELL AREA

5.1 Introduction

Several deposits in the greater Boston area have been identified as potentially liquefiable. These deposits include overbank river deposits and fluvioglacial deposits. We were able to obtain geotechnical data from sites in Lowell, figs 5-1 and 5-2, which contain these two types of deposits.

An analysis similar to that in Chapter 4 has been performed on the data from the Lowell sites. It has been found that the average recurrence rate of liquefaction for overbank river deposits is $\lambda_L=4.4\text{x}10^{-4}$/year and that for fluvioglacial deposits $\lambda_L=2.35\text{x}10^{-4}$/year. The SPT data displays better spatial correlation than the SPT data for the BackBay fill. Certain limitations to the liquefaction hazard evaluation procedure are identified and will be described later in the chapter.

5.2 Site Description

Data for this analysis was obtained from two adjacent sites in Lowell, with similar geology. A simplified profile of the deposits, fig. 5-3, proceeding downwards from ground surface, includes:

1- Overbank river deposits or flood plane deposits consisting mainly of light brown

yellow silty sand to fine sandy silt, about 15 ft in thickness. The deposit is medium dense to very loose. Figure 5-4 shows SPT and a representative grain size distribution curve for this material.

2- Fluvioglacial deposits, which are quite uniform and frequently contain loose layers of sand or silty sand. These deposits consist mainly of coarse to medium sand and medium to fine sand. The thickness of the layer ranges from 25 ft to 50 ft. Figure 5-5 shows SPT data and a representative grain size distribution curve.

3- Glacial till, which consists of compact to very compact silty coarse to fine sand with coarse to fine gravel and decomposed rock with some boulders. The till can be up to 15 ft in thickness.

4- Bed rock, which is mainly very hard coarse to fine grained quartz grano-diorite, slightly weathered in some places but sound overall.

5.3 Liquefiable Deposits

Based on the geological description, the first two layers are considered to be potentially liquefiable. The overbank river deposits will be referred to as layer I and the fluvioglacial deposits will be referred to as layer II. The grain size distribution curves, figs. 5-4 and 5-5, place layer I deposits within the range of fine silty sand, and layer II deposits within the range of clean medium sand. SPT data , figs 5-4 and 5-5, indicate that layer I has very low SPT values and that particular zones within layer II can be loose. This is further evidence that deposits I and II are potentially liquefiable. We also expect, based on the above data, that layer I be more susceptible to liquefaction than layer II (this prediction will be supported by formal analysis).

Layer I was found to be liquefiable under Massachusetts Building Code and was compacted to satisfy the code requirements (Soydemir and LeCount, 1984). Therefore, the

purpose of this analysis is not to characterize the site in its current state, but to evaluate the liquefiability of this type of geologic deposits, which are common within the greater Boston area. Since the two layers are different, each layer will be analyzed separately.

5.4 The Data Set

For each layer, the data consist of the minimum corrected SPT values along each borehole, as in Chapter 4. The SPT data from the two sites are comparable as they were obtained using similar samplers. No correction for weight of rod (WOR) is applied in this case.

The data includes 41 data points, as shown in tables 5-I and 5-II. The elevations listed are referenced to Lowell City Base, 55.20 ft above USC&GS mean sea level of 1929. For the purpose of this analysis, we assume that the ground surface is level. Figs. 5-6, 5-7, 5-8, 5-9 show the SPT data locations and values on a site map, separately for each layer. The data is clustered around the locations of the two source sites, which are relatively far apart. Performing separate analyses for the two clusters was not considered appropriate, because the right hand side cluster contains only six data points.

The water table at the site was observed to vary seasonally between 6 ft and 10 ft below ground level. In our analysis, we assume that water table is 6 ft below ground level, which represents the most critical value in that range.

5.5 Data Analysis and Modeling

The method of analysis for the Lowell sites is essentially the same as that described in Chapter 4. In what follows, we present the results, separately for layers I and II, using the notations of Chapter 4.

5.5.1 Analysis of layer I

The critical depth D, fig 5-10, shows no strong spatial trend. We therefore assume that D has, at all sites, the probability distribution estimated from the entire data set. Fig 5-11 shows a histogram of D.

As in the case of BackBay, the blow count number N_1 varies with D according to the correction factor $\sqrt{1/\sigma_{eff}}$, see the upper two plots in fig. 5-12. In the lower plot of fig. 5-12 the depth correction factors of the data points fit exactly the correction function curve. This is because the water table is assumed to be at a constant depth for all the points.

The distribution of N does not display strong regional dependence. The natural logarithms of N are fitted well by a normal distribution with mean m=1.62 and variance σ^2=0.285. Notice that this variance is much smaller than that for the fill material in BackBay, indicating that the present natural deposit is more uniform than the fill.

Spatial Correlations

To obtain the correlation distance in space we calculate the likelihood function for a variety of combinations of correlation distance and depth extension factor. From the results in Table 5-III, the correlation distance that maximizes the likelihood is about 80 ft. The likelihood function decreases by very small amounts with increasing extension factor. Hence, a good estimate of the depth extension factor is 10, even though the likelihood function does not have an absolute maximum at that value.

The correlation distance of 80 ft indicates that the data is better correlated in space than the fill data, which is again a consequence of the higher uniformity of the natural deposits.

Updating Model

In implementing the updating model described in Chapter 4, we have considered points to be "far" from the borings if they are more than 200 ft away from the closest point

of the data set. Updating is done on a grid of points with 50 ft spacing in both the X and Y directions and over a range of depth between 6 ft and 15 ft: the water table is at a depth of 6 ft and the average depth of layer I does not extend beyond 15 ft. The sand in this layer is silty, hence we have used the silty sand expression of Q_L in the conditional probability of liquefaction:

$$Q_L = 6.48 + 2.69\ln(CSRN) - 0.182(N_1)_{60} \quad (5.1)$$

For both layers we have assumed:

Unit weight of dry soil, $\gamma_d = 95 lb/ft^3$

Unit weight of wet soil, $\gamma_w = 120 lb/ft^3$

The seismicity hazard curve for the site is shown in fig 5-14. In the expression for the cyclic stress ratio, we have used a magnitude M=5.5. Notice that Lowell is closer to high seismicity sources than Boston, and events of magnitude between 5 and 6 are those that most frequently would cause liquefaction.

Hazard Maps

Two liquefaction hazard maps are produced for this layer. The first map shows the liquefaction recurrence rates at the points of the data sets, fig 5-15. The rates extend over a wide range, with an average value $\lambda_L = 4.4 \times 10^{-4}$/year.

The second map, fig 5-16, shows liquefaction rates at various grid locations using the updating model. At the generic site (blank space on map), $\lambda_L = 6.55 \times 10^{-4}$/year. The map shows that all the rates are of the order of 6 events per 10,000 years. Comparing the two maps, we notice that the model is sensitive to data points with low N_1 values (high rates) . However, near sites where N_1 is high (where rates are low), the model rapidly returns to higher liquefaction rates. This indicates some limitations of the model. An explanation of this behavior, which is more pronounced for layer II, will be given later. Fig. 5-17 shows a contour plot of the hazard map.

5.5.2 Analysis of Layer II

Fig. 5-18 shows a plot of D on Lowell map. Again D does not exhibit any strong spatial trend; hence, we assume that D has anywhere the probability distribution estimated from the entire data set, see fig. 5-19.

As in the case of layer I, the dependence of N_1 on D is well explained by the SPT correction factor, see fig. 5-20.

Moreover, the distribution of N does not exhibit strong regional dependence. In this case, the natural logarithm of N is fitted well by a normal distribution with mean m=2.166 and variance σ^2=0.162, fig. 5-21. As for layer I, the variance for the Backbay fill is much higher than the variance for the natural deposit.

Spatial Correlations

Ideally, we would use the correlation distance at which the likelihood function is maximum. Table 5-20 shows values of the likelihood function for a variety of correlation distances and extension factors. We notice that the function possesses a local maximum at low extension factors, but otherwise increases monotonically as the extension factor increases. By examining equation (4.7) we notice that, as the depth extension factor increases, the value of $\det(\Sigma)$ increases and hence $\sqrt{\det(\Sigma)}$ increases. At the same time the value of the exponential term increases. However, in our case the increase in the exponential term dominates and results in a monotonic increase in the value of the likelihood function. This behavior can be attributed to the spread of the data over a depth range of about 45 ft, which is amplified considerably as one increases the value of the extension factor. In the updating step we have decided to use a depth extension factor of 20, with a correlation distance of 80 ft.

Updating Model

The updating procedure is the same as that used for layer I, except for the depth range which for layer II is 15 ft to 62 ft.

The sand of this layer seems to contain very little if any fines. We therefore used the clean sand expression for Q_L, which is (Liao, 1986):

$$Q_L = 16.5 + 6.46\ln(CSRN) - 0.40(N_1)_{60} \quad (5.2)$$

The reference magnitude is 5.5, as for layer I.

Hazard Maps

As in the analysis of layer I, two liquefaction hazard maps are produced for layer II. Figure 5-22 shows the liquefaction recurrence rates at the points of the data set, with an average rate of $\lambda_L=2.35\text{x}10^{-4}$/year.

Figure 5-23 shows liquefaction rates for layer II at various grid locations. It is not possible to plot a contours for this hazard map because of the very small variation in the values of the rates. At the generic site (blank space on map) $\lambda_L=2.35\text{x}10^{-4}$/year. The rates on this map are only very slightly affected by information provided by the data points. Most of the values are close to the rate for the generic site. The explanation is that the depth extension factor of 20 makes even close points "far", especially because we are working within a depth range of about 45 ft. To test this hyposethesis we have obtained hazard maps using an extension factor of 10 and correlation distance of 80 ft, extension factor of 5 and correlation distance of 50 ft, and extension factor of 1 and correlation distance of 50 ft. The correlation distances are chosen to be the values at which the likelihood is maximum for the given extension factor. By comparing the 4 maps, figs. 5-23, 5-24, 5-25, 5-26, we observe that, as the extension factor decreases from 20 to 1, the model becomes more sensitive to data points with high liquefaction rates, but remains quite insensitive to data points with lower than average rates.

5.6 Sensitivity Analysis for M

In order to evaluate the impact of the chosen value of the earthquake magnitude M on the liquefaction rates, we have obtained hazard maps also for M=6.5. Figs. 5-27 and 5-28 show the hazard rates for layers I and II respectively, for M=6.5. We notice that there is an increase of about 50% in the rates. M=6.5 is an upper limit for the magnitude of the earthquakes to be expected at the site. Hence, the uncertainty in the results is expected to be less than a factor of 50%.

5.7 Discussion

Together with BackBay the Lowell sites offer an opportunity to compare results for natural and artificial deposits. The latter sites also help to pinpoint some of the limitations of the model.

The SPT values in the natural deposits seem to be more uniform and better correlated in space than the SPT values in artificial fill. This greater uniformity is also reflected in the reduced variance of the natural logarithm of the blow count data.

The average liquefaction recurrence rate is about 4.4 events per 10,000 years for layer I and about 2.35 events per 10,000 years for layer II. This result is in good agreement with qualitative evaluation based on the assessment of the engineering properties of the two deposits (see section 5.3). Such a result tends to support the suitability of the model in evaluating the relative liquefaction susceptibility of different deposits.

A problem that arises from the application of the model to the Lowell sites is its insensitivity to high SPT values. The explanation for this behavior is that we assume that everywhere in the deposit the critical depth has the marginal distribution of D from the entire data set. This assumption is accurate except for points close to boreholes where the critical depth should be rather well constrained. The model could be improved by applying to D an updating procedure similar to the one used for N.

5.8 Conclusion

Based on the above analysis, overbank river deposits in the Lowell area have a liquefaction rate of about $4\text{-}6\text{x}10^{-4}$ events/year, and fluvioglacial deposits have a liquefaction rate of about $2\text{-}3\text{x}10^{-4}$/year.

The analysis indicates that the geologic deposits are more uniform and are better correlated in space than the artificial fill of BackBay. This makes it possible to characterize liquefaction hazard for a given geologic deposit based on fewer SPT data.

It is noted again that the present results have no bearing on the site because of soil improvement measures that have been taken there. However, the results are useful in evaluating the liquefaction susceptibility of other sites with similar geologic conditions.

NUMBER OF POINTS: 41 LOWELL LAYER I

X FT	Y FT	Z SURFACE	D FT	BLOWS/FT UNCORRECTED	BLOWS/FT CORRECTED
1410.0	244.0	43.5	6.5	2.00	3.83
680.0	996.0	44.0	11.5	4.00	6.30
1053.0	844.0	45.0	11.5	4.00	6.30
566.0	379.0	44.0	20.5	6.00	7.51
885.0	411.0	46.5	11.0	4.00	6.41
1272.0	695.0	45.8	11.0	6.00	9.61
1136.0	382.0	44.6	16.0	2.00	2.77
1484.0	470.0	45.8	6.5	6.00	11.50
1437.0	250.0	42.6	6.5	4.00	7.67
1381.0	472.0	40.5	7.0	6.00	11.23
1158.0	558.0	41.1	6.5	4.00	7.67
810.0	806.0	45.0	10.5	8.00	13.03
1052.0	741.0	46.8	11.0	10.00	16.01
1172.0	709.0	46.2	10.5	8.00	13.03
1414.0	644.0	46.5	6.5	8.00	15.33
778.0	685.0	47.4	15.5	6.00	8.42
898.0	653.0	44.8	10.5	4.00	6.52
1019.0	621.0	42.4	6.0	4.00	7.86
1261.0	556.0	40.2	6.0	8.00	15.72
1502.0	491.0	44.4	10.5	8.00	13.03
866.0	532.0	47.6	6.5	10.00	19.17
987.0	500.0	47.1	10.5	4.00	6.52
1108.0	467.0	45.7	11.5	2.00	3.15
1265.0	425.0	44.8	11.0	4.00	6.41
1373.0	396.0	43.0	11.0	6.00	9.61
713.0	444.0	47.4	6.5	8.00	15.33
834.0	411.0	47.0	11.5	4.00	6.30
954.0	379.0	47.0	11.5	4.00	6.30
1075.0	347.0	45.7	11.0	1.00	1.60
1317.0	282.0	43.2	6.0	10.00	19.65
931.0	774.0	46.8	6.0	10.00	19.65
1381.0	523.0	41.8	6.0	4.00	7.86
710.0	574.0	47.6	6.0	12.00	23.58
1470.0	370.0	41.6	6.5	8.00	15.33
1196.0	314.0	45.2	11.5	4.00	6.30
3400.0	300.0	45.0	6.5	4.00	7.67
3300.0	300.0	45.0	6.5	2.00	3.83
3200.0	300.0	44.0	7.5	6.00	10.98
3400.0	400.0	44.5	6.5	6.00	11.50
3300.0	400.0	42.0	6.0	8.00	15.72
3200.0	400.0	43.0	6.0	6.00	11.79
0000.00	000.0	00.0	0.0	0.0	0.0

NOTE: LAYER I LOOSE FINE SAND AND SILT

ASSUMED WATER LEVEL 6 FT BELOW GROUND SURFACE

Table 5-I: Data Base, Lowell, layer I

NUMBER OF DATA POINT: 41 LOWELL LAYER II

X FT	Y FT	Z SURFACE	D FT	BLOWS/FT UNCORRECTED	BLOWS/FT CORRECTED
1410.0	244.0	43.5	40.5	6.00	5.57
680.0	996.0	44.0	55.5	8.00	6.42
1053.0	844.0	45.0	45.5	6.00	5.28
566.0	379.0	44.0	59.5	10.00	7.76
885.0	411.0	46.5	66.5	8.00	5.89
1272.0	695.0	45.8	31.0	10.00	10.46
1136.0	382.0	44.6	45.5	12.00	10.55
1484.0	470.0	45.8	42.0	10.00	9.12
1437.0	250.0	42.6	20.5	8.00	10.01
1381.0	472.0	40.5	36.5	6.00	5.83
1158.0	558.0	41.1	31.5	14.00	14.54
810.0	806.0	45.0	35.0	8.00	7.93
1052.0	741.0	46.8	30.5	4.00	4.22
1172.0	709.0	46.2	26.5	14.00	15.69
1414.0	644.0	46.5	30.5	6.00	6.32
778.0	685.0	47.4	25.5	6.00	6.84
898.0	653.0	44.8	40.5	16.00	14.84
1019.0	621.0	42.4	40.5	12.00	11.13
1261.0	556.0	40.2	34.0	12.00	12.05
1502.0	491.0	44.4	51.0	8.00	6.67
866.0	532.0	47.6	15.5	10.00	14.03
987.0	500.0	47.1	16.5	10.00	13.68
1108.0	467.0	45.7	35.5	12.00	11.82
1265.0	425.0	44.8	51.0	12.00	10.01
1373.0	396.0	43.0	25.5	6.00	6.84
713.0	444.0	47.4	15.5	8.00	11.23
834.0	411.0	47.0	56.5	8.00	6.36
954.0	379.0	47.0	61.5	10.00	7.64
1075.0	347.0	45.7	45.5	6.00	5.28
1317.0	282.0	43.2	42.0	16.00	14.60
931.0	774.0	46.8	25.5	12.00	13.68
1381.0	523.0	41.8	45.5	14.00	12.31
710.0	574.0	47.6	41.0	18.00	16.60
1470.0	370.0	41.6	26.5	8.00	8.97
1196.0	314.0	45.2	16.5	12.00	16.42
3400.0	300.0	45.0	66.5	3.00	2.21
3300.0	300.0	45.0	66.5	4.00	2.95
3200.0	300.0	44.0	65.5	6.00	4.45
3400.0	400.0	44.5	30.5	6.00	6.32
3300.0	400.0	42.0	45.5	10.00	8.79
3200.0	400.0	43.0	45.5	10.00	8.79
0000.00	000.0	0.0	0.0	0.0	0.0

NOTE: LAYER II MEDIUM DENSE SAND WITH SOME GRAVEL

ASSUMED WATER ELEVATION 6 FT BELOW GROUND SURFACE

Table 5-II: Data Base, Lowell, Layer II

DEPTH EXTENSION FACTOR	CORRELATION DISTANCE (FT) 10	50	90	130	170
0	5.8185	7.9003	8.2900	7.0149	4.8013
2	5.8163	7.8815	8.2800	7.0146	4.8123
4	5.8122	7.8286	8.2500	7.0100	4.8379
6	5.8060	7.7499	8.2015	6.9953	4.8640
8	5.8020	7.6540	8.1372	6.9674	4.8799
10	5.7994	7.5480	8.0601	6.9256	4.8805

LIKELIHOOD

DEPTH EXTENSION FACTOR	CORRELATION DISTANCE (FT) 50	60	70	80	90
0	7.9003	8.2227	8.3791	8.3937	8.2900
2	7.8815	8.2059	8.3645	8.3814	8.2800
4	7.8286	8.1583	8.3228	8.3455	8.2500
6	7.7499	8.0863	8.2585	8.2891	8.2015
8	7.6540	7.9969	8.1773	8.2163	8.1372
10	7.5480	7.8960	8.0840	8.1312	8.0601

LIKELIHOOD

Table 5-III: Likelihood Function Values, Layer I

DEPTH EXTENSION FACTOR	CORRELATION DISTANCE (FT) 10	50	90	130	170
0	17.353	17.997	17.205	14.919	11.796
2	17.344	17.862	17.238	15.217	12.381
4	17.346	17.753	17.312	15.619	13.173
6	17.348	17.763	17.471	16.034	13.889
8	17.348	17.808	17.642	16.400	14.483
10	17.348	17.850	17.789	16.702	14.967
12	17.348	17.883	17.909	16.949	15.365
14	17.349	17.907	18.007	17.153	15.696
16	17.349	17.925	18.087	17.323	15.975
18	17.348	17.939	18.115	17.467	16.212
20	17.348	17.949	18.212	17.591	16.415
22	17.348	17.956	18.262	17.698	16.592

LIKELIHOOD

DEPTH EXTENSION FACTOR	CORRELATION DISTANCE (FT) 50	60	70	80	90
20	17.949	18.114	18.213	18.244	18.212

LIKELIHOOD

Table 5-IV: Likelihood Function Values, Layer II

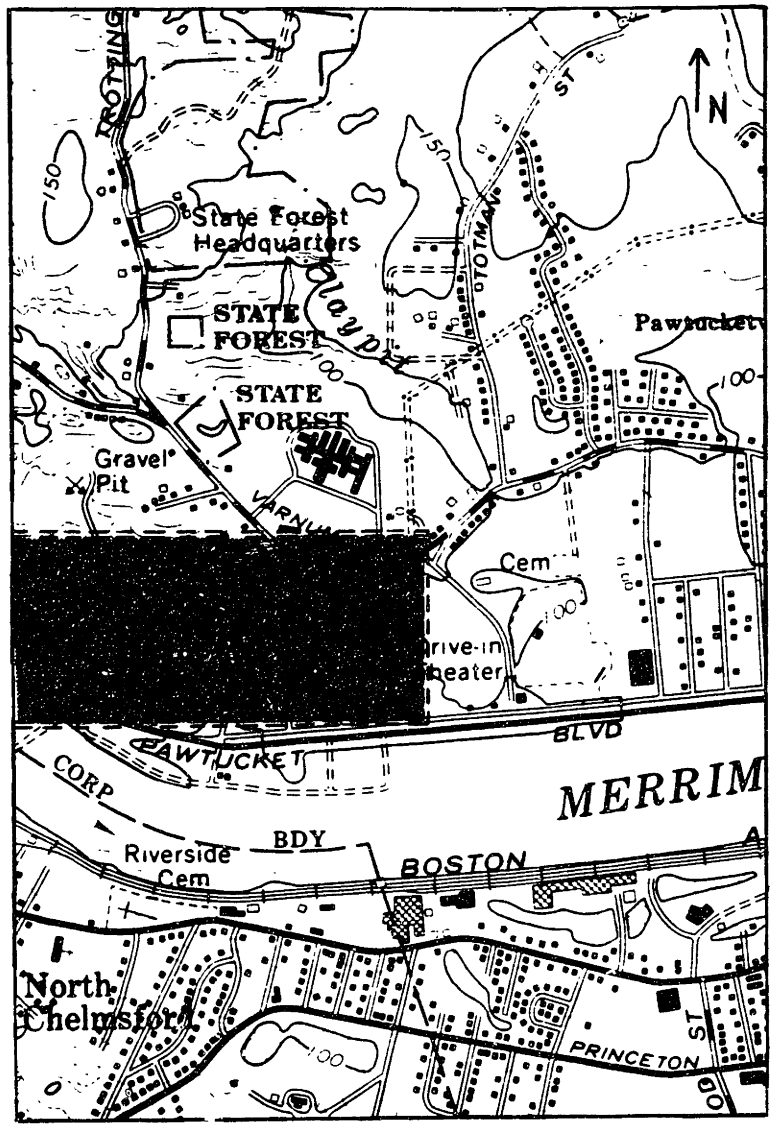

Figure 5-1: Location of the Lowell Sites (USGS Lowell Quadrangle)

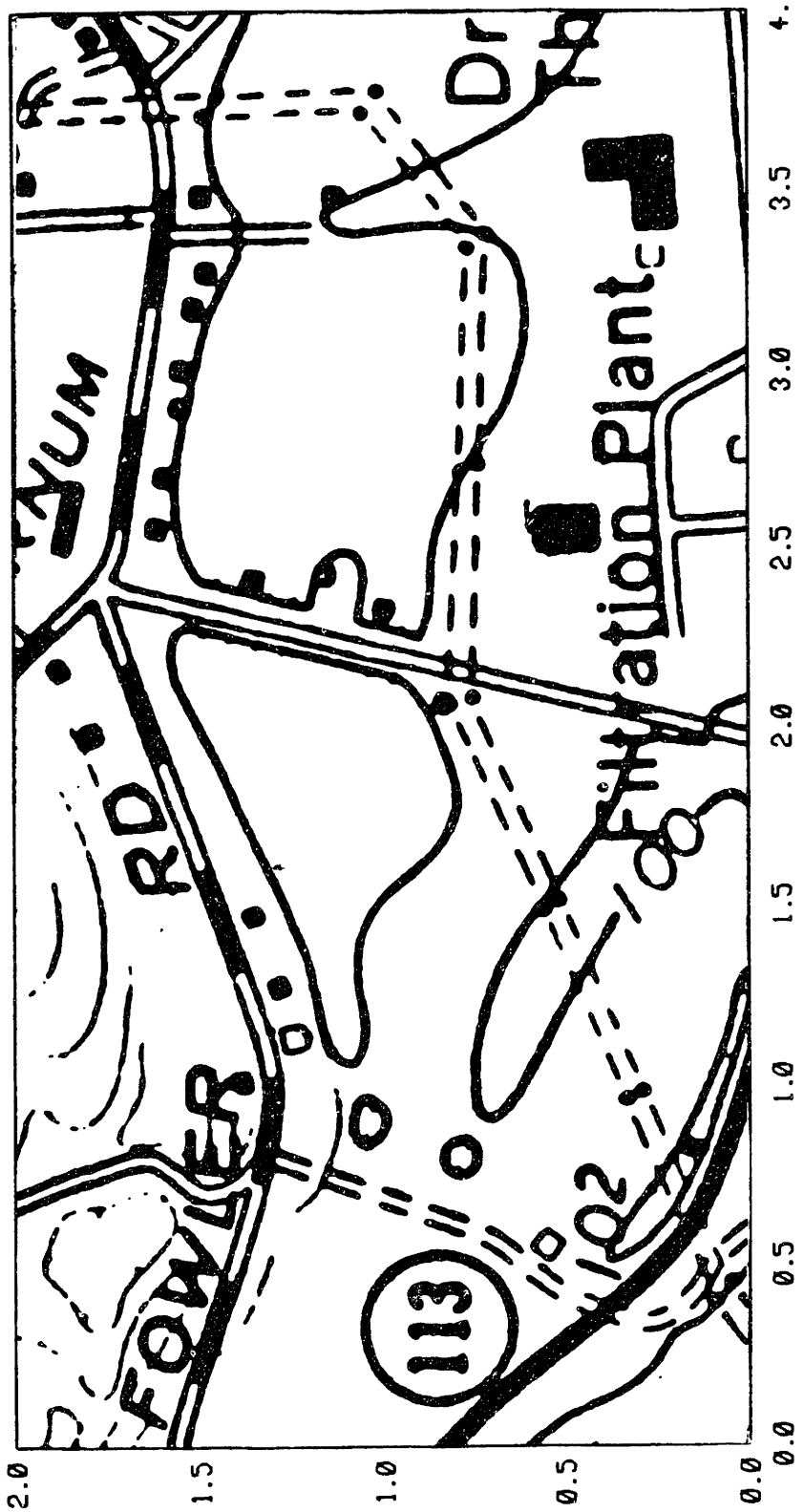

Figure 5-2: Reference Axes (Scale in 1000 feets)

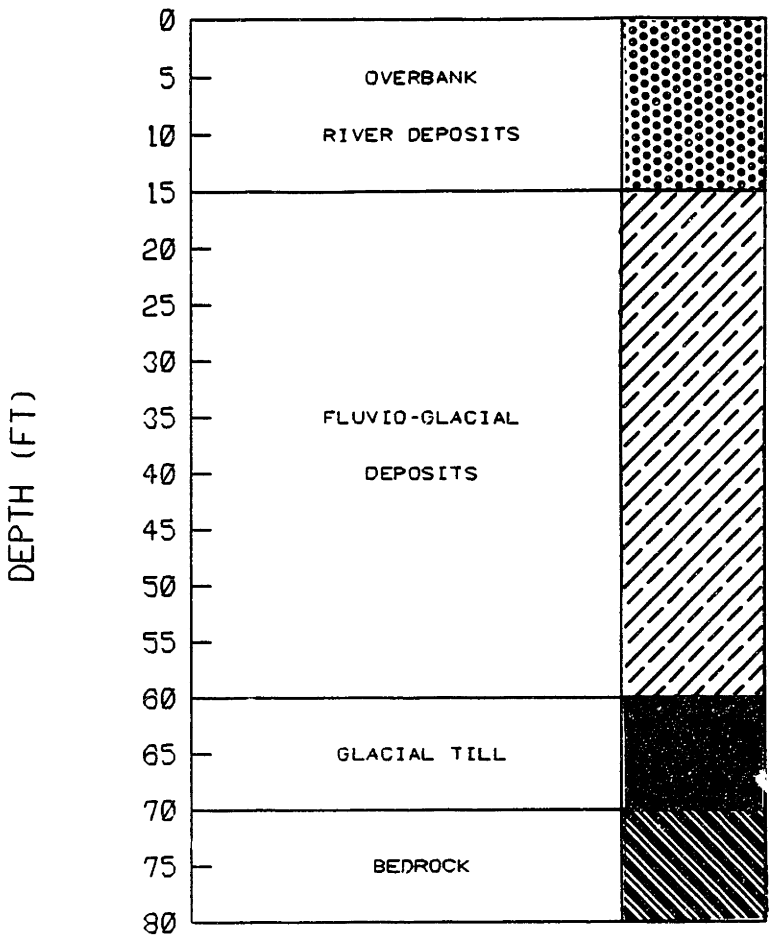

Figure 5-3: Geologic Profile, Lowell

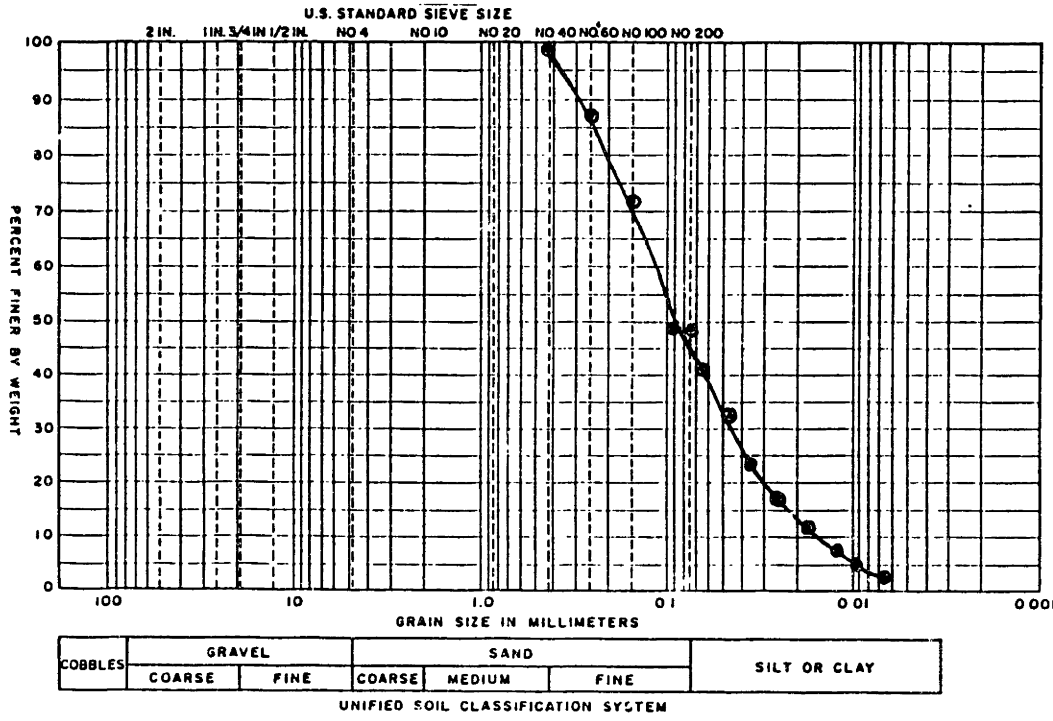

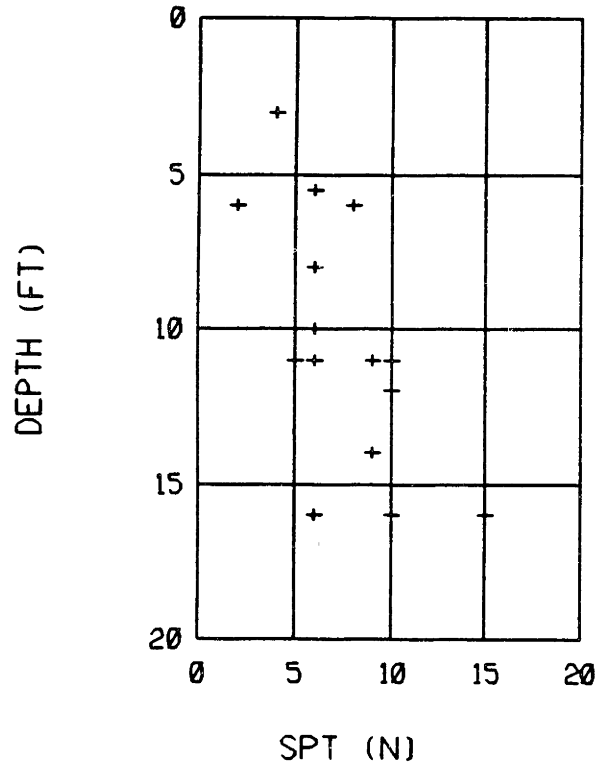

Figure 5-4: OverBank River Deposits, Lowell

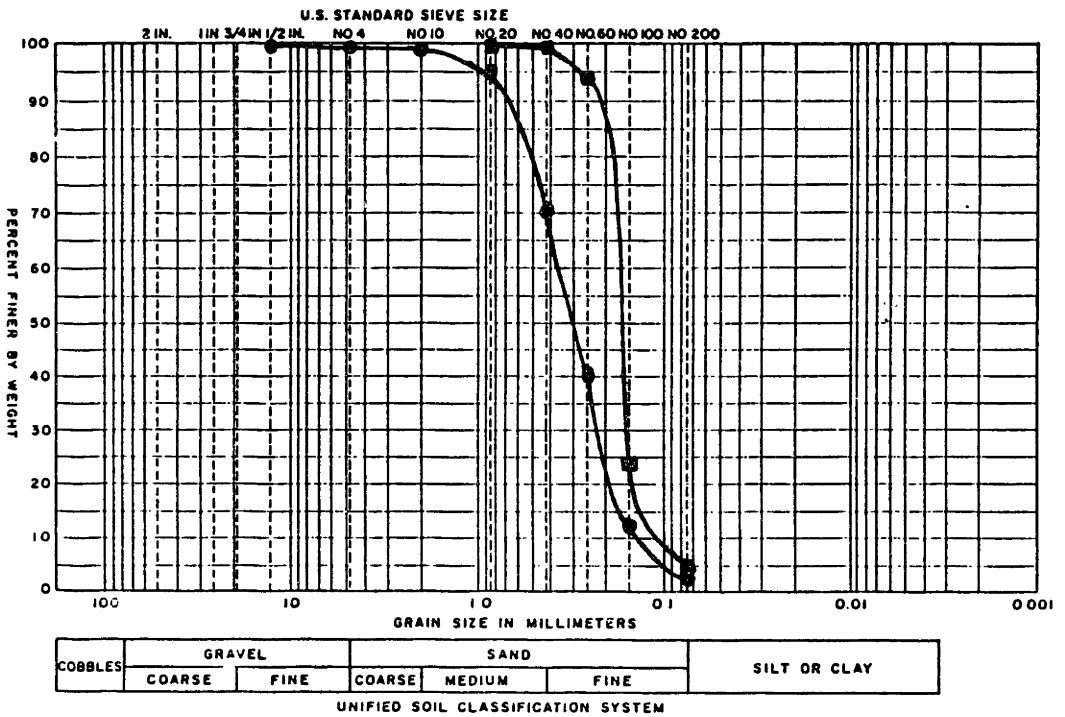

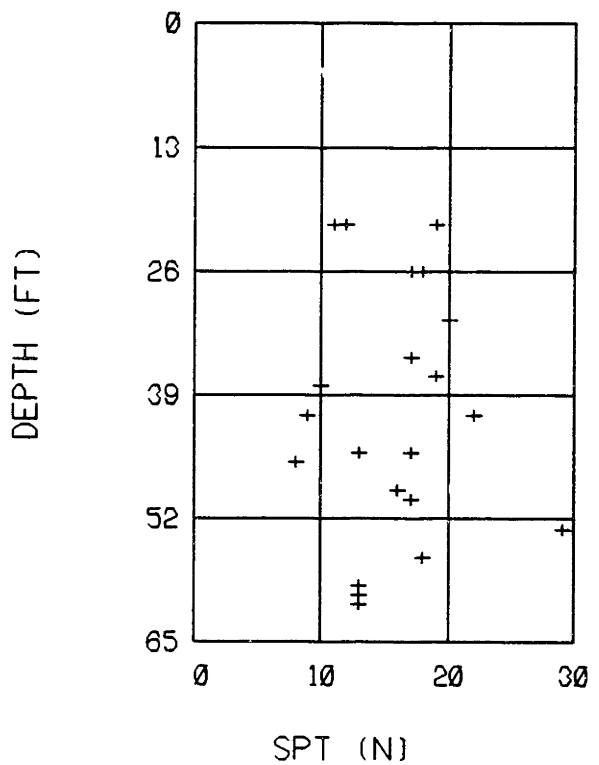

Figure 5-5: Fluvioglacial Deposits, Lowell

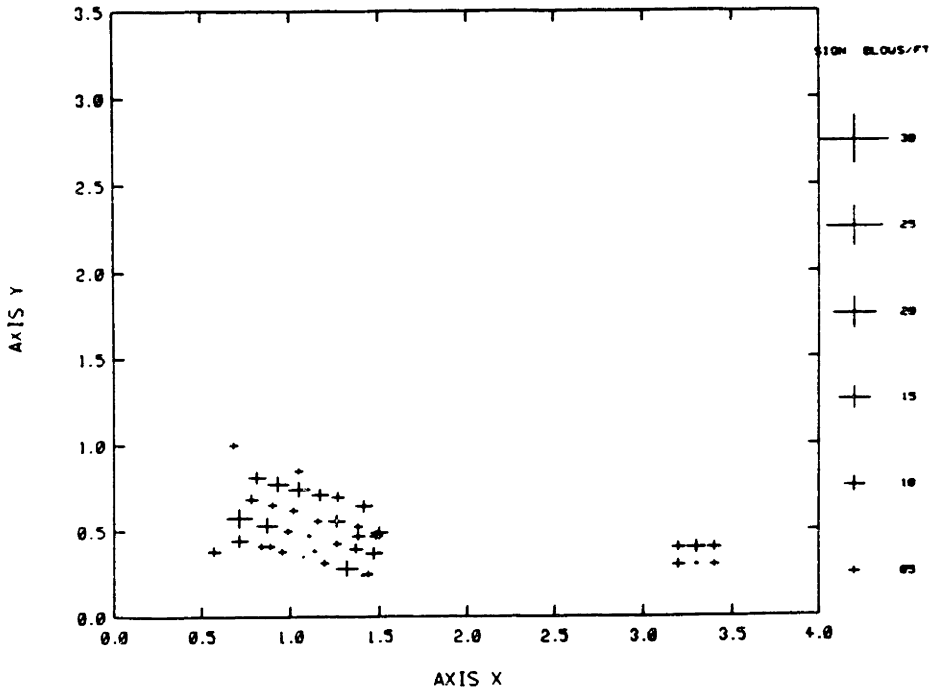

Figure 5-6: Map of Uncorrected Blow Count, Layer I

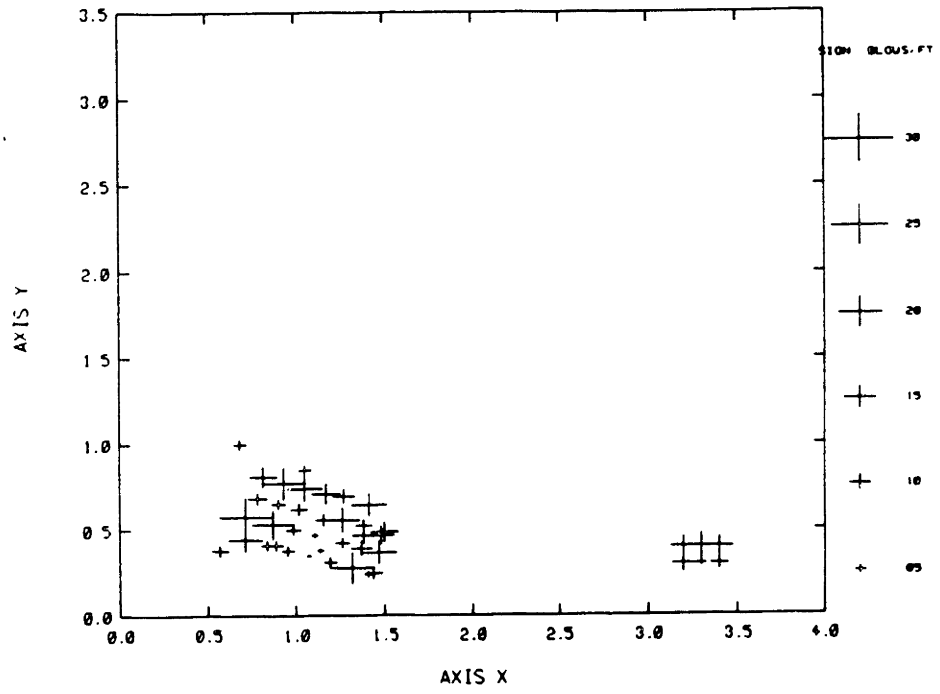

Figure 5-7: Map of Corrected Blow Count, Layer I

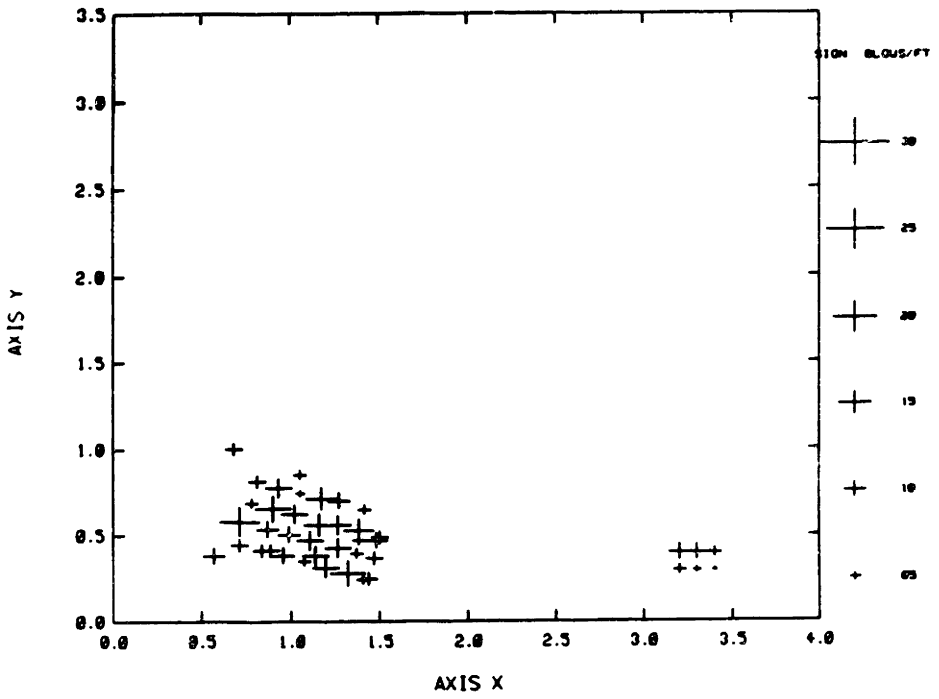

Figure 5-8: Map of Uncorrected Blow Count, Layer II

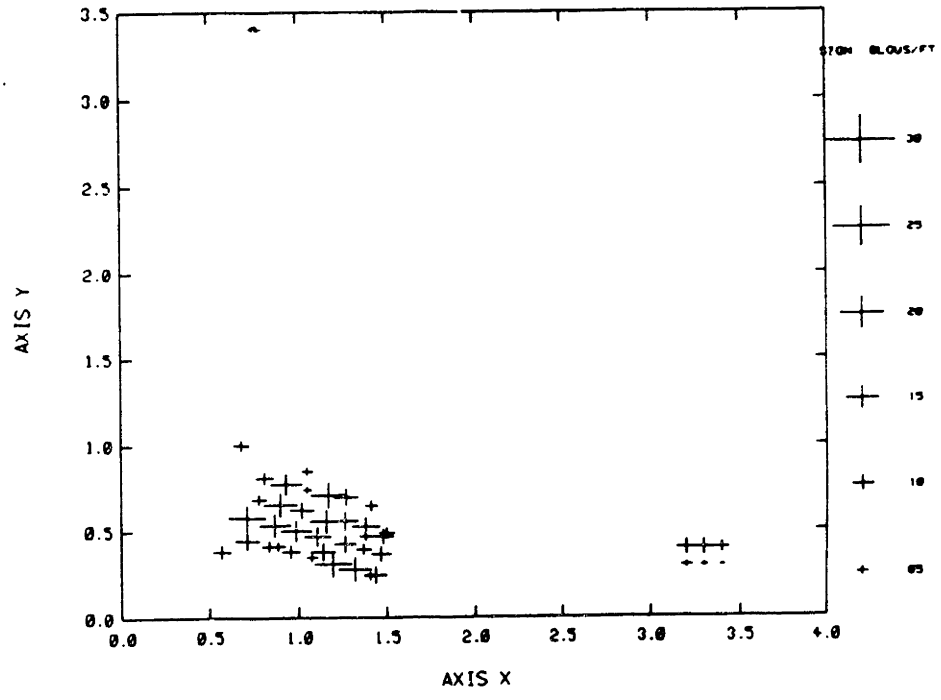

Figure 5-9: Map of Corrected Blow Count, Layer II

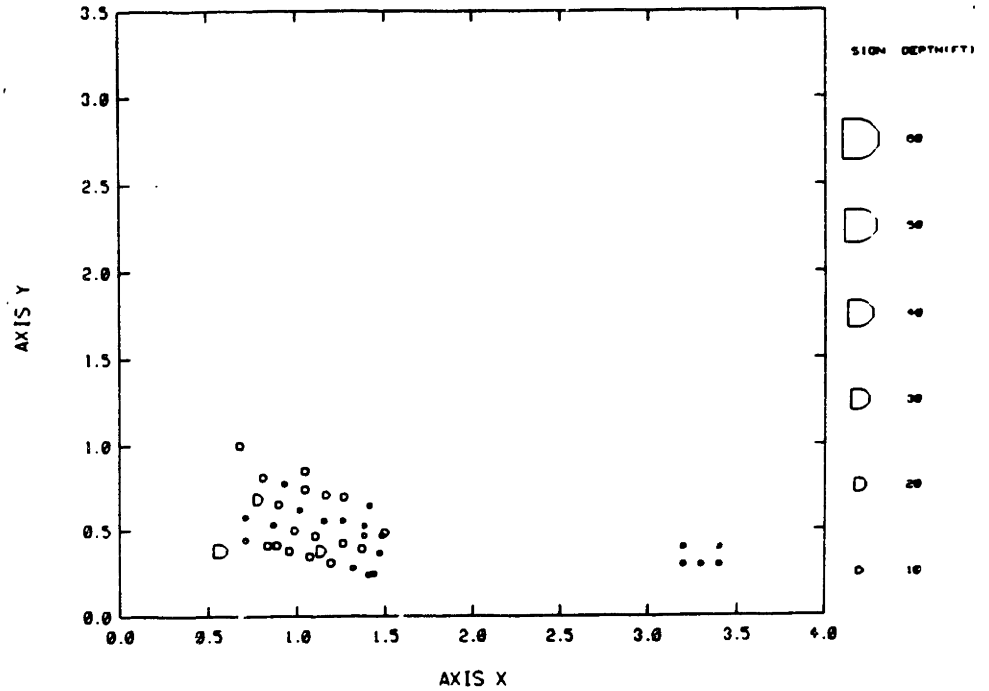

Figure 5-10: Map of Critical Depth, Layer I

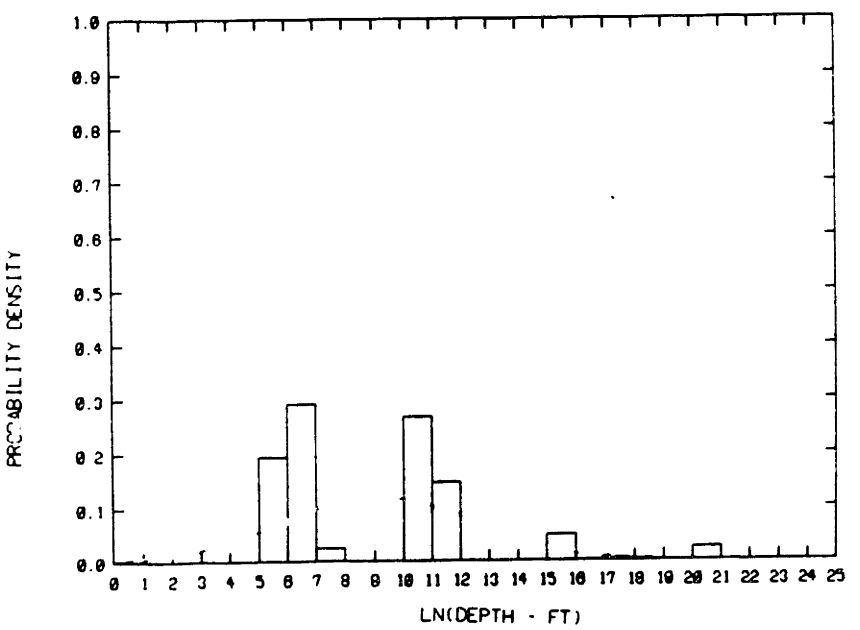

Figure 5-11: Histogram of Critical Depth, Layer I

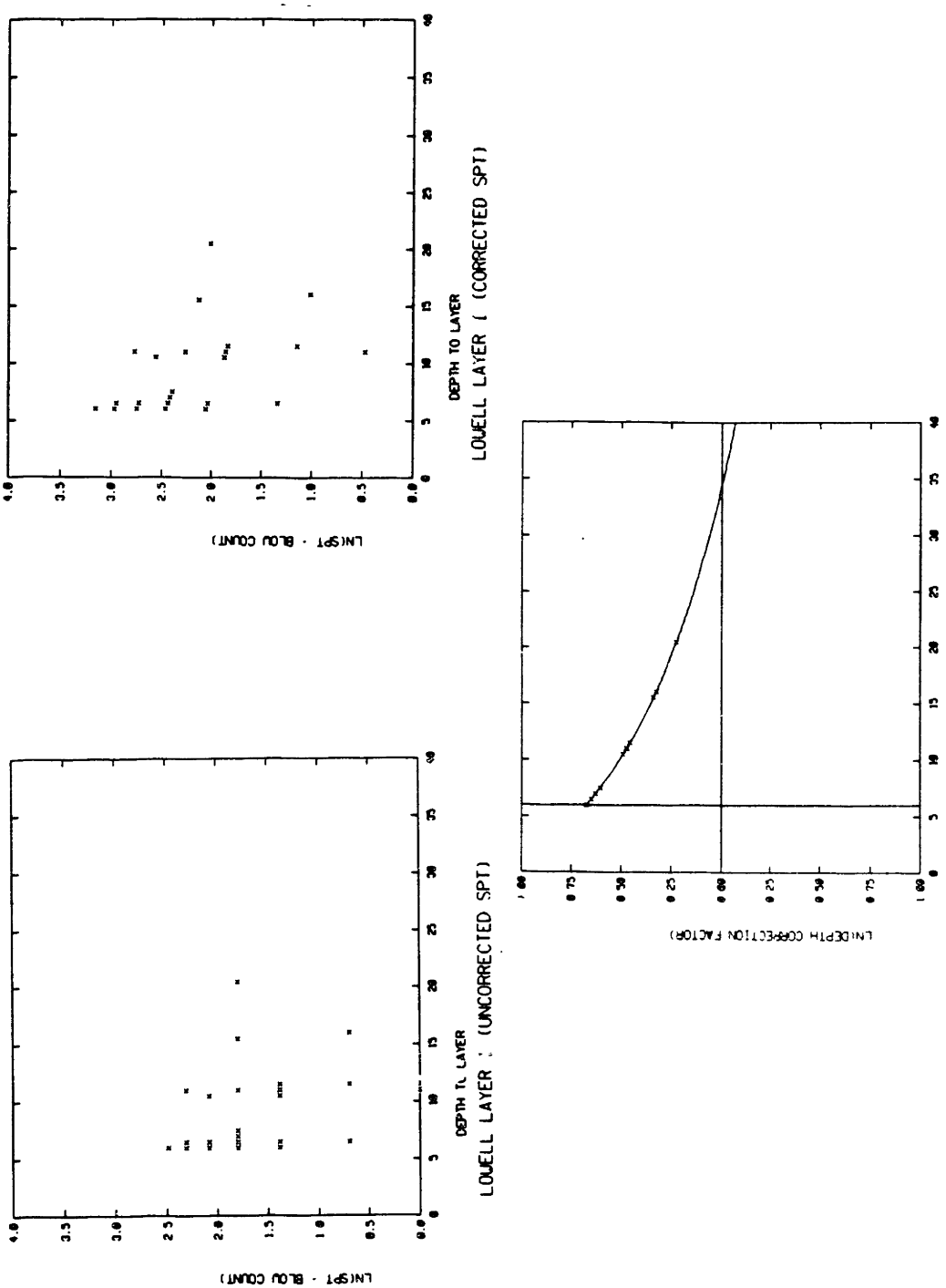

Figure 5-12: N and N_1 Depth Dependence, Layer I

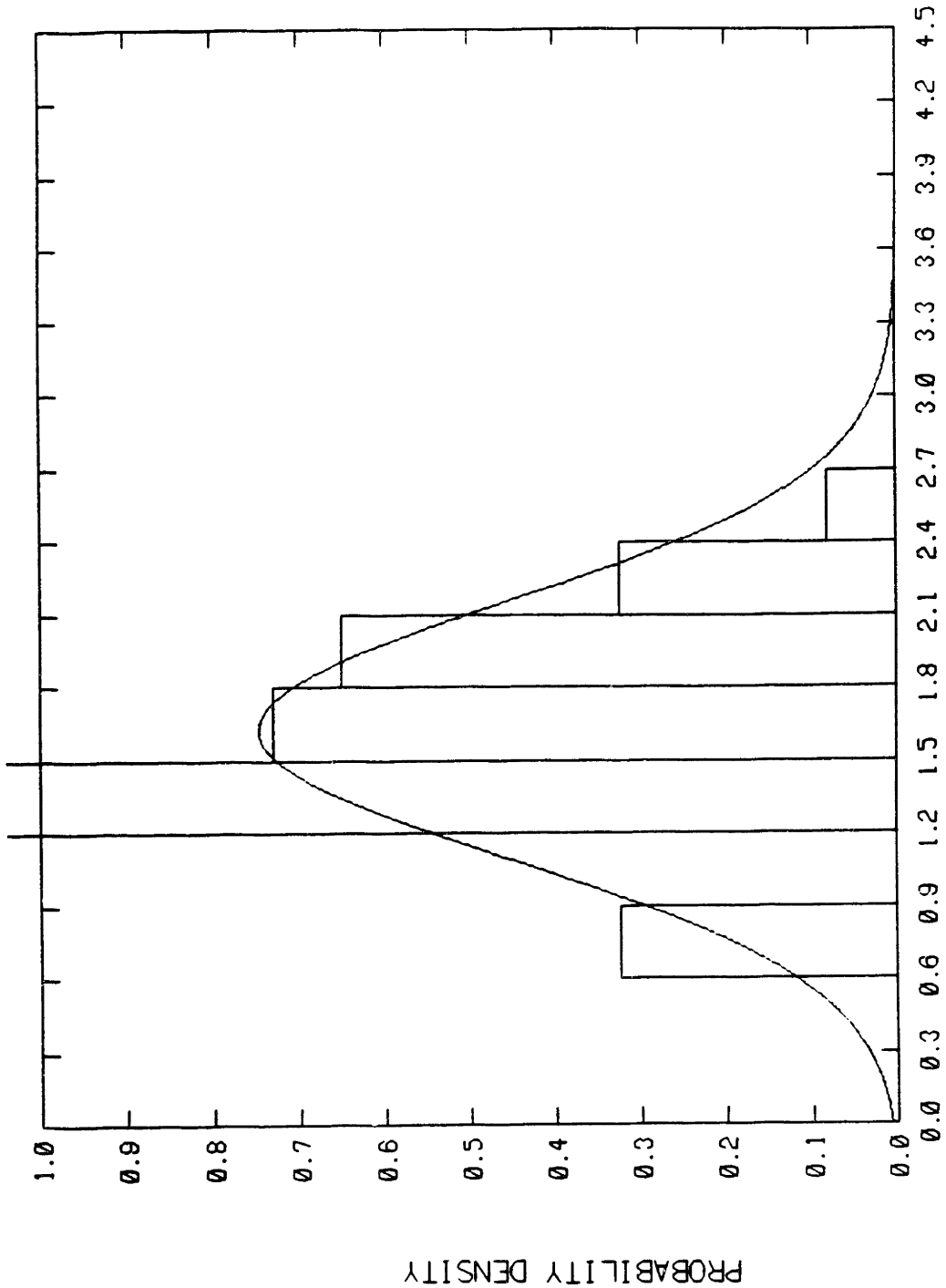

Figure 5-13: Distribution of ln(N), Layer I

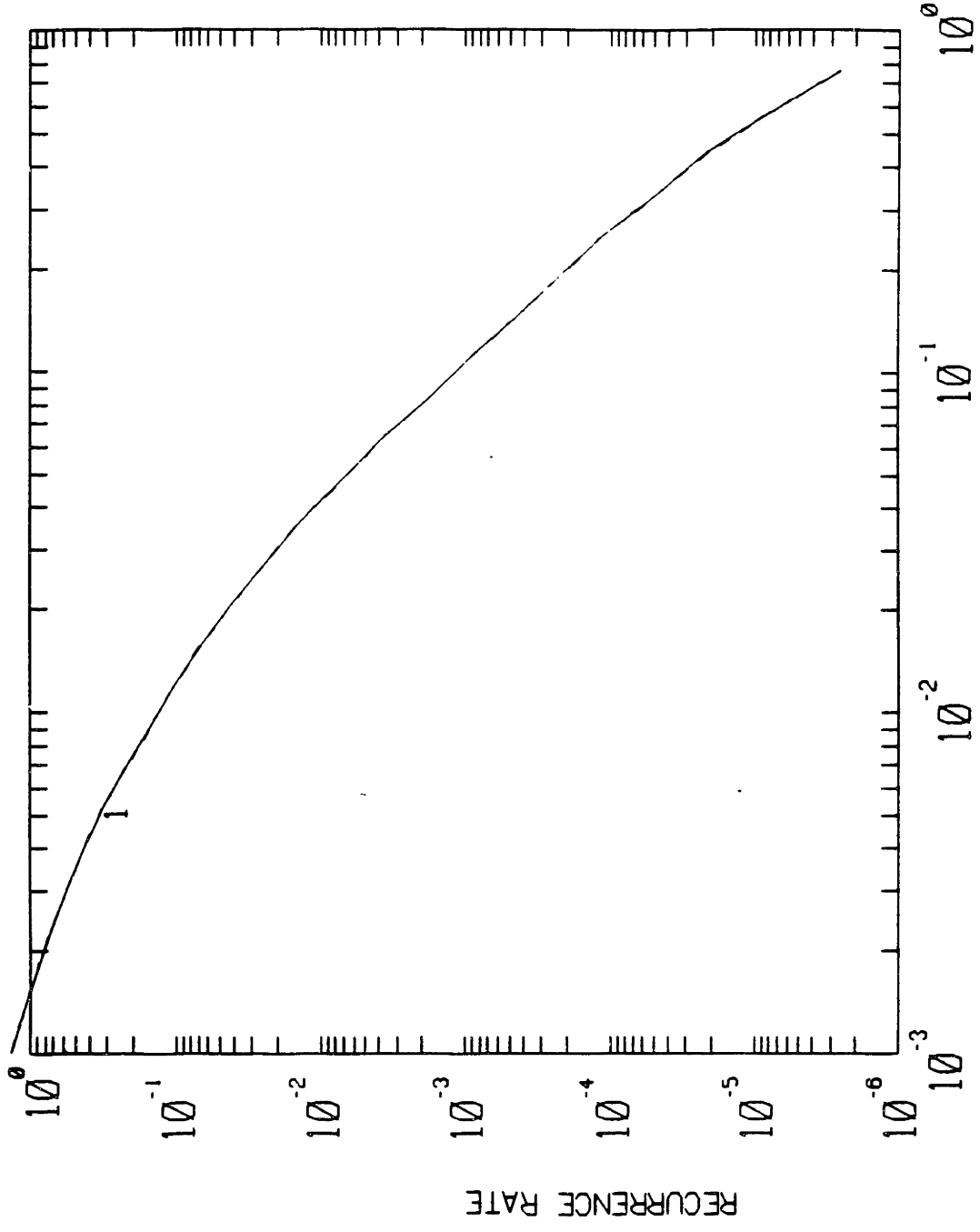

Figure 5-14: Seismic Hazard Curve, Lowell

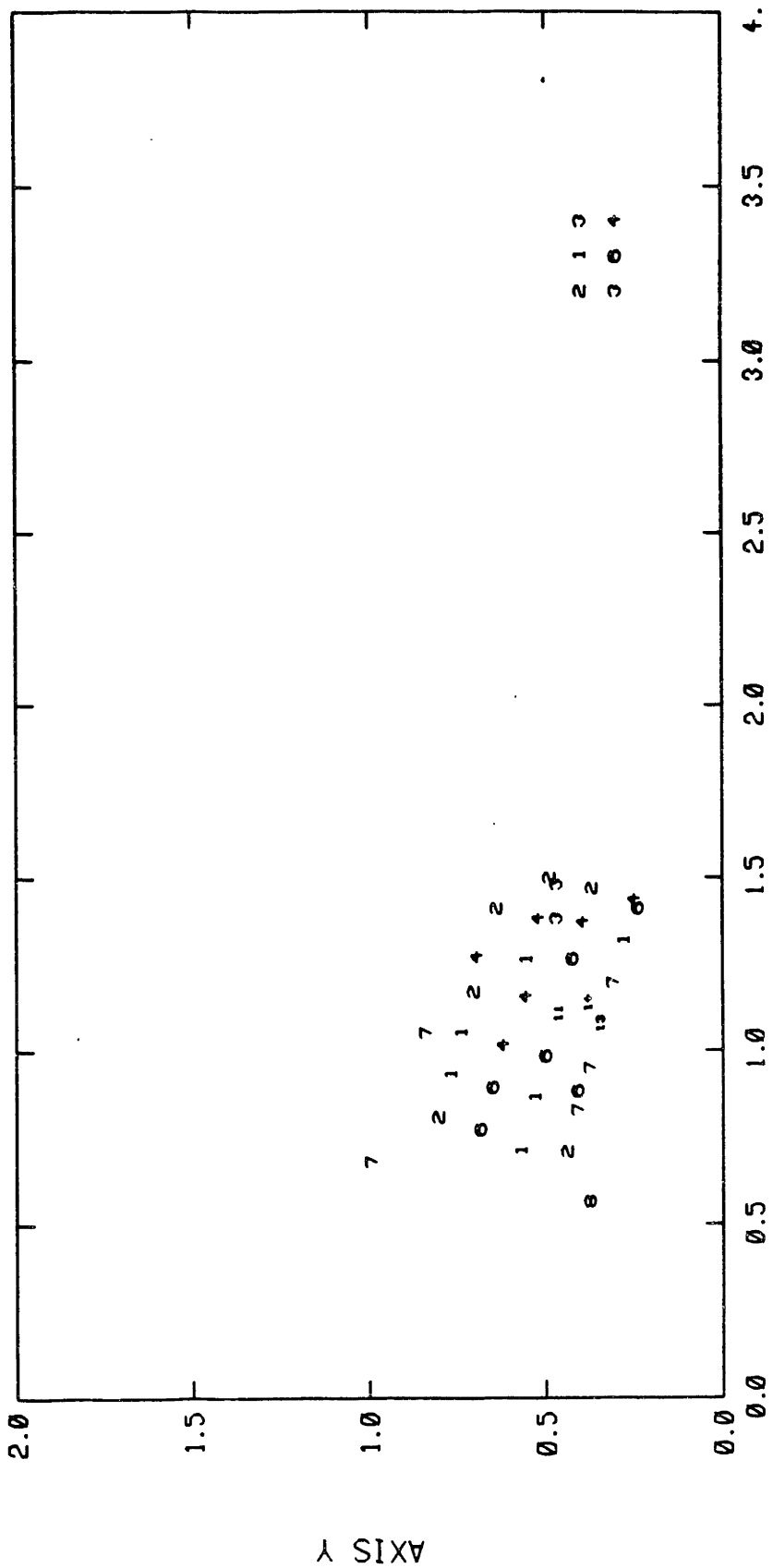

Figure 5-15: Liquefaction Recurrence Rates x10^4 at Data Points, Layer I

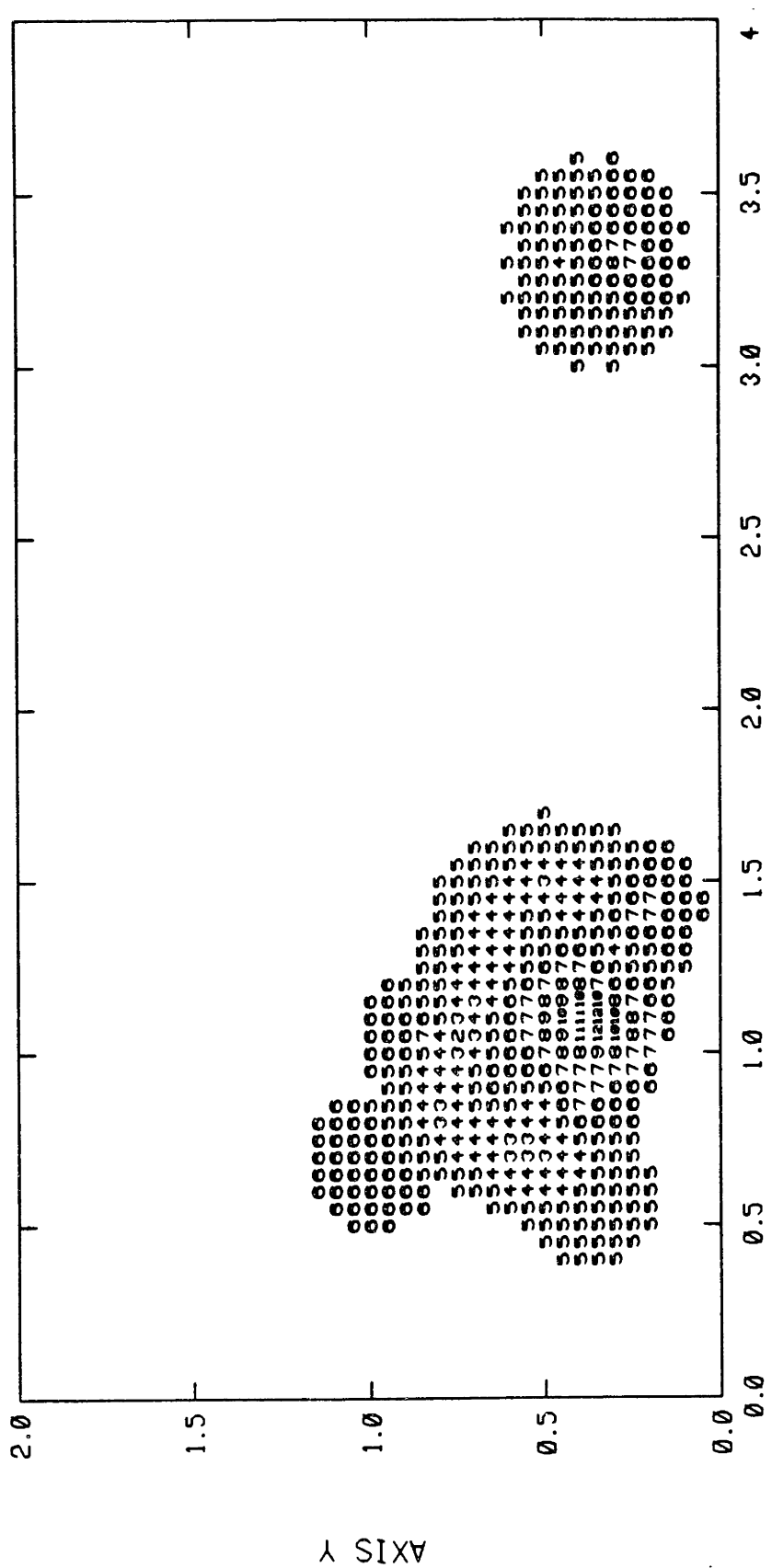

Figure 5-16: Liquefaction Hazard Map, Layer I (Rate x10^4/year)

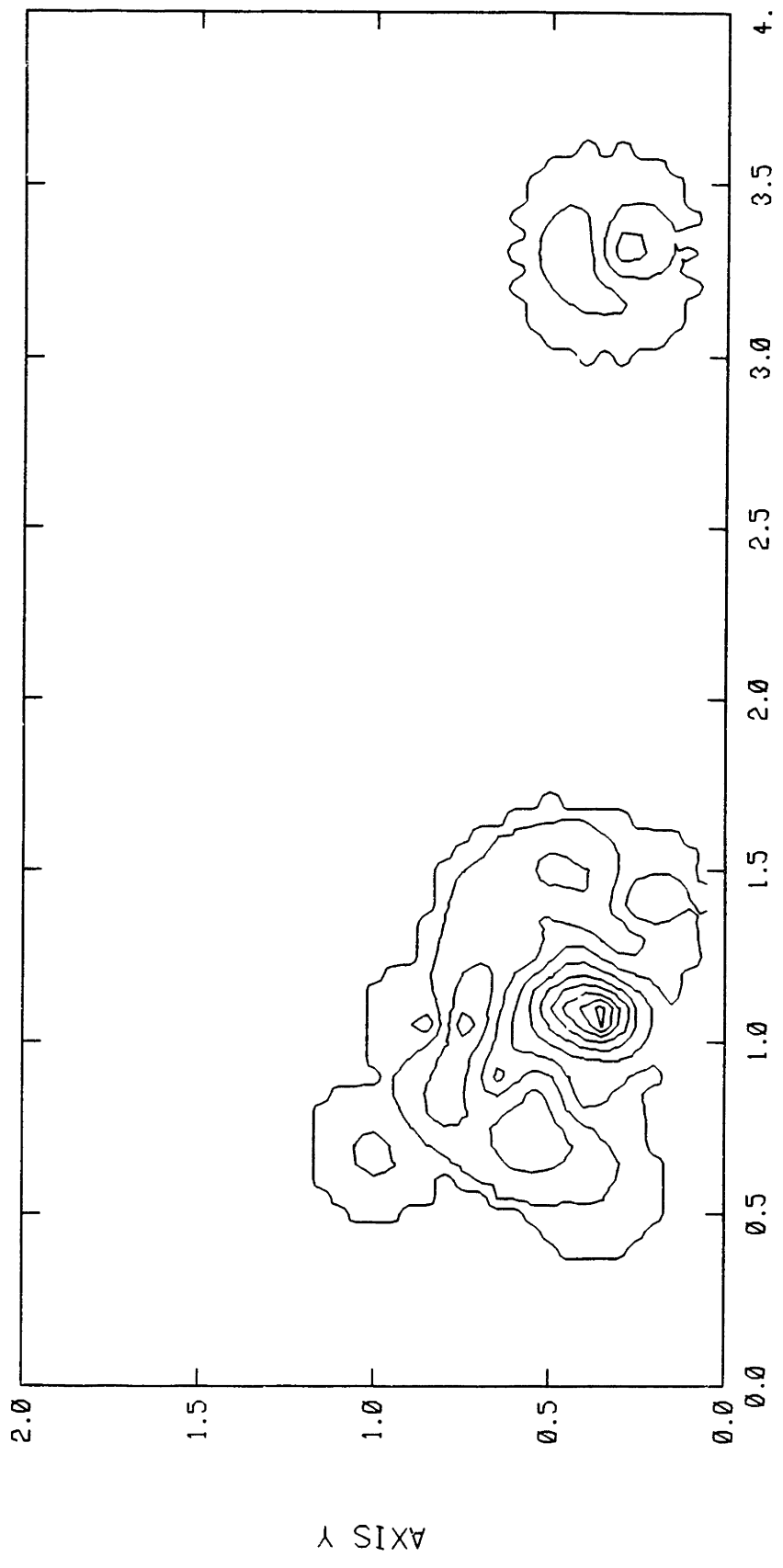

Figure 5-17: Liquefaction Hazard Map, Layer I (Contours of Rates)

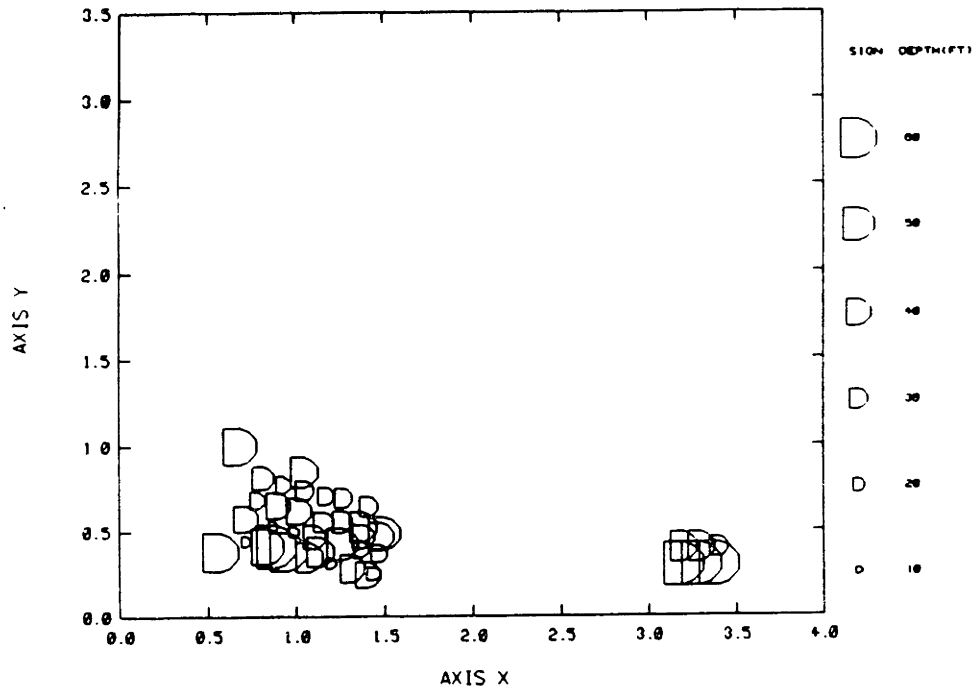

Figure 5-18: Map of Critical Depth, Layer II

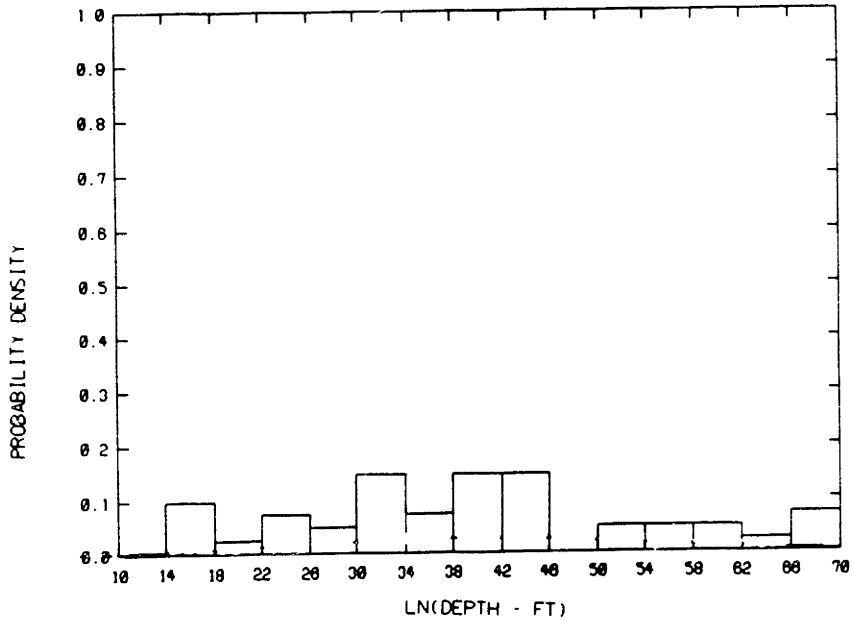

Figure 5-19: Histogram of Critical Depth, Layer II

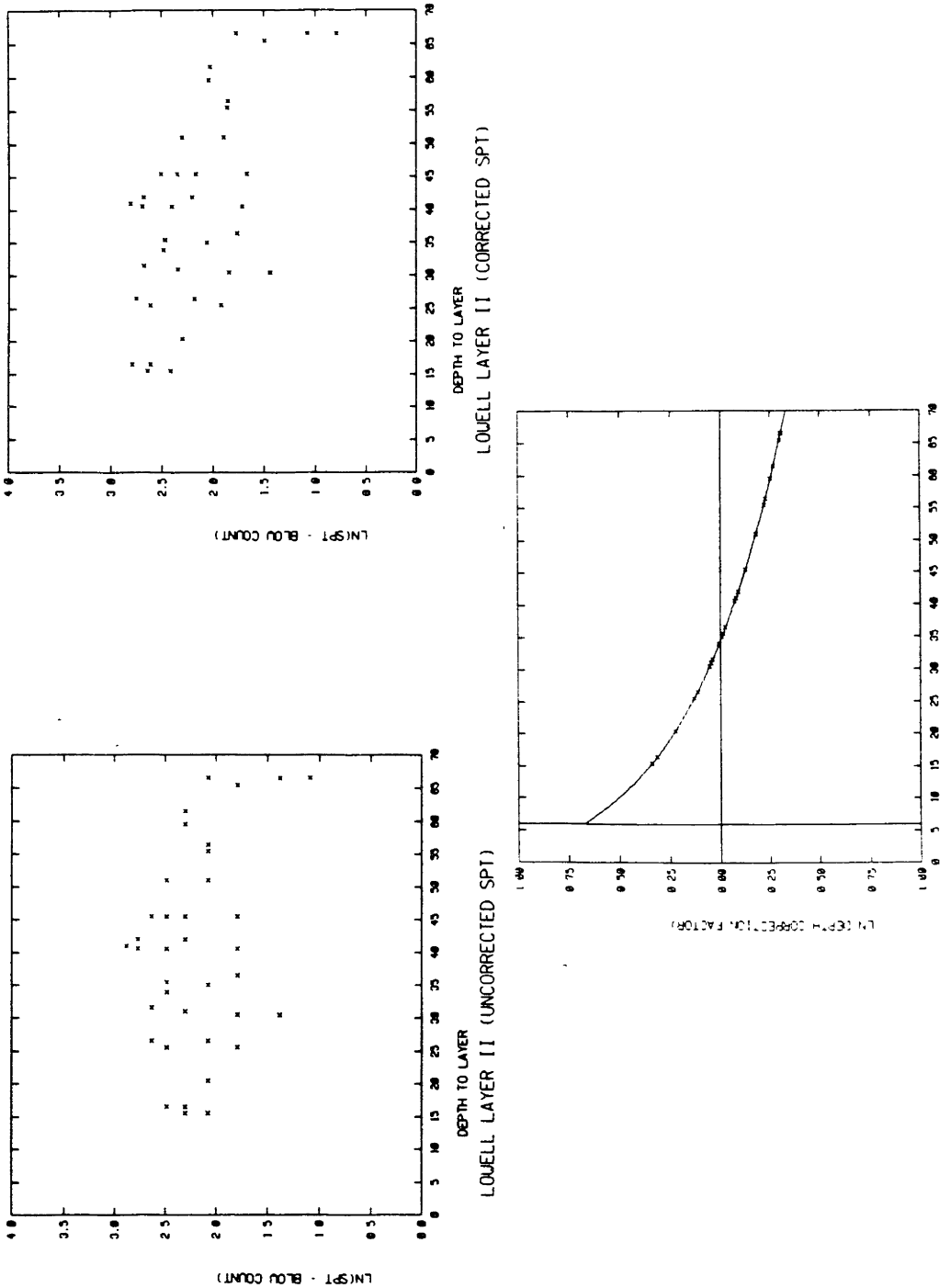

Figure 5-20: N and N_1 Depth Dependence, Layer II

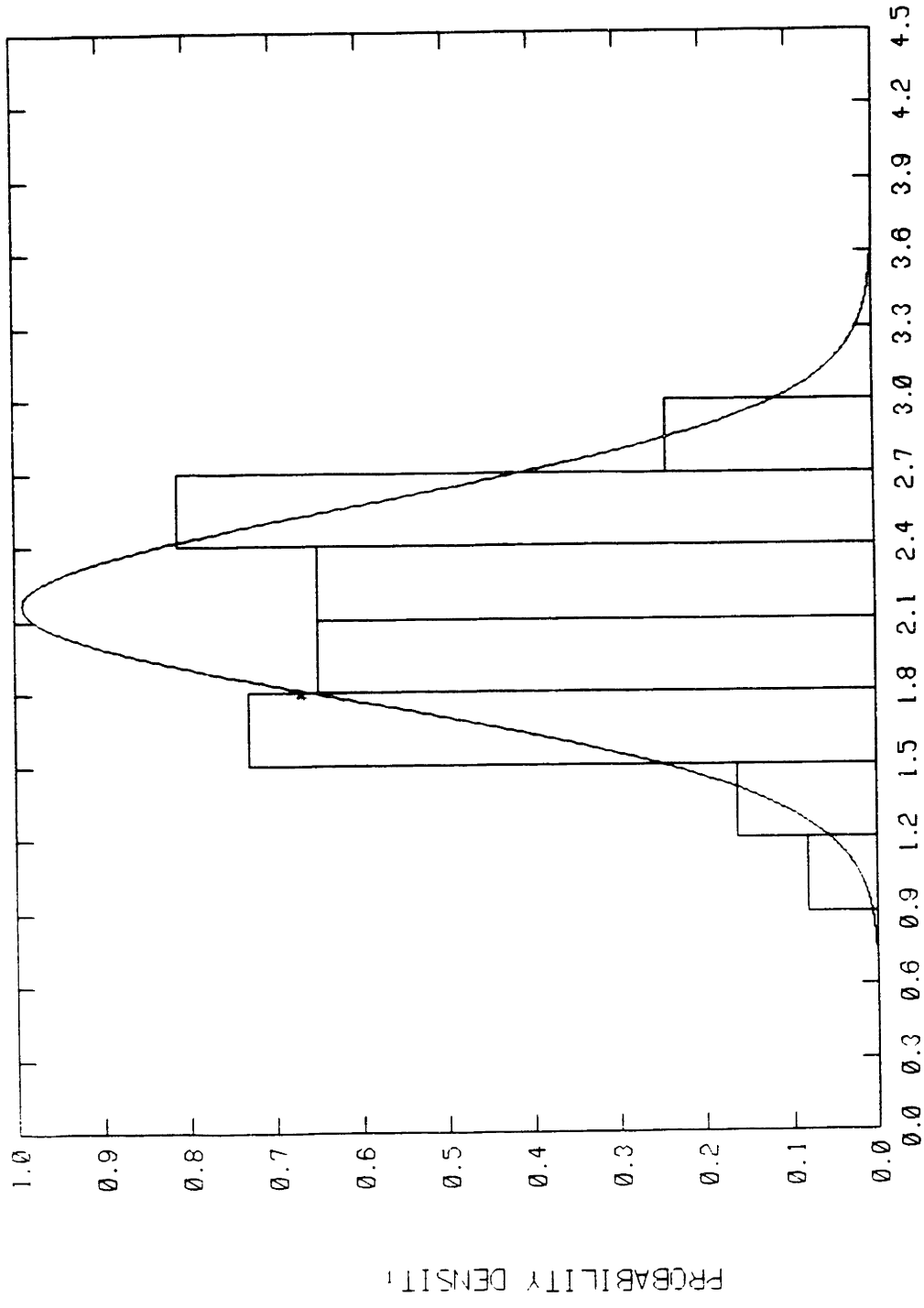

Figure 5-21: Distribution of ln(N), Layer II

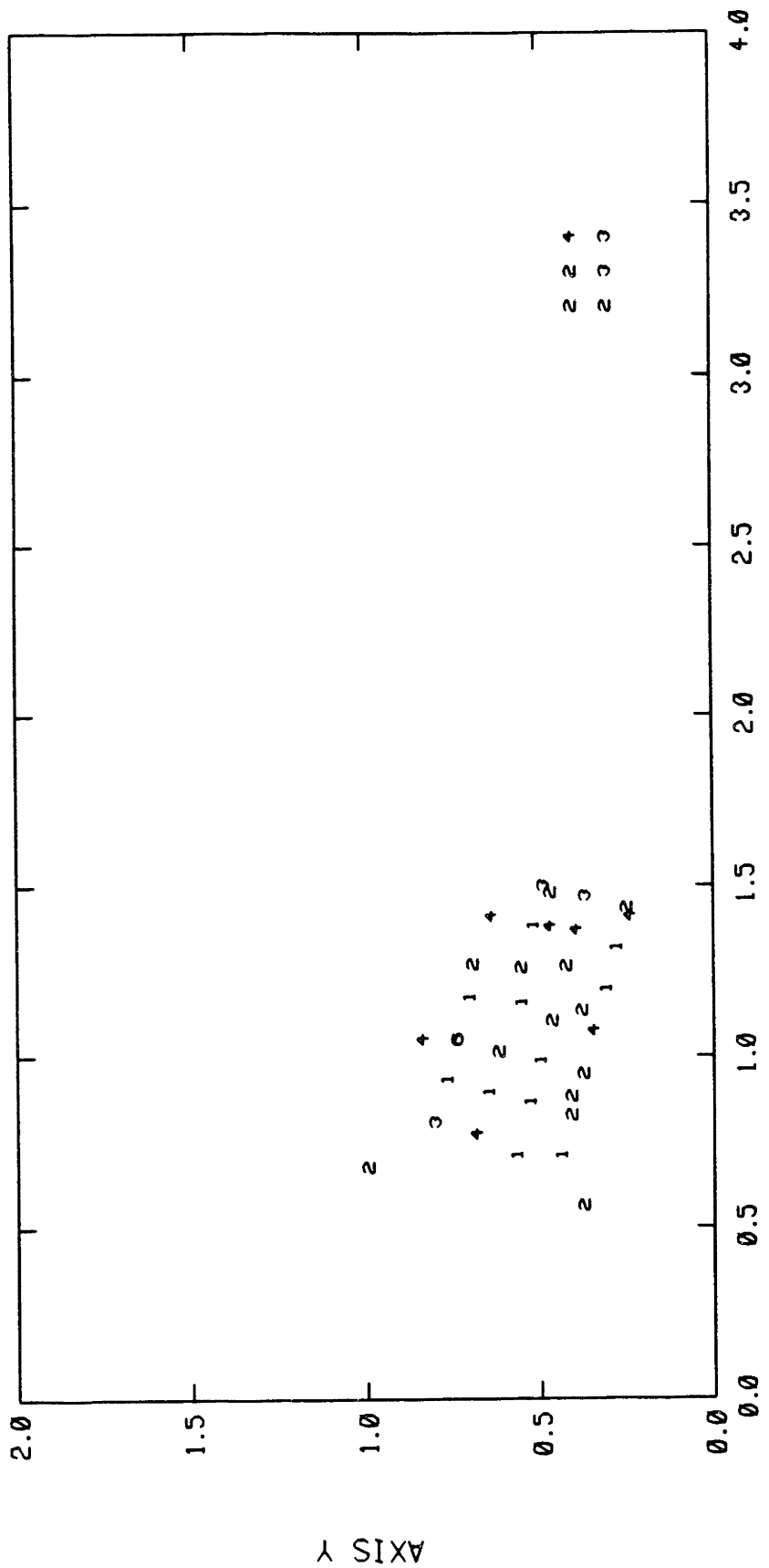

Figure 5-22: Liquefaction Recurrence Rates x10^4 at Data Points, Layer II

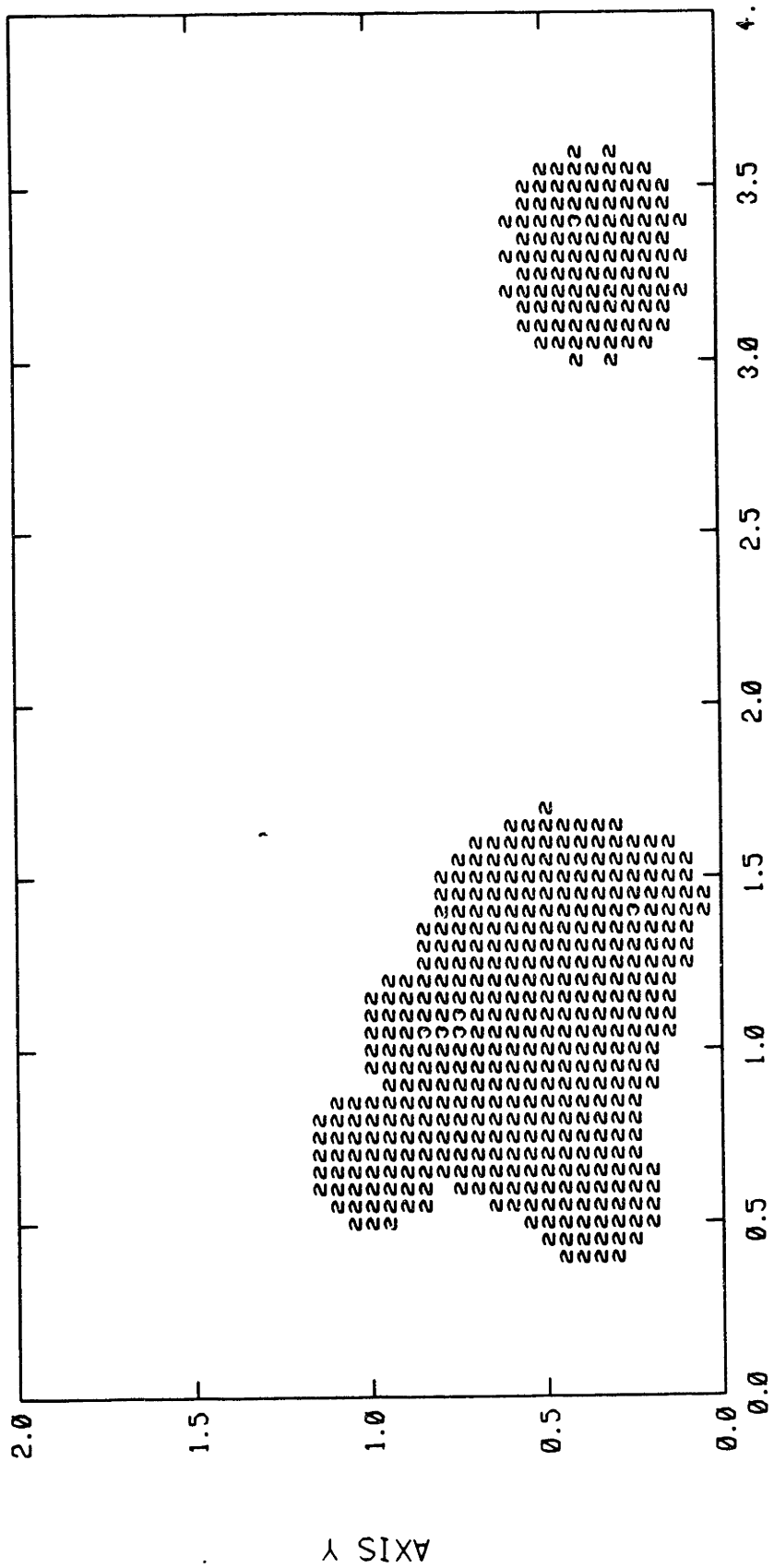

Figure 5-23: Liquefaction Hazard Map, Layer II (Rate x10^4/year)

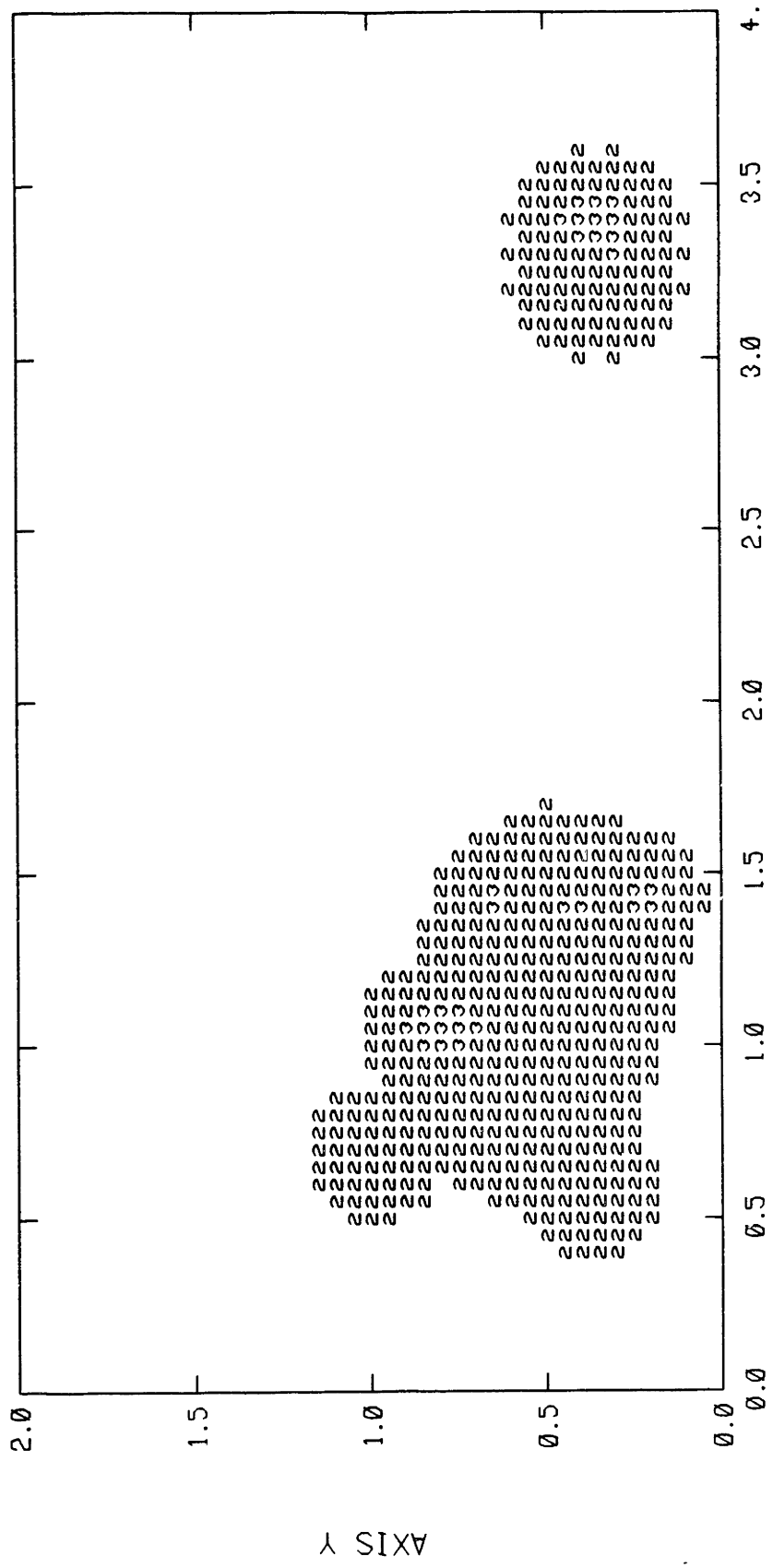

Figure 5-24: Liquefaction Hazard Map, Layer II (Extension Factor: 10)

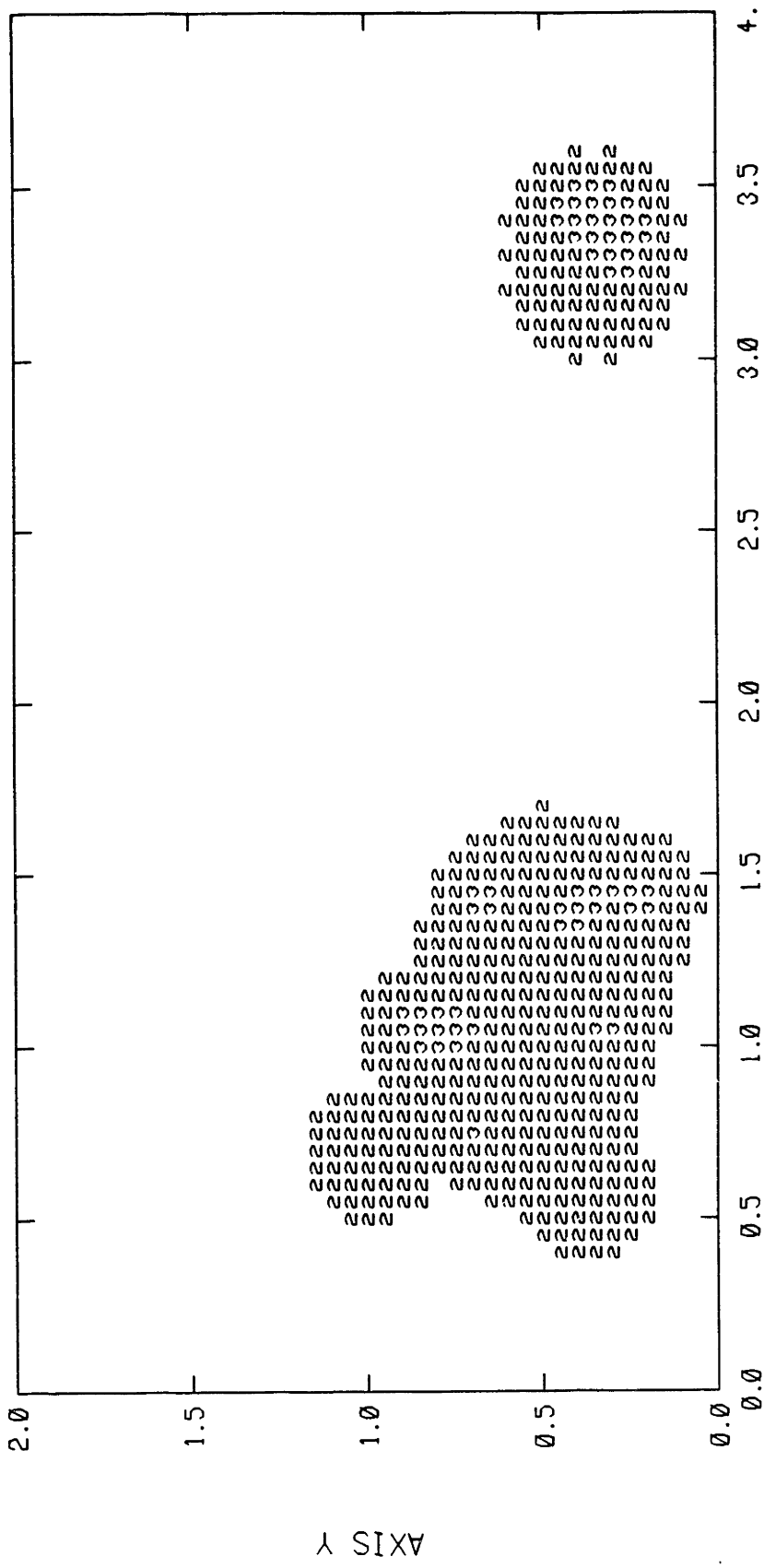

Figure 5-25: Liquefaction Hazard Map, Layer II (Extension Factor: 5)

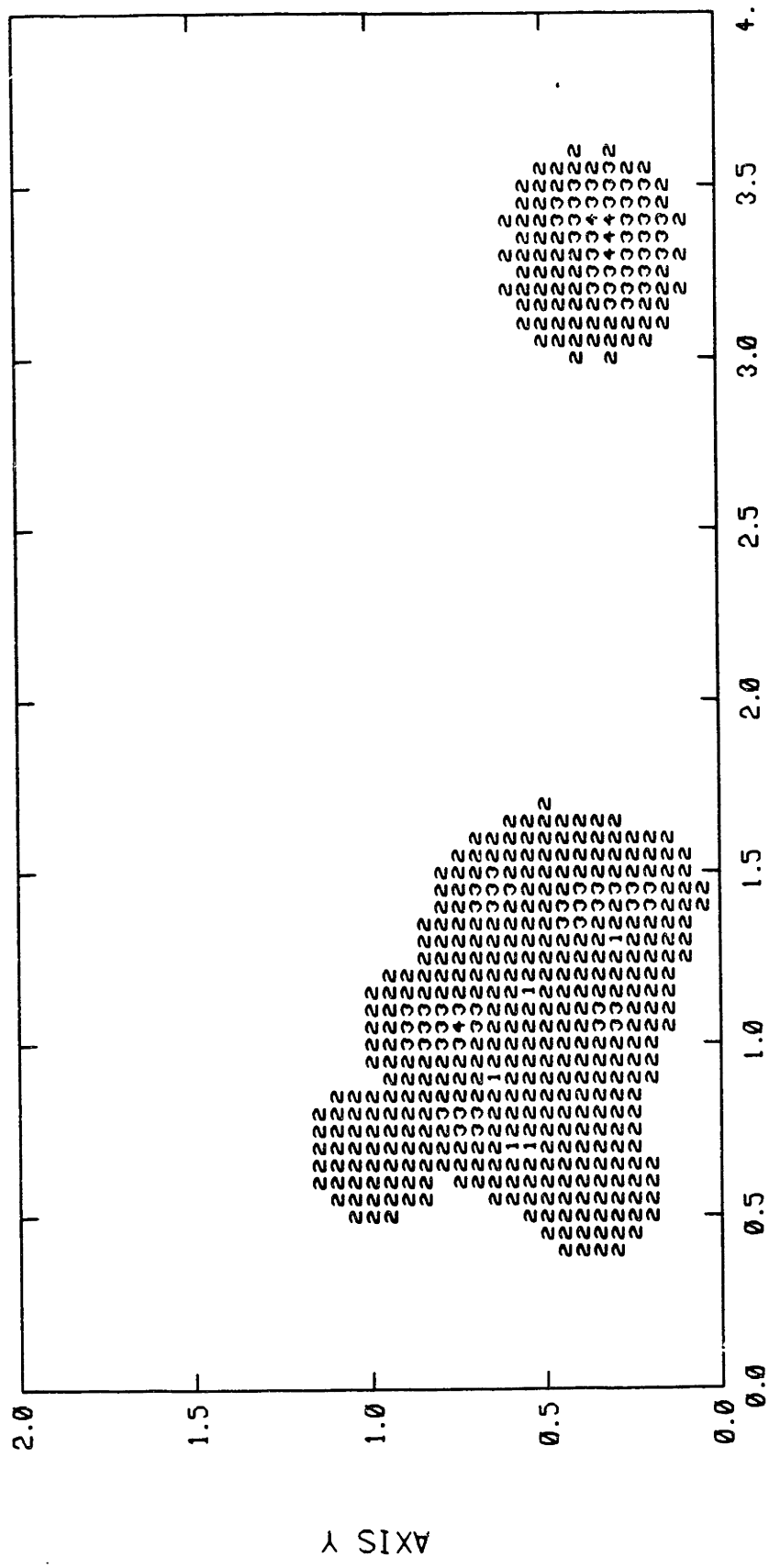

Figure 5-26: Liquefaction Hazard Map, Layer II (Extension Factor: 1)

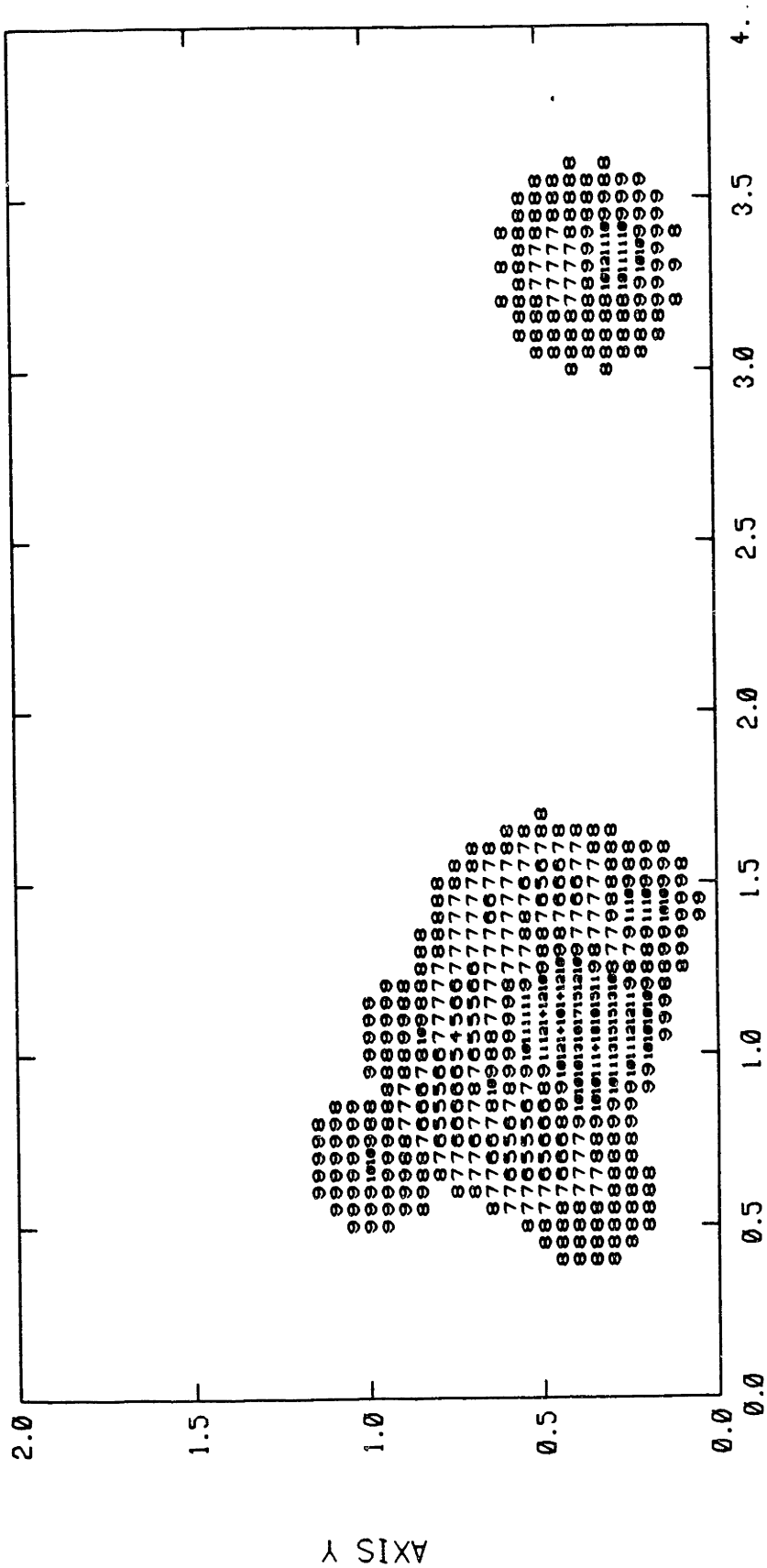

Figure 5-27: Liquefaction Hazard Map, Layer I, M=6.5

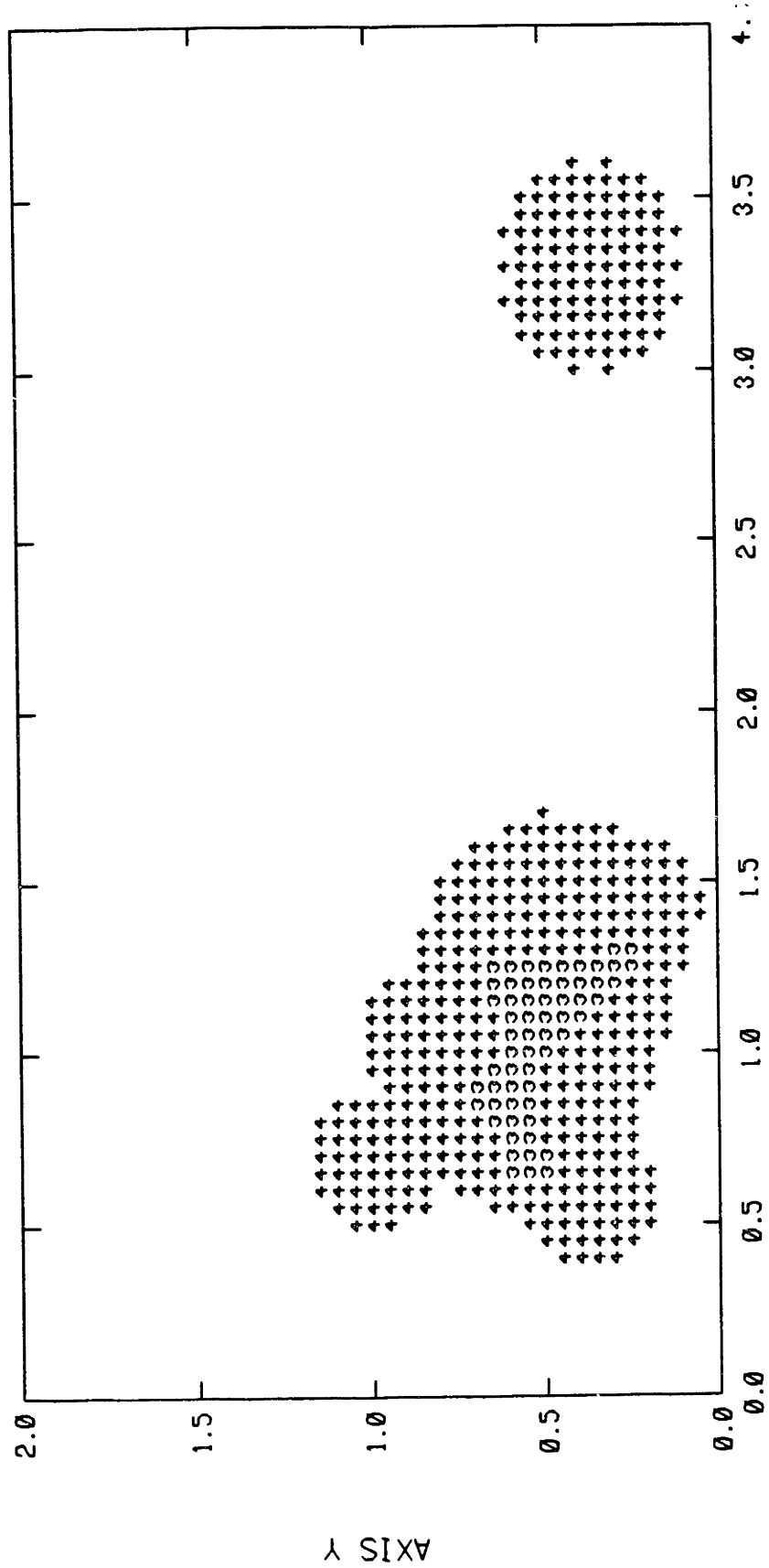

Figure 5-28: Liquefaction Hazard Map, Layer II, M=6.5

Chapter 6

LIQUEFACTION HAZARD EVALUATION of GLACIOMARINE DEPOSITS in NEWBURYPORT, MASSACHUSETTS

6.1 Introduction

In this chapter we develop a new technique to evaluate the liquefaction hazard in deposits where liquefaction is known to have occurred during a ground shaking event. The only information needed for this evaluation is the magnitude and epicentral location of the earthquake, and the extent of ground failure. No insitu testing is strictly necessary. The method is also useful to calibrate to local conditions the liquefaction probability models developed by Liao(1986) and used in chapters 4 and 5.

Later in the chapter, the methodology is applied to Newburyport glaciomarine deposits which are known to have liquefied during the 1727 earthquake.

6.2 The Concept

In order to evaluate liquefaction potential at a site, one needs information on soil type and soil resistance to liquefaction, and on seismicity and ground motion attenuation. The main problem in evaluating the liquefaction potential is how to assess the resistance of the soil deposit to liquefaction. In the analysis of chapters 4 and 5 we use the SPT data as an indicator of liquefaction resistance. In other approaches to liquefaction (see review in chapters 2 and 3), measures of resistance are derived from laboratory or other insitu tests.

These tests provide only limited information on soil susceptibility to liquefaction. A possibly more reliable indicator of the liquefaction resistance of a deposit is its behavior during past earthquakes.

From a review of the historical records or from borehole profiles one can sometimes determine whether a deposit has or has not liquefied during past earthquakes of known intensity. It is easy to understand how important such a piece of information is, especially for deposits that are known to have liquefied under moderate earthquakes or have not liquefied under intense ground shaking.

There might be redundancy in the available information, for example because the strength of the soil can be determined either from available test results or from known performance during historical earthquakes. One should make use of this redundancy to better constrain model parameters and therefore generate more accurate liquefaction hazard estimates. The adjustment of the models can be performed in an iterative fashion until the predictions are compatible with all the input data.

6.3 Methodology

A possible use of historical data on liquefaction is as follows:

Suppose that, for a given historical earthquake one can estimate the fraction of surface area that has experienced ground failure (γ), and the peak ground acceleration (PGA) at the site. The model described in chapters 4 and 5 gives the probability of ground failure P_L as a function $f(N_1,PGA)$ of the blow count number N_1 and of PGA. By setting P_L equal to γ, one can estimate N_1 for the given value of PGA. Then, from the estimate of N_1 and the seismic hazard curve at the site, one can evaluate the recurrence rate of liquefaction at the site. Fig. 6-1 shows a flow chart of the proposed method. In most cases, the parameters used will not be known exactly. For example, PGA may be estimated with

uncertainty from an attenuation equation using a known magnitude and epicentral distance. As a consequence, N_1 is itself not determined exactly.

Historical information can be used to calibrate the liquefaction model. For example, if for a given earthquake and a given site one knows exactly PGA, γ, and N_1, then one can adjust the coefficients of the liquefaction probability model $P_L(PGA,N_1)$ so that it is consistent with the observations. If the site has experienced partial or total liquefaction more than once, then one would have more data points to calibrate the liquefaction probability model and better constrain its parameters.

In our method there is an inherent assumption that the N values measured after historical earthquakes reflect the strength of the deposit at the time of the event. This is not necessarily true. During strong earthquakes, the soil undergoes large strains which, in the case when liquefaction occurs, cause changes in relative density and soil particle configuration. The net result may be an increase in liquefaction resistance. When dealing with multiple liquefaction events one can account for the change in N by, for example, introducing to the model a function which modifies N after every event. Such function is not developed here.

6.4 Application to Newburyport Glaciomarine Deposits

6.4.1 Site Geology

The local geology has been described in detail by Tuttle et al. (1987), it includes as main features a layer of glaciomarine sand overlain by glaciomarine clay. The clay is relatively impermeable and can be laminated with very fine sand 1-2m in thickness. In some areas, the ground water is artesian because of the impermeable clay cap. Fig. 6-2 shows a typical geologic crossection of the site.

6.4.2 Ground Failure Event

In 1727, an earthquake of magnitude 5.0 occurred near Newburyport. Historical records report ground failure events in the town, in the form of lateral spreading and sand boils (Tuttle at al., 1987). There have been reports of ground failure in nearby areas during a second earthquake in 1755, which however does not seem to have caused liquefaction in Newburyport. Tuttle et al. (1987) reports that the stratigraphy in the region near Newburyport is disturbed, a possible indication that the area has experienced liquefaction-related phenomena during the past few thousand years.

The earthquake catalogue described in Chapter 4 gives the epicentral location of the 1727 event as 42.8°N, 70.6°E and estimates epicentral MM intensity I_0 as 7-9. Using the attenuation model of eq. (4.12), the peak ground acceleration at the site is therefore estimated to be $PGA=e^{4.824+\varepsilon}(cm/sec^2)$ where ε is a normally distributed random variable with mean value zero and standard deviation $\sigma=0.6$.

6.4.3 Analysis

From the geologic profile, it is reasonable to assume a depth of 15 ft for the most liquefiable sand layer. Considering the possibility of artesian conditions, the water table is considered to be at the ground surface. Although these assumptions are possibly inaccurate, they may be acceptable here because the results of the analysis are not sensitive to the depth of the critical layer and to the depth of the water table.

Estimating Blow Count Number

The natural logarithm of N is assumed to have normal distribution with mean m and variance $\sigma^2=0.26$. This variance is considered to be reasonable for a natural material, based on the analysis of Chapter 5. For the probability of liquefaction $P_L=f(N,a)$, we use the clean sand model which is also given in Chapter 5, see eq. (5.2).

Since for the Newburyport site we do not have an accurate estimate of the fraction γ of the area that experienced liquefaction during the 1727 event and we do not know well the blow count number, we first produce a plot of γ v.s. N_m, where $N_m=e^m$,(see fig. 6-3). The value of γ for given N_m is calculated using the following equation:

$$\gamma(N_m)=\sum_N \sum_a P_L(N,a)\times P(N|m,\sigma)\times P(a) \tag{6.1}$$

where

$P(N|m,\sigma)$ = discretized probability of N, given m and σ (see eq. (4.4))

$P(a)$ = discretized probability of peak site acceleration in the 1727 event
$=P(\varepsilon)$

One can use the plot of fig. 6-3 to estimate the mean uncorrected blow count number from any given estimate of the fraction of liquefied area, γ. The mean blow count number so inferred should be interpreted as an equivalent blow count number rather than the field mean value. At the time of this study, field SPT data are not yet available to make a comparison.

Estimating the Liquefaction Rate

Fig. 6-4 shows the seismic hazard curve for the Newburyport site in terms of the peak ground acceleration. Using a relationship of the type in equation (4.20), one can estimate the liquefaction rate λ_L for given N_m:

$$\lambda_L=\sum_a \sum_N P_L(N,a)\times P(N|m,\sigma)\times \lambda(a) \tag{6.2}$$

Fig.6-5 shows a plot of the liquefaction rate λ_L as a function of N_m. Using the estimate of N_m from the previous analysis, one can evaluate the expected liquefaction rate at the site.

Liquefaction Hazard Curves

One can also combine fig. 6-3 with fig. 6-5 and plot the liquefaction rate λ_L as a function of the fraction liquefied area γ during the 1727 earthquake. This is done in fig. 6-6. An advantage of this curve is that one does not have to go through an explicit estimation of SPT.

The two main sources of uncertainty in the present evaluation of liquefaction hazard are the estimate of PGA for the 1727 event and the estimate of the variance of N. Fig. 6-7 shows a plot of λ_L vs. γ for different values of the variance of N. Notice that as the variance increases, λ_L decreases for γ less than about 10%. However, for γ greater than 10%, the variance of N has very little effect on the liquefaction rate. The mean value of N, which is very low for γ>10%, is the dominant parameter for this range of γ.

Fig. 6-8 shows a plot of λ_L vs. γ for different estimates of the 1727 PGA. As one would expect, rate increases with decreasing PGA (smaller values of PGA for the 1727 event mean weaker sand deposits).

6.5 Discussion

Tuttle (1988) estimates that for certain areas of Newburyport, γ has a value around 1% for the 1727 event. Using a PGA of 0.125g and the plot of fig. 6-8, one finds a corresponding rate of liquefaction at the generic site of 1.5×10^{-4}/year. If there is an error in the estimate of γ and for example the actual value ranges between 1% and 10%, then the estimate of λ_L itself varies by up to one order of magnitude.

During the 1727 event, it was observed that sites in different areas of Newburyport experienced liquefaction to different degrees. This means that γ should not be assigned a single value for the entire region. The reason for the spatial variation of γ and therefore of liquefaction resistance might be due to a difference in the water table level, in the gradation, in the relative density of the soil, etc.... A better method to use the curves in fig. 6-8 would

then be to divide the region into several areas and assign a different γ to each area. Some areas would have high values of γ and consequently high liquefaction rates, while in others γ and λ_L would be lower. The result is a liquefaction hazard map similar to the maps produced in chapters 4 and 5.

A problem arises when we apply the method to other earthquakes. For example, for the 1755 earthquake, the estimate of PGA at Newburyport is about 0.1g, but apparently no or minimal liquefaction occurred. If one estimates γ for this earthquake using the results from the 1727 event (with γ=0.01) one gets γ=0.6%, which is larger than zero. Three explanations can be given for this discrepancy:

1- The soil did liquefy during the 1755 earthquake but liquefaction was not observed or reported,

2- As a result of the 1727 earthquake, the soil densified and its strength increased. The implication is that the hazard curve in fig. 6-6 is not applicable after 1727.

3- There is uncertainty on the fraction γ that would liquefy for a given (N,PGA) combination and this uncertainty should be accounted for in reconciling observations from different earthquakes.

A simple way to include variability of γ is to discretize the region into n cells and assume that each cell liquefies with probability P_L, independently of the other cells. Then the fraction γ of liquefied cells given P_L is a random variable with distribution directly related to the binomial distribution. In fact, the probability that n_L cells liquefy is:

$$P(n_L|P_L)=\binom{n_L}{n}P_L^{n_L}(1-P_L)^{n-n_L} \tag{6.3}$$

and $\gamma=n_L/n$

Fig. 6-9 shows a plot of the distribution in eq. (6.3). Methods can then be developed to estimate the mean blow count number in using observations from several earthquakes. Some such methods are currently under study.

6.6 Conclusions

The method developed in this chapter allows one to evaluate liquefaction hazard at sites where liquefaction has occurred as a result of historic events, without the need for insitu testing. The method is also useful to calibrate parameters of the liquefaction model to local conditions.

Application of the method to Newburyport using liquefaction information for the 1727 earthquake gives a liquefaction rate of about 10^{-4}-10^{-3}/year.

Before the method can be recommended for general use, it should be tested in other areas where more data are available about the extent of liquefaction and about geotechnical parameters.

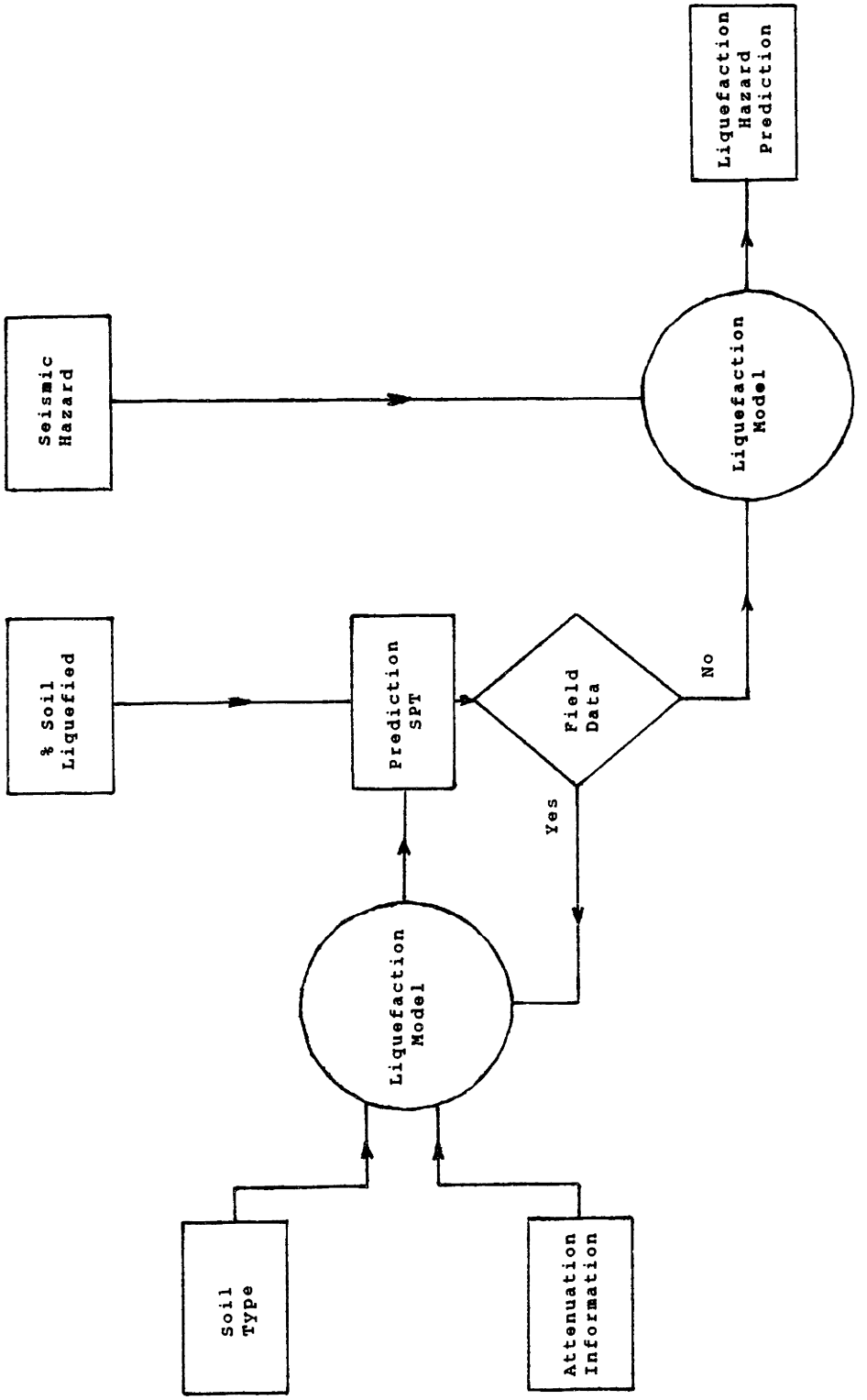

Figure 6-1: Flow Chart of Liquefaction Hazard Evaluation Method

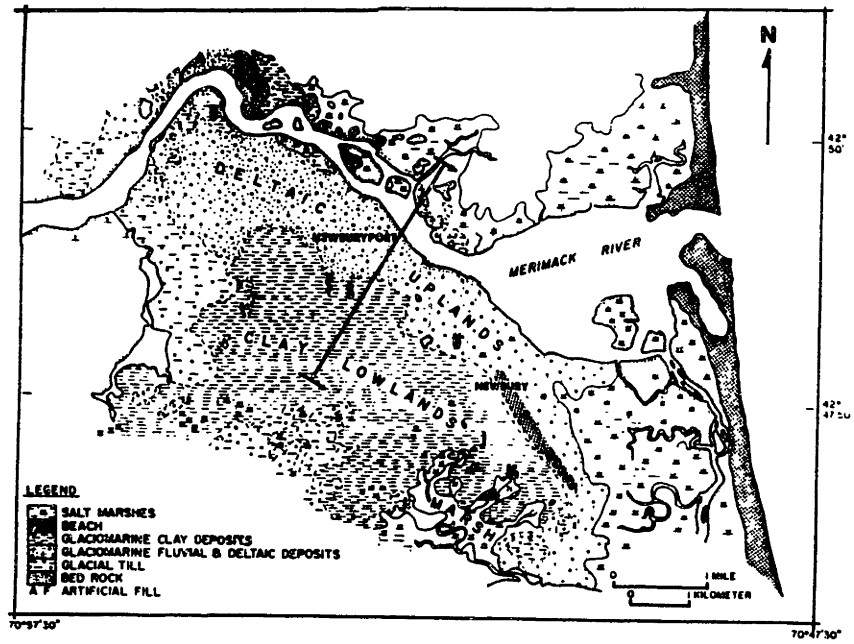

CROSS SECTION OF NEWBURYPORT DELTA BASED ON BOREHOLE DATA

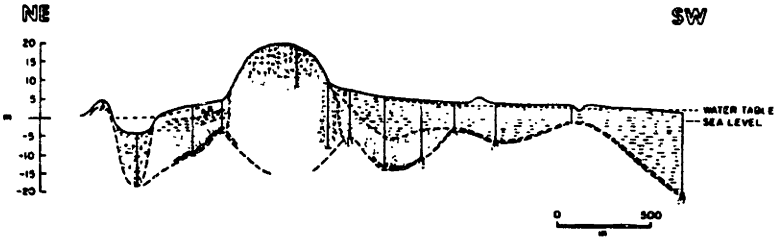

Figure 6-2: Geologic Crossection in Newburyport (Tuttle, 1987)

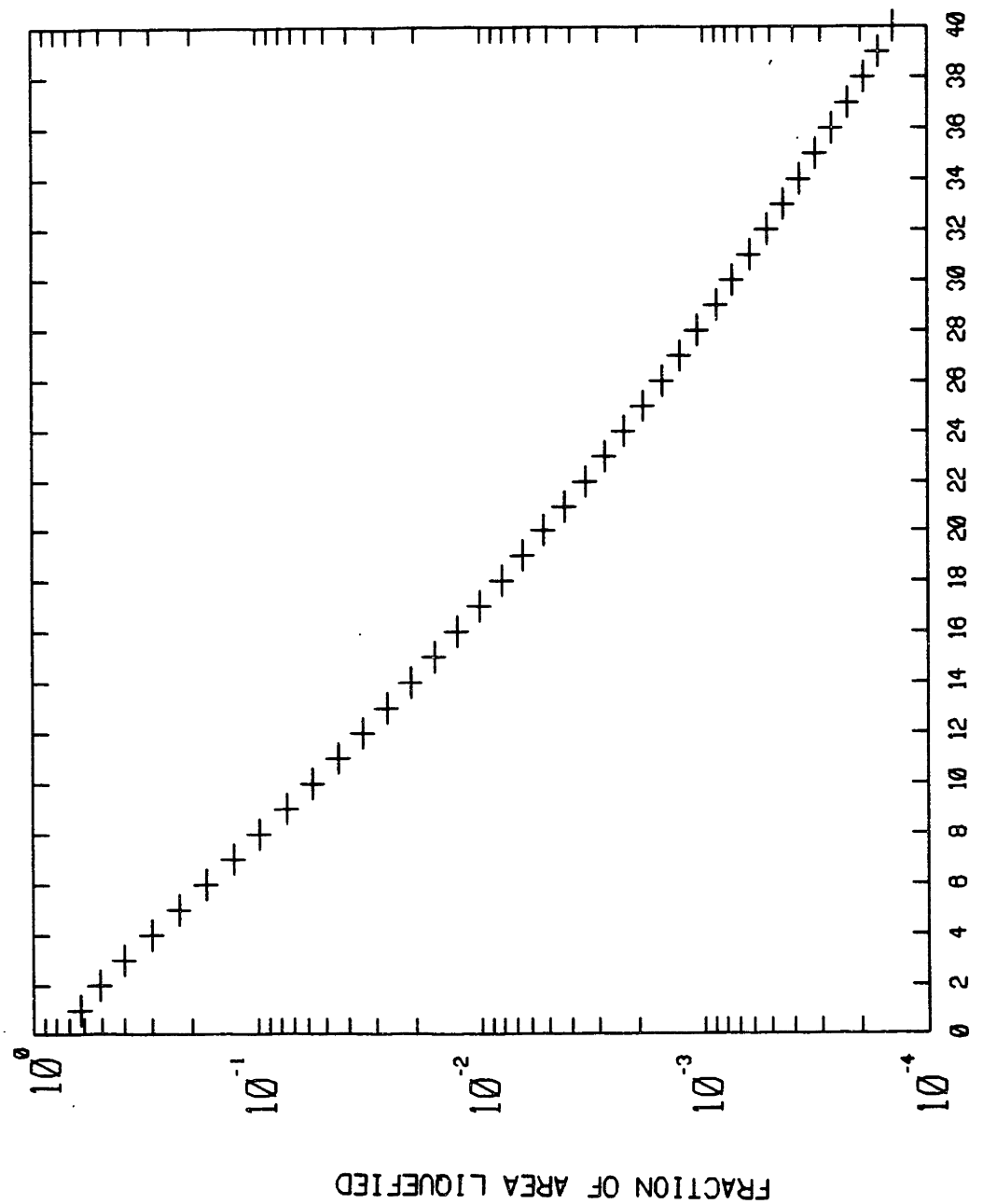

Figure 6-3: Plot of γ vs. N_m

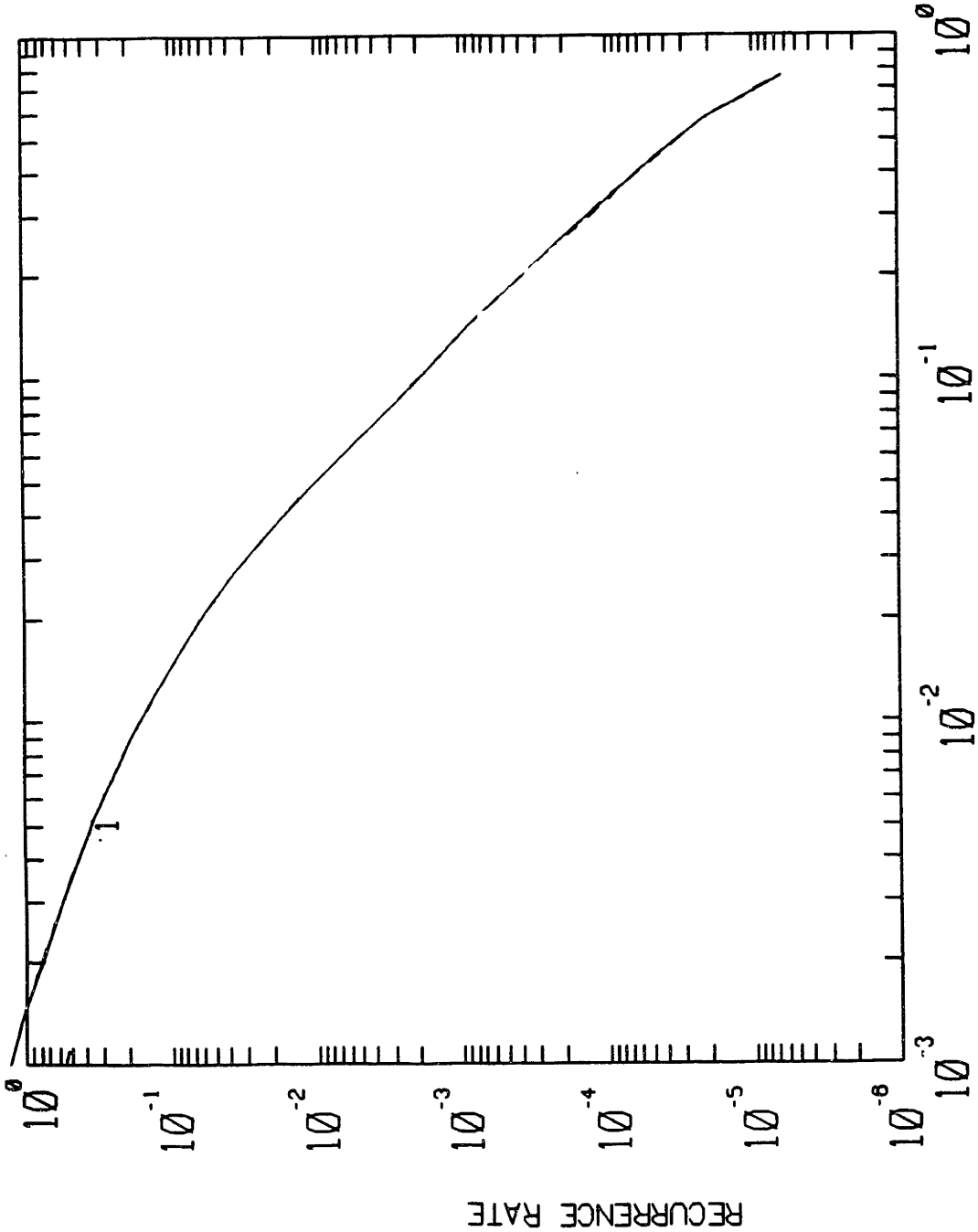

Figure 6-4: Seismic Hazard Curve for Newburyport

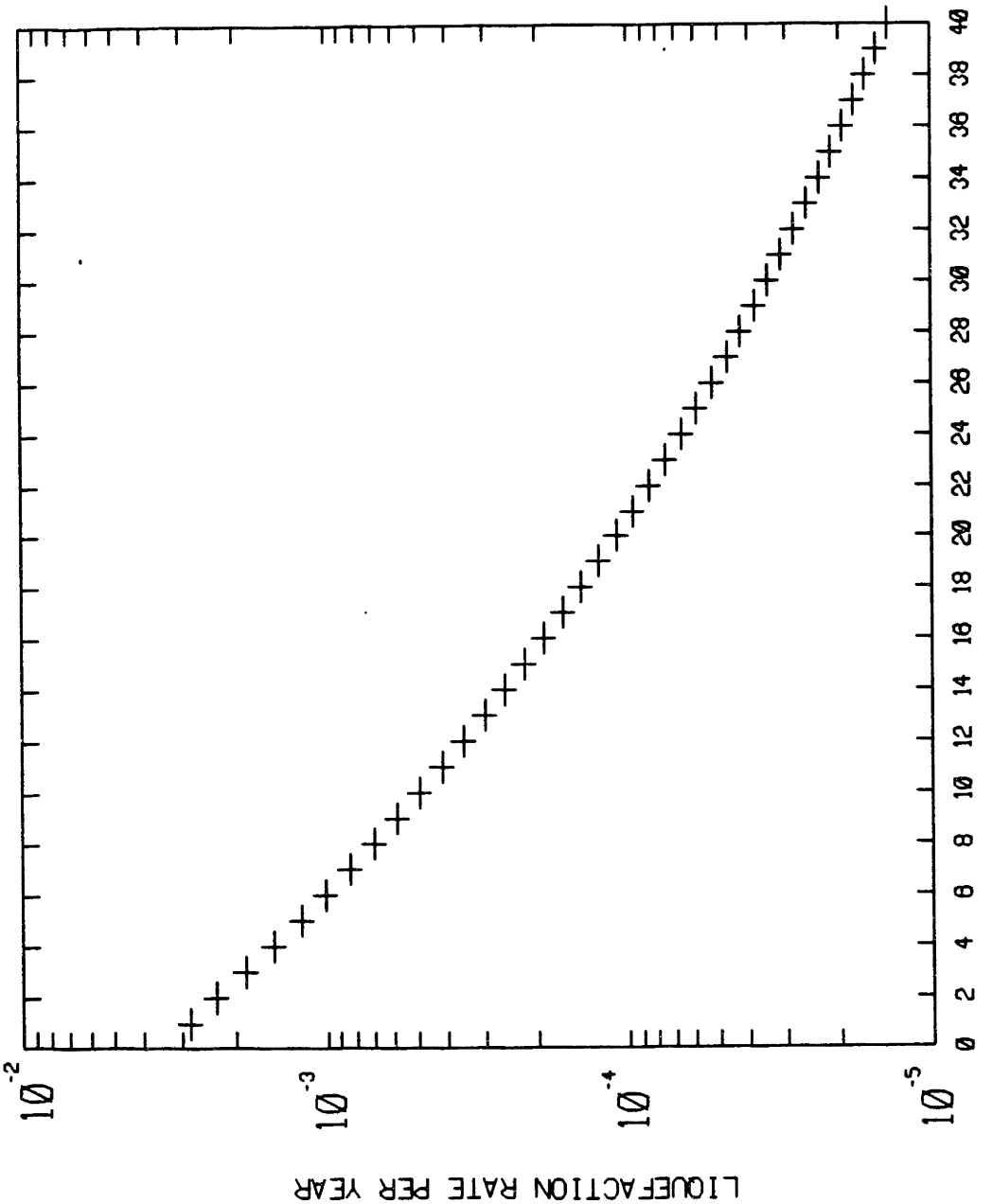

Figure 6-5: Plot of λ_L vs. N_m

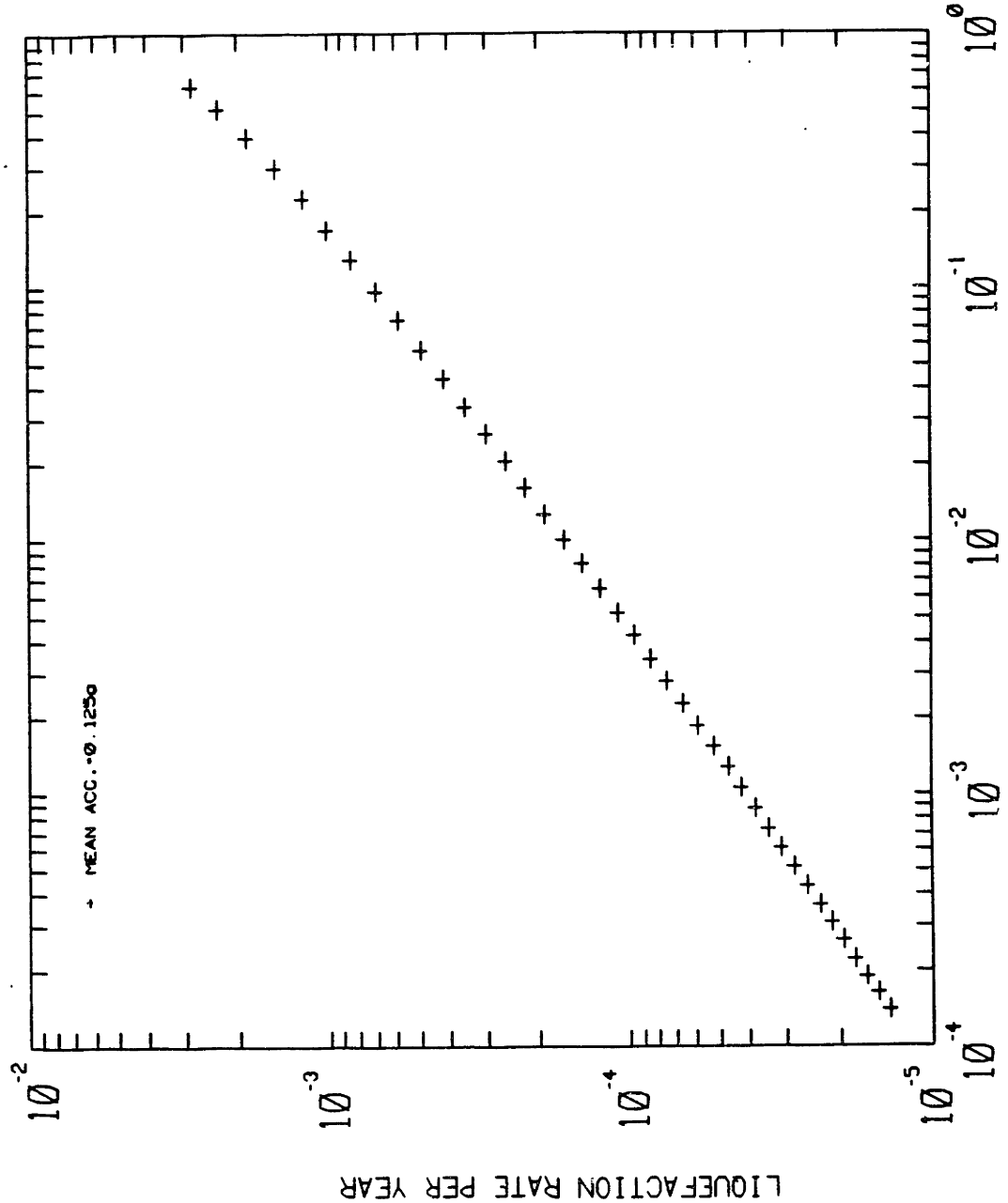

Figure 6-6: Liquefaction Hazard Curve

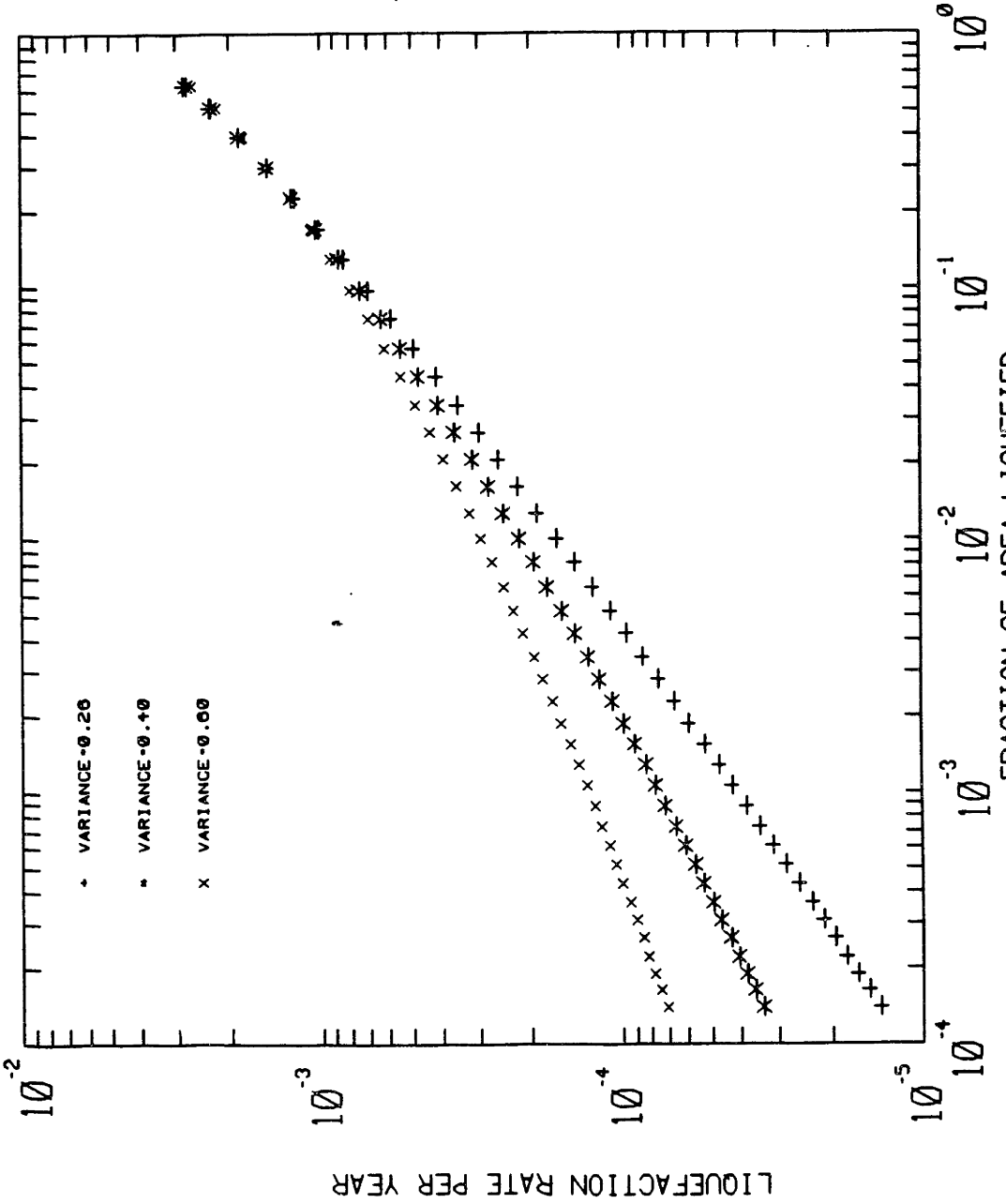

Figure 6-7: Liquefaction Hazard Curve for Different σ^2

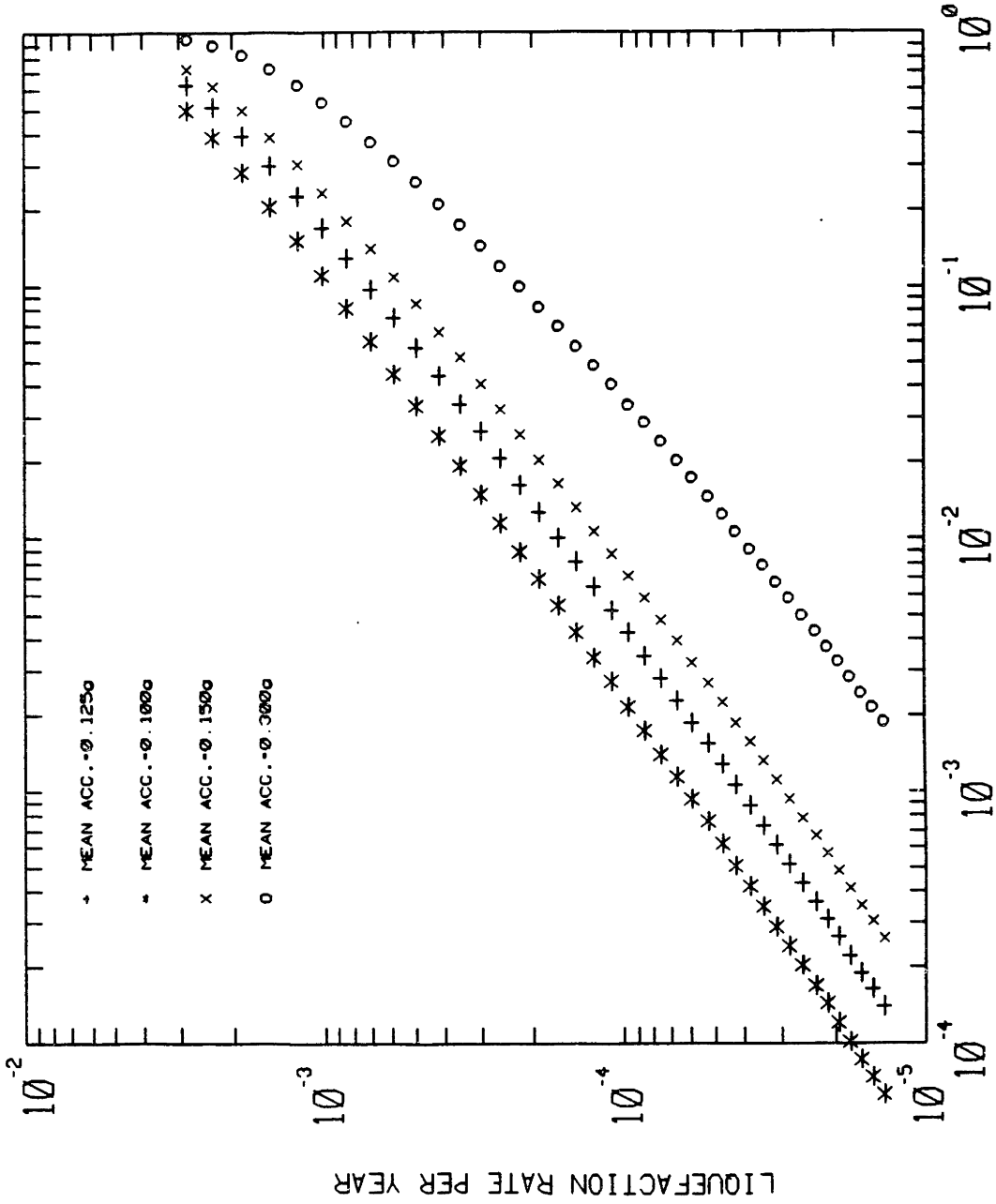

Figure 6-8: Liquefaction Hazard Curve for Different PGA

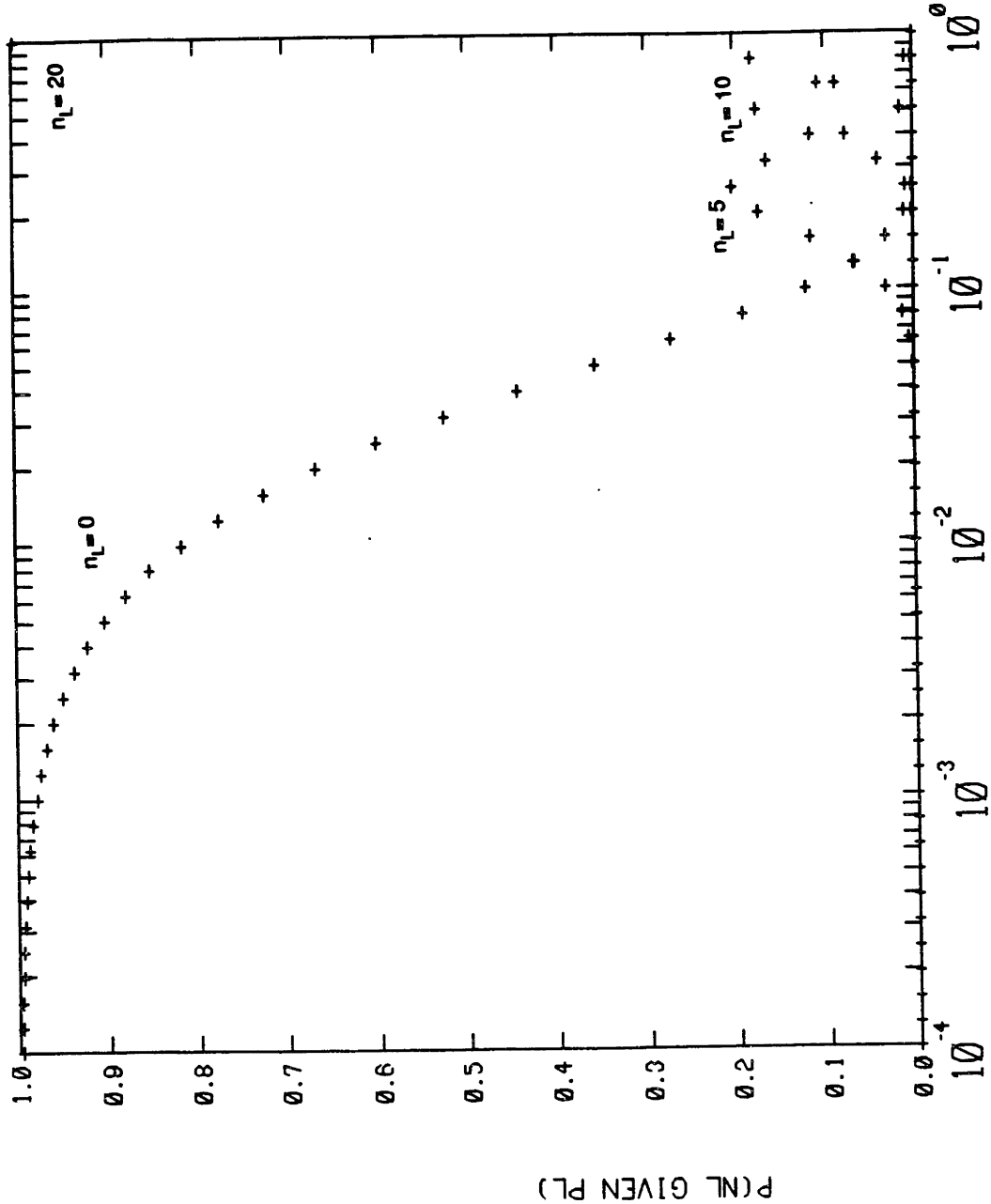

Figure 6-9: $P(n_L' | P_L)$ n=20 cells

Chapter 7

LIQUEFACTION DANGER MAPS NORTH OF BOSTON

7.1 Introduction

The eventual objective of this study is to produce liquefaction risk maps of class D for the Greater Boston Area, which is the area approximately encircled by Interstate 495. A first step in this direction is to produce Class B liquefaction danger maps identifying potentially liquefiable soil deposits.

In this chapter we use information from surficial geology maps and some geotechnical data, (class A), to produce two liquefaction maps covering selected areas north of Boston. This work is an illustration of the type of liquefaction danger maps that can be produced for the Boston area. Time constraints and unavailability at the time of this research of more detailed geotechnical information prevented us from producing similar maps for areas west and south of Boston.

7.2 Procedure

Two liquefaction danger maps are produced covering eight USGS quadrangles north of Boston. Map 1 covers Lawrence, Reading, Wilmington, and South Groveland quadrangles. Map 2 covers Salem, Ipswich, Georgetown, and Marblehead North quadrangles. The two liquefaction danger maps are presented in Appendix I of this thesis.

On the basis of geologic descriptions in USGS surficial geology maps as well as some geotechnical data obtained from local engineering firms, we qualitatively assessed the liquefiability of the various surficial deposits in each quadrangle. The various liquefiable

deposits are marked on the danger maps using different types of crosshatching. The maps are thus class B1 maps.

Several deposits are identified as potentially liquefiable based on their geologic description, grain size distribution and on previous records of liquefaction events in similar deposits in other regions. These deposits include:

- Windblown deposits (loess); they consist mainly of fine sand and silt. These deposits are known to collapse after being exposed to water for long periods of time.

- Overbank fluvial deposits; they consist of medium to fine sand. Overbank deposits can contain layers which are loose.

-Glacio-lacustrine and fluvioglacial deposits; based on some geotechnical data we observe that some of the deposits have very low SPT values. Grain size distribution curves of the deposits place them within the range of liquefiable soils. This category includes kame plain and kame terrace deposits as well as fluvioglacial lake deposits.

- Glaciomarine clays and sands; these deposits have experienced liquefaction during the 1727 earthquake in Newburyport (Tuttle et al., 1987). See also Chapter 6.

Other local deposits are identified as potentially liquefiable and will be discussed later. The following is a description of the potentially liquefiable deposits identified in the liquefaction danger maps.

7.3 Map 1

This map includes the Lawrence, Reading, Wilmington, and South Groveland quadrangles. The potentially liquefiable deposits identified in this map include wind blown deposits, overbank river deposits, glacial lake deposits, and kame plain and kame terrace deposits.

The following is a detailed description of the deposits identified in each quadrangle covered by this map.

7.3.1 Lawrence Quadrangle

Four major deposits in this quadrangle are identified as potentially liquefiable based on the surficial geology map of the quadrangle and some geotechnical information. These deposits are wind blown deposits, overbank river deposits, glacial lake deposits, and fluvioglacial deposits of kame terrace and kame plain types.

Wind blown deposits are limited to few areas in this quadrangle. These deposits are composed of unstratified fine to medium sand. They can take the form of dunes near the shores of glacial lake Methuen. Based on Obermeier et al (1987) one knows of dunes which have liquefied, this knowledge is used as the basis for the classification here.

Overbank river deposits are found mainly along the banks of the Merrimack river and a few other local rivers. The deposit consists of well sorted fine sands and silts. Analysis of SPT records in similar deposits in Lowell, along the Merrimack river, (Chapter 4), indicate that these deposits are potentially liquefiable.

Glacial lakes provide a suitable environment for the low density deposition of soil brought in by glacial meltwater. Lake bottoms are characterized by well sorted sands and silts. This type of deposit is similar to layer II in the Lowell sites, Chapter 4, which contains loose seams of sand and has a very low blow count number.

Kame plains and -terraces are fluvioglacial deposits which consist of coarse gravel and sand deposits but contain finer granular deposits as well. These deposits can be less susceptible to liquefaction because of the presence of some gravel. However, borehole data of kame deposits around Haggets pond, fig. 7-1, show that grain size distribution places the deposit within the range of liquefiable deposits. Low SPT values, less than 10 blows/ft, occur within that deposit.

There are other deposits that might liquefy in this quadrangle, that are not however identified in Map 1. Some of the local sand deposits can be included under this category as well as some artificial fill.

7.3.2 Reading Quadrangle

Two major deposits are identified in this quadrangle as potentially liquefiable: overbank river deposits and kame plain and -terrace deposits. Wind blown deposits exist in this quadrangle but are not identified on the surficial geology maps. The most interesting aspect in this quadrangle is that boundaries of an old glacial lake are identified. The area is now overlain by a variety of deposits including kames and marches. It is possible that the glacial deposits underlying this area are potentially liquefiable.

Fill as well as some unstratified sand exist in this quadrangle. These deposits are not marked in Map 1.

7.3.3 Wilmington Quadrangle

The three potentially liquefiable deposits identified in this quadrangle are wind blown deposits, flood plane deposits, and kame plain, -terrace and -delta deposits. Kame terraces include in some areas valley train deposits which are unlikely to liquefy. However, it is not possible to distinguish the valley train deposits from kame plane and kame terrace deposits. The kame deltas, in this quadrangle, are included as potentially liquefiable because they are described as containing some fine sand. Figure 7-2 shows a grain size distribution curve and some SPT data for kame type deposits close to Lowell Junction in Wilmington.

Unmapped deposits that might be prone to liquefaction are local fluvial deposits and local deposits of sand , as well as artificial fill. A particular problem in this quadrangle is that the geologic map does not show the continuation of the old glacial lake identified in the Reading quadrangle, which should extend to the Wilmington quadrangle. However, in the

text description of the Wilmington geologic map, varved lake bottom deposits are described which are found at some depth near Grove street close to the border of the Reading quadrangle. Hence, it is likely that lake bottom deposits underlie several swamps in the area.

7.3.4 South Groveland Quadrangle

No USGS geologic map is available for this quadrangle; however, the surficial geology of a portion of the quadrangle (northeast section) is described in Sammel, (1967). The only deposits identified as liquefiable in this quadrangle are the kame plain and -terrace deposits.

7.4 Map 2

This map covers the Georgetown, Salem, Ipswich, and Marblehead North quadrangles. The main potentially liquefiable deposits identified in this map are windblown deposits, overbank fluvial deposits, and glaciomarine deposits. The glaciomarine deposits, as discussed in Chapter 6, have liquefied in the past in Newburyport area, just to the north of the Ipswich quadrangle.

The following is a detailed description of the potentially liquefiable deposits in each quadrangle covered by Map 2.

7.4.1 Georgetown Quadrangle

Three major deposits are described in this quadrangle: overbank river deposits, kame plain and -terrace deposits, and glaciomarine deposits. The overbank river deposits are not distinguished on the geologic quadrangle map but are included as part of "undivided sand deposits" and were described as "fine to medium well sorted sand, may include some alluvium and marine sand". The identification of the kame plain and -terrace deposits

proved to be problematic. Kame plains and -terraces are included under different categories in the geologic map; namely fine to medium well sorted fluvioglacial sand river deposits in the Parker River Area, medium well sorted sand deposits in Ipswich River Area, and scattered poorly sorted collapsed drift deposits. Sammel, (1967), identifies different deposits as Kame type deposits. We include the kame deposits identified in Sammel, (1967), in the danger map to be on the conservative side.

Two types of glaciomarine deposits exist in this quadrangle; glaciomarine clays and glaciomarine sands. Only glaciomarine sands are identified as liquefiable in Map 2. However, it is possible that the clays are underlain by liquefiable glaciomarine sands, as in the case of Newburyport, (Tuttle, 1987).

7.4.2 Ipswich Quadrangle

Four deposits are mapped as liquefiable in this quadrangle; dune/windblown deposits, overbank fluvial deposits, kame plain and -terrace deposits, glaciomarine deposits. Dune deposits are found mainly along the beaches. The geologic map does not distinguish between glaciomarine sands and clays. To be conservative we classified all glaciomarine deposits as liquefiable.

7.4.3 Salem Quadrangle

Overbank fluvial deposits, glaciomarine deposits and kame plain and kame terrace deposits are identified as potentially liquefiable in this quadrangle. As in the Ipswich quadrangle, it was not possible to differentiate between glaciomarine clays and glaciomarine sands. The kame plain and -terrace deposits are not identified in the geologic map as such, but are included under several other categories (such as early fluvioglacial deposits in Danvers River valley, fluvioglacial deposits in Danvers River and Miles River valleys, and late fluvioglacial deposits in the Ipswich River valley). Kames are, hence, identified on the basis of the geologic description of the various categories while maintaing continuity with Kame plain and terrace deposits identified in adjacent maps.

Eolian deposits are present over much of the area but are not identified on the geologic quadrangle map.

7.4.4 Marblehead North Quadrangle

No geologic maps or other geotechnical information on surficial deposits is available in this quadrangle.

7.5 Conclusion

Class B1 maps are produced identifying different potentially liquefiable deposits north of Boston. One should be careful in using these maps because of several limitations:

First, the boundaries of the deposits on the maps are not accurate. In several areas earthmoving work has resulted in local changes of surficial geology. At many localities accurate description of the deposits is not available. Assumptions are made as to the boundaries of the deposits and their susceptibility to liquefaction. It is quite possible that in some areas we are overly conservative while in others we have missed liquefiable deposits. Maps 1 & 2 are based on surficial geology information. However, some underlying deposits may liquefy. We suspect, for example, that many of the marches and swamps are underlain by liquefiable fluvioglacial deposits. Information about the underlying deposits is not included in the danger maps. Extensive borehole information is needed to establish the geologic profile of the area.

The water level in the mapped area is unknown. A deposit has to be saturated to liquefy. Some of the deposits identified might lie above the water table and hence might not be liquefiable.

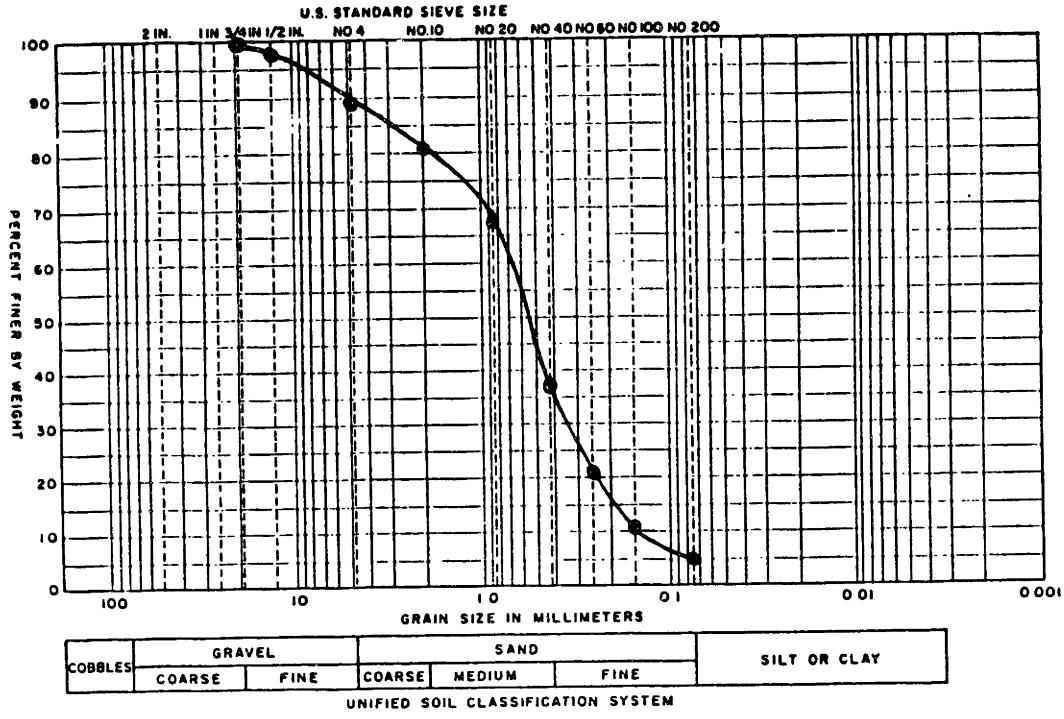

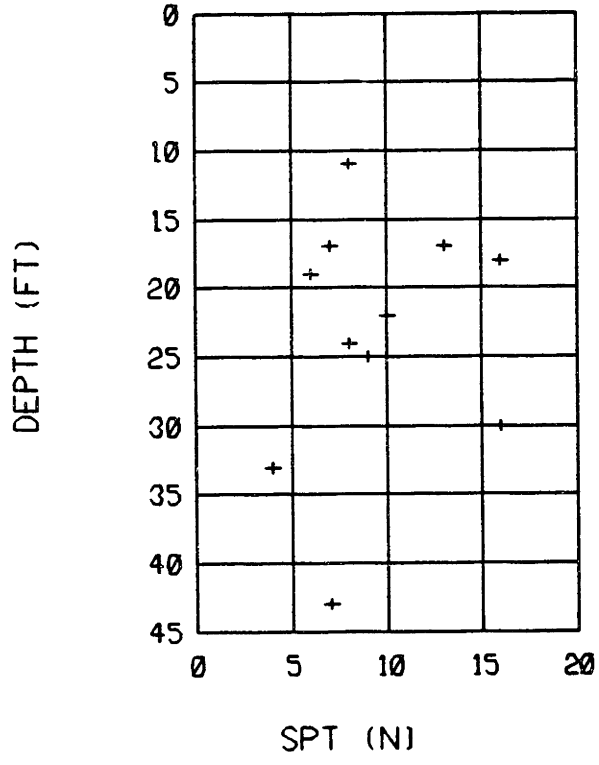

Figure 7-1: Kame Deposits, Haggets Pond, Lawerence

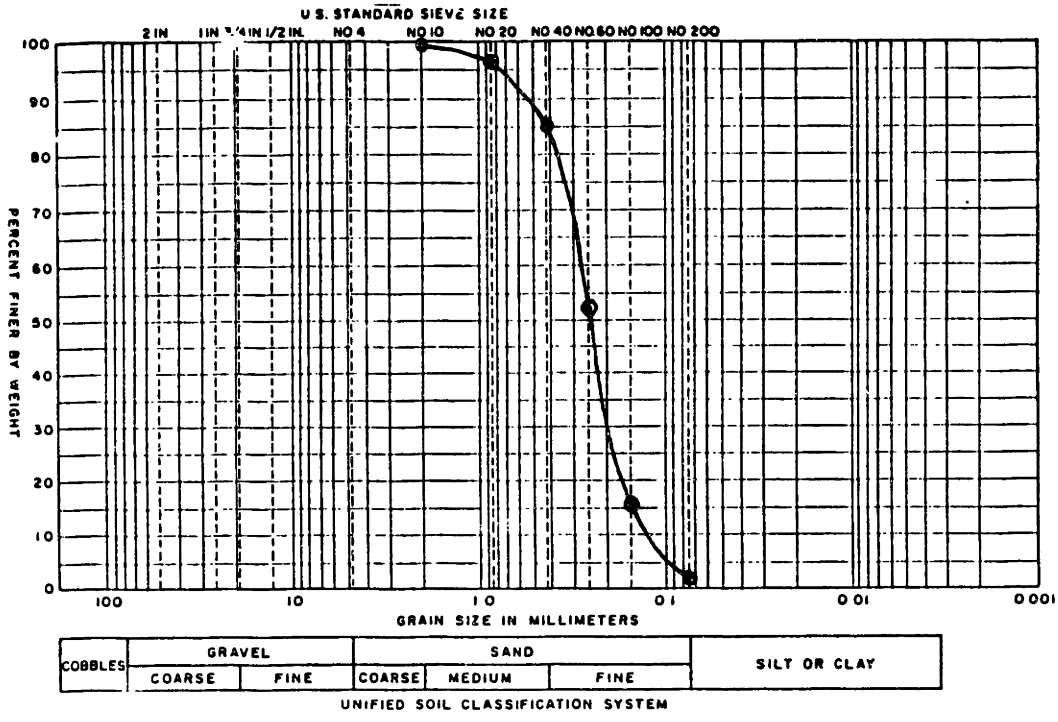

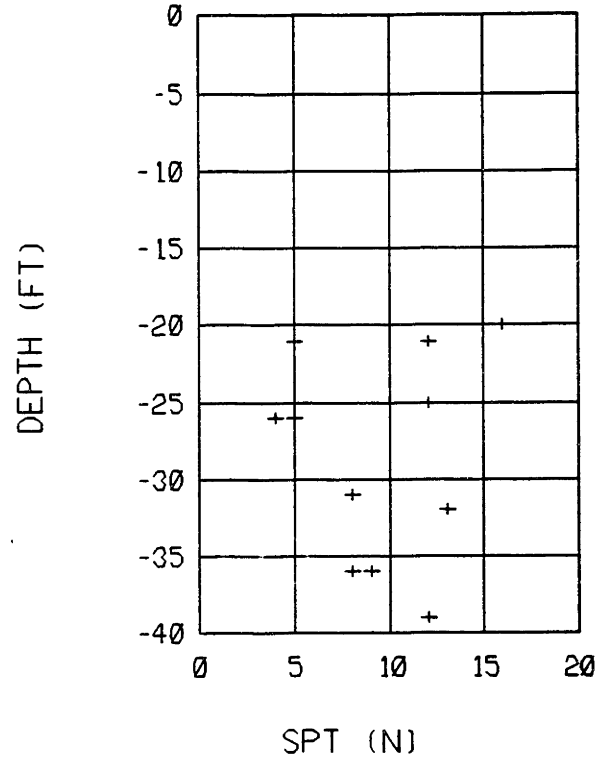

Figure 7-2: Fluvioglacial Deposits, Lowell Junction, Wilmington

Chapter 8

CONCLUSION

8.1 Major Results

Three techniques to produce geographical maps of liquefaction hazard or liquefaction danger (see definitions in section 3.3) are described in this thesis and applied to selected areas of Greater Boston. Specifically, liquefaction hazard maps are produced for the BackBay fill and for an area with fluvial and fluvioglacial deposits in Lowell. The estimated liquefaction rate ranges between 10^{-4}/year to 10^{-3}/year, which can be considered moderate. These are spatially averaged rates. Specific sites in the mapped regions exhibit higher or lower rates.

A new method is proposed to evaluate liquefaction hazard using past liquefaction records. When this method is applied to glaciomarine deposits in Newburyport. that are known to have partially liquefied during the 1727 earthquake, the estimated liquefaction rate is again between 10^{-4} and 10^{-3} events/year.

Finally, two liquefaction danger maps are produced, which identify liquefiable deposits in areas north of Boston. The main problem encountered in the production of these maps is the lack of adequate geologic and geotechnical information.

8.2 Recommendations for Future Work

Several additions and improvement can be made to the mapping methods developed here. For the method that produces liquefaction hazard maps (Chapter 4), a spatial correlation and updating technique similar to that used for SPT data should be implemented for the critical depth. Possible problems arising from not properly updating the critical depth were discussed in chapter 5.

The analyses of SPT records from the BackBay and Lowell areas indicate that SPT counts are better correlated in natural deposits than in artificial fill. Analysis of additional SPT records in the region is needed to establish characteristic spatial variability patterns. Having good spatial correlation of blow count data enables one to extrapolate results from a few test sites to other sites in the same geologic deposit.

Soil deposits described in chapters 4,5,&7 are identified as liquefiable based on the geologic description of the material and sometimes using grain size distribution information. Field and laboratory investigations (such as those described in Chapter 2) are needed to better establish the liquefiability of these deposits.

In the danger maps produced in chapter 7 we identify all potentially liquefiable deposits without taking the location of the ground water table into consideration. Investigations are needed to determine the location and seasonal fluctuation of the ground water table. In the same maps, we only identify the liquefiable surficial deposits. Information on the soil profile in the mapped areas is needed to identify any underlying potentially liquefiable deposit.

Bibliography

Aldrich,H.P. (1970), BackBay Boston Part I, Journal of the Boston Society of Civil Engineers, V57, No.1, pp1-33.

Aldrich,H.P. & Lambrechts,J.R. (1986), BackBay Boston Part II: Ground Water Levels, Civil Engineering Practice, pp31-64.

Anderson,L.R. and Keaton,J., (1982), Development of a Liquefaction Potential Map. Soil Dynamics and Earthquake Engineering Conference, Southampton, pp899-910.

Arulmoli,K., Arulanandan,K., and Seed,H.B., (1985), New Method for Evaluating Liquefaction Potential. ASCE Journal of Geotechnical Engineering, Vol.111, No.1, pp95-114.

BSCE, (1969-1970), Boston Society of Civil Engineers Journal.

Budhu,M., Vijayakumar,V., Giese,R.F., and Baumgras,L., (1987), Liquefaction Potential for New York State: A Preliminary Report on Sites in Manhatten and Baffalo. National Center for Earthquake Engineering Research, Technical Report, NCEER-87-0009.

Casagrande,A., (1975), Liquefaction and Cyclic Deformation of Sands, A Critical Review. Vth Pan American Conference on Soil Mechanics and Foundation Engineering, pp80-133.

Castle,R.O., (1958), Surficial Geology of the Lawrence Quadrangle, Massachusetts - New Hampshire. Scale 1:31,680. Geologic Quadrangle Maps of the United States. U.S. Geological Survey. Map GQ-107.

Castle,R.O., (1959), Surficial Geology of the Wilmington Quadrangle, Massachusetts. Scale 1:31,680. Geologic Quadrangle Maps of the United States. U.S. Geological Survey. Map GQ-122.

Cupples,N.P., (1969), Surficial Geology of the Georgetown Quadrangle, Massachusetts. Scale 1:24,000. Geologic Quadrangle Maps of the United States. U.S. Geological Survey. Map GQ-850.

DM7, (1982), Design Manual. Naval Facilities Engineering Command. Department of the Navy.

Einstein,H.H., (1988), Landslide Risk Assessment Procedure. International Symposium on land slides, Switzerland.

El Hosri,M.S., Biarez,J., and Hicher,P.Y., (1984), Liquefaction Characteristics of Silty Clay. 8th World Conference on Earthquake Engineering, San Francisco, Vol. III, pp277-287.

Hawkes,M., (1987), Surficial Geology of the Boston Basin, MA. Master's Thesis. Massachusetts Institute of Technology, 313p.

Heidari,M., (1987), Statistical Methods of Earthquake Attenuation. Ph.D. Thesis, Dept. of Civil Engineering, MIT.

Hoshiya,M. and Saito,E., (1986), Linearized Liquefaction Process by Kalma Filter. ASCE Journal of Geotechnical Engineering. Vol.112, No.2, pp155-189.

Jamiolkowski,M., Baldi,G., Belloti,R., Ghionna,V., and Pasqualini,E., (1985),Penetration Resistance and Liquefaction of Sands. Proc 11th Int. Conf. on Soil Mech. and Found. Eng., V4, pp1891-1896.

Kasim,A.G., Chu,M-Y., and Jensen,C.N., (1986), Field Correlation of Cone and Standard Penetration Tests. Technical Note, ASCE Journal of Geotechnical Engineering, Vol. 112, No.3, pp368-372.

Kavazanjian,E., Roth,R.A., and Echezuria,H., (1985), Liquefaction Potential Mapping for San Franscisco. ASCE Journal of Geotechnical Engineering, Vol. 111,No. 1, pp54-76.

Kavazanjian,E. and Ho,C., (1984), Non-linear Probabilistic Evaluation of Equivalent Uniform Cycles for Liquefaction Analysis. 8th World Conference on Earthquake Engineering, Vol.III, pp231-238.

Lew,M., (1984), Risk and Mitigation of Liquefaction Hazard. 8th World Conference on Earthquake Engineering, Vol.III, pp183-190.

Liao,S., (1986), Statistical Modelling of Earthquake-Induced Liquefaction. Doctoral Thesis. Massachusetts Institute of Technology.

Liao,S. and Whitman,R.V., (1986), Overburden Correction Factors For SPT in Sand. ASCE Journal of Geotechnical Engineering, Vol 112, No. 3, pp373-377.

Maugri,M. and Carruba,P., (1985), Microzoning Using SPT data. Proc. 11th International Conference on Soil Mechanics and Foundation Engineering, pp1831-1836.

NRC, (1985), Liquefaction of Soils During Earthquakes. National Research Council. National Academy Press, 240p.

Obermeier,S.F., Weems,R.E., and Jacobson,R.B., (1987), Earthquake-Induced Liquefaction Features in the Coastal South Carolina Region. Seismic Hazards, Ground Motions, Soil Liquefaction and Engineering Practice in Eastern North America. A Symposium Sponsored by NCEER.

Oldale,R.N., (1962), Surficial Geology of the Reading Quadrangle, Massachusetts. Scale 1:24,000. Geologic Quadrangle Maps of the United States. U.S. Geological Survey. Map GQ-168.

Oldale,R.N., (1964), Surficial Geology of the Salem Quadrangle, Massachusetts. Scale 1:24,000. Geologic Quadrangle Maps of the United States. U.S. Geological Survey. Map GQ-271.

Perkins,J.B., (1987), Cumulative Damage Potential from Earthquake Ground

Shaking, San Mateo County, California. US Geological Survey Miscellaneous Investigation Series, Map I-1257-I.

Pires,J.E., Wen,Y.K., and Ang,A.H-S., (1984), Probabilistic Analysis of Seismic Safety Against Liquefaction. 8th World Conference on Earthquake Engineering, Vol.III, pp159-167.

Poulos,S.J., Castro,G., and France,J.W., (1985), Liquefaction Evaluation Procedure. ASCE Journal of Geotechnical Engineering, Vol.111, No.6, pp772-792.

Robertson,P.K. and Campanella,R.G., (1985), Liquefaction Potential of Sands using the CPT. ASCE Journal of Geotechnical Engineering. Vol.111, No.3, pp384-403.

Roth,R.A. and Kavazanjian,E., (1984), Liquefaction Susceptibility Mapping for San Franscisco, California. Bulletin of the Association of Engineering Geologists, Vol XXI, No. 4, pp459-478.

Sammel,E.A.,(1963), Surficial Geology of the Ipswich Quadrangle, Massachusetts. Scale 1:24,000. Geologic Quadrangle Maps of the United States. U.S. Geological Survey. Map GQ-189.

Sammel,E.A., (1967), Water Resources of the Parker and Rowley River Basins, Massachusetts. Hydrologic Investigations Atlas, HA 247. US Geological Survey.

Seed,H.B., (1987), Design Problems in Soil Liquefaction. ASCE Journal of Geotechnical Engineering, Vol. 113, No.8, pp827-845. B **Seed,H.B., Idriss,I.M., and Arango,A.**, , (1983), Evaluation of Liquefaction Potential Using Field Performance Data. ASCE Journal of Geotechnical Engineering, Vol. 109, No.3, pp458-482.

Soydemir,C. and LeCount,P.L., (1984), Foundation Design for Potential Liquefaction. 8th World Conference on Earthquake Engineering, Vol.III, pp191-198.

Symes,M.J., Shibuya,S., Hight,D.W., and Gens,A., (1985), Liquefaction with

Cyclic Principal Stress Rotation. Proc. 11th Int. Conf on Soil Mech. and Found. Eng., V4, pp1919-1922.

Tokimatso,K., and Yoshimi,Y., (1984), Criteria of Soil Liquefaction with SPT and Fines Content. 8th World Conference on Earthquake Engineering, Vol.III, pp255-262.

Tuttle,M.P., (1988), Personal Communication.

Tuttle,M.P., Seeber,L., and Bradley,L., (1987), Liquefaction of Glaciomarine Sediments During the 1727 Earthquake in Newburyport, Massachusetts. Seismic Hazards, Ground Motions, Soil Liquefaction and Engineering Practice in Eastern North America. A Symposium Sponsored by NCEER.

Ty,R. (1987), History and Characteristics of Man Made Fill in Boston and Cambridge. Master's Thesis. Massachusetts Institute of Technology, 135p.

U.S. Geological Survey, Georgetown Quadrangle, MA, Ipswich Quadrangle, MA, Lawerence Quadrangle, MA-NH, Marblehead North Quadrangle, MA, Reading Quadrangle, MA, Salem Quadrangle, MA, South Groveland Quadrangle, MA, Wilmington Quadrangle, MA. Topographic Maps, Scale 1:25,000.

Vaid,Y.P., Chern,J.C., and Tumi,H., (1984), Confining Pressure, Grain Angularity, and Liquefaction. ASCE Journal of Geotechnical Engineering, Vol. 111, No. 10, pp1229-1235.

Veneziano,D. and Chouinard,L., (1987a), Local Models of Seismicity and their Estimation. Proc. Symp. on Seismic Hazards, Ground Motions, Soil Liquefaction and Engineering Practice in Eastern North America, Sterling Forest, New York.

Veneziano,D. and Chouinard,L., (1987b), Combination of Seismic Source and Historic Estimates of Earthquake Hazard, in press.

Whitman,R.V., (1985), On Liquefaction. Proceedings of 11th Int. Conf. on soil Mechanics and Foundation Engineering, V4, pp1923-1926.

Yegian,M.K., (1984), Probabilistic Seismic Hazard Analysis for Pore Pressure Buildup in Sands. 8th World conference on Earthquake Engineering, Vol.III, pp167-174.

Yoshimi,Y., Hatanaka,M., Oh-Oka,H., and Makihara,Y., (1985), Liquefaction of Sand Sampled by insitu Freezing. Proc. 11th Int. Conf. on Soil Mech. and Found. Eng., V4, pp1927-1930.

Youd,T.L., (1984), Recurrence of Liquefaction at the Same Site. 8th World conference on Earthquake Engineering, Vol.III, pp231-238.

Youd,T.L. and Bennet,M.J., (1983), Liquefaction Sites, Imperial Valley, California. ASCE Journal of Geotechnical Engineering, Vol.III, pp191-198.

Youd,T.L. and Perkins,J.B., (1978), Mapping Liquefaction-Induced Ground Failure Potential. ASCE Journal of Geotechnical Division, GT4, pp433-446.

Youd,T.L. and Perkins,D.M.,(1987), Mapping Liquefaction Severity Index, ASCE Journal of Geotechnical Engineering, Vol. 113, No. 11, pp1374-1392.

Youd,T.L. and Perkins,JB, (1987), Map Showing Liquefaction Susceptibility of San Mateo County, California. US Geological Survey Miscellaneous Investigation Series, Map 1-1257-G.

Youd,T.L., Tinsley,J.C., Perkins,D.M., King,E.J., and Preston,R.F., (1978), Liquefaction Potential Map of San Fernando Valley, California. 2nd International Microzoning Conference Proceedings, pp268-278.

Zen,K., Umehara,Y., and Ohneda,H., (1985), Evaluation of drainage Effects in Sand Liquefaction. Proc. 11th Int. Conf. on Soil Mechanics and Foundation Engineering, V4, pp1931-1934.

Ziony,J.I., (1976), The Evaluation of Potential Geologic Effects of Earthquakes, CENTO Seminar on Recent Advances in Earthquake Hazard Minimization, Tehran, pp116-128.

Appendix I

Please see the next two pages for:

Liquefaction Danger Map 1

Liquefaction Danger Map 2

The maps are reduced from originals which are on a scale of 1:50,000.

LIQUEFACTION DANGER MAP

USGS TOPOGRAPHIC MAPS

QUADRANGLES:

LAWRENCE SOUTHGROVELAND
WILMINGTON READING

MASSACHUSETTS

SCALE 1:50,000

MAP 1
MIT 1988

Wind Blown Deposits High

Cherbank River Deposits Moderate

Glacial Lake Deposits Low

Kame Terraces Kame Plains Low

— Boundary of Old Glacial Lake

LIQUEFACTION DANGER MAP

USGS TOPOGRAPHIC MAPS

QUADRANGLES:

GEORGETOWN IPSWICH
SALEM MARBLEHEAD NORTH

MASSACHUSETTS

SCALE 1:50,000

MAP 2
MIT 1988

Wind Blown Deposits High	Overbank River Deposits Moderate	Glacial Lake Deposits Low	Kame Terraces Kame Plains Low	Glaciomarine Deposits Moderate